Functional MRI of Rat and Monkey Models of Absence Epilepsy: A Dissertation

A Dissertation Presented

By

Jeffrey R. Tenney

Submitted to the Faculty of the

University of Massachusetts Graduate School of Biomedical Sciences, Worcester

In partial fulfillment of the requirements for the degree of

DOCTOR OF PHILOSOPHY

May 28, 2004

Ph.D./M.D. Program in the Biomedical Sciences

COPYRIGHT

FUNCTIONAL MRI OF RAT AND MONKEY MODELS OF ABSENCE EPILEPSY

A Dissertation Presented

By

Jeffrey R. Tenney

Approved as to style and content by:

John Fray, Ph.D., Chair of Committee

Paul Gardner, Ph.D., Member of Committee

Peter Grigg, Ph.D., Member of Committee

Paul Marshall, M.D., Member of Committee

Michael Rivkin, M.D., Member of Committee

Craig Ferris, Ph.D.,Dissertation Mentor

Anthony Carruthers, Ph.D., Dean of the
Graduate School of Biomedical
Sciences

Ph.D./M.D. Program in the Biomedical Sciences

May 28, 2004

ACKNOWLEDGEMENTS

I would first like to thank my mentor, Craig Ferris, for the wonderful opportunities he created for me during my thesis research. While providing the necessary guidance I needed in order to complete a successful thesis, he also gave me the freedom to explore my own ideas. The completion of this thesis would not have been possible without the help of all the members of the CCNI, especially Jean King, Tara Messenger, and Mat Brevard, who have been with me since I started this journey. Jean, you have been my advocate, advisor, and cheerleader since day one and your constant encouragement has meant a great deal to me. In addition, I would like to thank the members of my dissertation committee for their insights and thoughtful comments.

My family has provided me with love and support throughout this process. My mother and sister, Kate, have always encouraged me and made me believe that I can accomplish anything. My fiancée, Nicole, has been my constant companion and partner since I first applied to medical school. Nicole, thank you for enduring the long nights and my crazy schedule. You are my best friend and the love of my life.

Finally, thank you to all the teachers that have encouraged and impacted me over the years. This dissertation is for you.

ABSTRACT

A seizure is defined as an abnormal electrical discharge from the brain that results in the affected area losing its normal function and reacting uncontrollably. A particular subset of seizures, known as absence seizures, are characterized by brief, paroxysmal losses of consciousness that are associated with bilaterally synchronous 3 Hz spike and wave discharges (SWDs) on electroencephalography (EEG). The optimal way to understand any disease state is to study it within the human. Unfortunately, well controlled experiments in humans are difficult due to small patient populations, treatment medications which alter the seizure, and the ethical problems associated with invasive experimental procedures. Animal models of absence seizures provide a means of avoiding the above difficulties but the model should mimic, as closely as possible, the human condition. The goal of this thesis was to develop an animal model of absence epilepsy that could be used to explore, non-invasively, the underlying mechanisms of absence seizures. Functional magnetic resonance imaging (fMRI) was used to non-invasively monitor brain activity during absence seizures in various animal models.

In this dissertation I report the development of a pharmacological rat model of absence seizures for use in fMRI investigations. Imaging was performed after absence seizure induction using γ-butyrolactone (GBL) and it was found that the cortico-thalamic circuitry, critical for the formation of SWDs,

showed robust signal changes consistent with electroencephalographic recordings in the same animals.

Since a major disadvantage of the GBL rat model is that it produces acute, drug-induced seizures, a genetic rat model with spontaneous absence seizures was subsequently developed for fMRI. EEG-triggered fMRI was used to identify areas of brain activation during spontaneous SWDs in the epileptic WAG/Rij rat strain under awake conditions. Significant signal changes were apparent in several areas of the cortex and several important nuclei of the thalamus. These results draw an anatomical correlation between areas in which there is increased fMRI signal and those where SWDs have been previously recorded using electrophysiologic techniques.

One way in which absences differ between humans and both of these rat models is that the SWD frequency in humans is classically 3 Hz while in rats it varies from 7 to 11 Hz. Marmoset monkeys were found to model the human absence seizure condition better than other animals because GBL administration in these non-human primates results in the formation of 3 Hz SWDs. This monkey model was developed for awake functional imaging and changes in signal intensity in the thalamus and sensorimotor cortex correlated with the onset of 3 Hz SWDs. The change in BOLD signal intensity was bilateral but heterogeneous, affecting some brain areas more than others.

TABLE OF CONTENTS

List of Tables

List of Figures

CHAPTER I

INTRODUCTION

Epilepsy

Definition and Classifications

A seizure is defined as an abnormal electrical discharge from the brain. The area affected by the seizure looses its normal function and may react uncontrollably. Epilepsy is a term used to describe a chronic disease state which consists of repetitive seizures. Epilepsy is one of the most common neurological disorders with a prevalence of approximately 2.5 million in the United States (1). Estimates suggest that 3% of the population will suffer from the condition at some point in their lives and the highest incidences occur in young children and the elderly (1).

Seizures vary widely in their clinical presentations and are currently classified into two broad categories, according to their clinical features: partial or generalized. Partial seizures begin in one or more localized brain regions, which is defined as a "focus". Generalized seizures, in contrast, have long been defined as beginning in both hemispheres of the brain simultaneously, without a "focus" of origin. Generalized seizures can be further subdivided into the convulsive and non-convulsive types, depending on whether the seizure is associated with tonic/clonic movements. The prototypic non-convulsive seizure and the focus of the thesis is the typical absence seizure found in children.

Pathophysiology

Neurons are cells that respond to excitatory and inhibitory signals with electrical discharges. Seizures are the result of aberrant excitations in groups of neurons. Electrical recording of brain activity has been in the past and is currently, the major diagnostic and research tool for epilepsy. The electrical activity of individual neurons, recorded with the use of intracellular electrodes, has provided a great deal of information regarding the pathophysiology of seizures. In addition, extracellular recordings of neurons, through the use of electroencephalography (EEG), have provided the ability to measure the synchronized activity of large numbers of cells, non-invasively from the scalp.

The use of intracellular recordings and EEG has provided some insight into the pathophysiology of seizures. Partial seizures appear to result when the stereotyped and synchronous electrical activity of a focus of neurons begins to spread to other brain areas (2). It is not clearly understood what causes this spread of electrical activity, but generally the seizure activity spreads along known cortical connections. Generalized seizures appear to be the result of a malfunctioning circuit between the thalamus and cortex. The origination of generalized seizures has been debated for many years, but it is widely accepted that corticothalamic malfunctioning is a necessary component.

Absence Epilepsy

Clinical Description

Typical absences are characterized as generalized seizures that consist of multiple, brief (up to 20 seconds) impairments of consciousness that have an abrupt onset and offset. Absences are unique among seizure types due to their pharmacologic treatments and characteristic bilaterally synchronous 3 Hz spike and wave discharges (SWDs) on EEG. The incidence of absence seizures in the United States is 1.9 to 8 per 100,000, usually occurring in children between the ages of 4 years and adolescence, with girls affected more than boys (3). Childhood absence epilepsy accounts for 2-8% of all the patients with epilepsy (1). A typical absence seizure is manifested behaviorally as a "staring spell" and can be accompanied by atonic postures such as drooping of the head and/or automatisms such as lip smacking.

Absence epilepsy has been shown to be genetically determined with a 16-45% positive family history, but incomplete penetrance (4). In addition, concordance rates of 70-85% have been found in monozygotic twins (4). As of this time, only two gene mutations have been identified in probands with absence epilepsy. These mutations were found in the subunits of the γ-aminobutyric acid type A ($GABA_A$) receptor and voltage-gated Ca^{++} channels (5).

Thalamocortical Circuitry

There is a rich literature from human and animal studies pointing to aberrant thalamocortical rhythms as contributing to absence. The importance of this neural circuitry to the pathophysiology of this seizure disorder necessitates a discussion of the normal functioning of intrinsic corticothalamic, thalamocortical, and intrathalamic connections.

EEG is a state-dependent measurement because the electrical activity of the mammalian brain varies with the level of consciousness. During the alert state, the EEG is dominated by desynchronization and low amplitude, fast waveforms (6). In contrast, certain consciousness states (i.e., sleep) are correlated with synchronized EEG activity, consisting of high amplitude, low frequency recordings (6). This shifting of consciousness is mainly due to changes in intrathalamic and thalamocortical activity.

One of the important functions of the thalamus is to regulate the transmission of stimuli from the external world to the cortex. This is facilitated by the ability of thalamic neurons to shift between oscillating and tonic firing modes. The ability of thalamic neurons to shift firing states is related to changes in consciousness, with the alert, desynchronized state caused by tonic firing of thalamocortical neurons (7). In contrast, when thalamocortical firing is shifted to an oscillatory, rhythmic form, signal transmission to the cortex is dampened and the level of consciousness is lowered (8).

Oscillatory activity within the thalamocortical circuit relies upon thalamic neurons within the nucleus reticularis thalami (nRT), which possesses intrinsic oscillatory behavior (9). The nRT is located along the dorsal and lateral thalamus and essentially forms a shell around the thalamus (Figure 1) (10). The nRT is composed almost entirely of inhibitory neurotransmitter, GABA neurons that project to each other and to almost all thalamic relay neurons. Fibers passing from the thalamus to the cortex, via the thalamic relay neurons, and corticothalamic fibers projecting from lamina VI of the cortex to the thalamus, must pass through the nRT (11-12). Therefore, the nRT is in a unique position to influence the thalamocortical and corticothalamic circuitry as evidenced by its correlation with EEG activity. During synchronized EEG activity, the cells of the nRT show rhythmic burst firing while during desynchronized, wakeful EEG activity the cells show tonic, single spike firing (12-14).

The ability of the nRT cells to shift between oscillatory and tonic firing modes seems to be due to the low threshold Ca^{++} spike. This Ca^{++} spike is thought to result from $GABA_B$ receptor-mediated inhibitory postsynaptic potentials (IPSPs) (15). The importance of Ca^{++} potentials in the pathogenesis of absence seizures is underscored by the fact that the efficacy of some antiepileptics is related to their ability to decrease low threshold calcium currents (16).

Figure 1

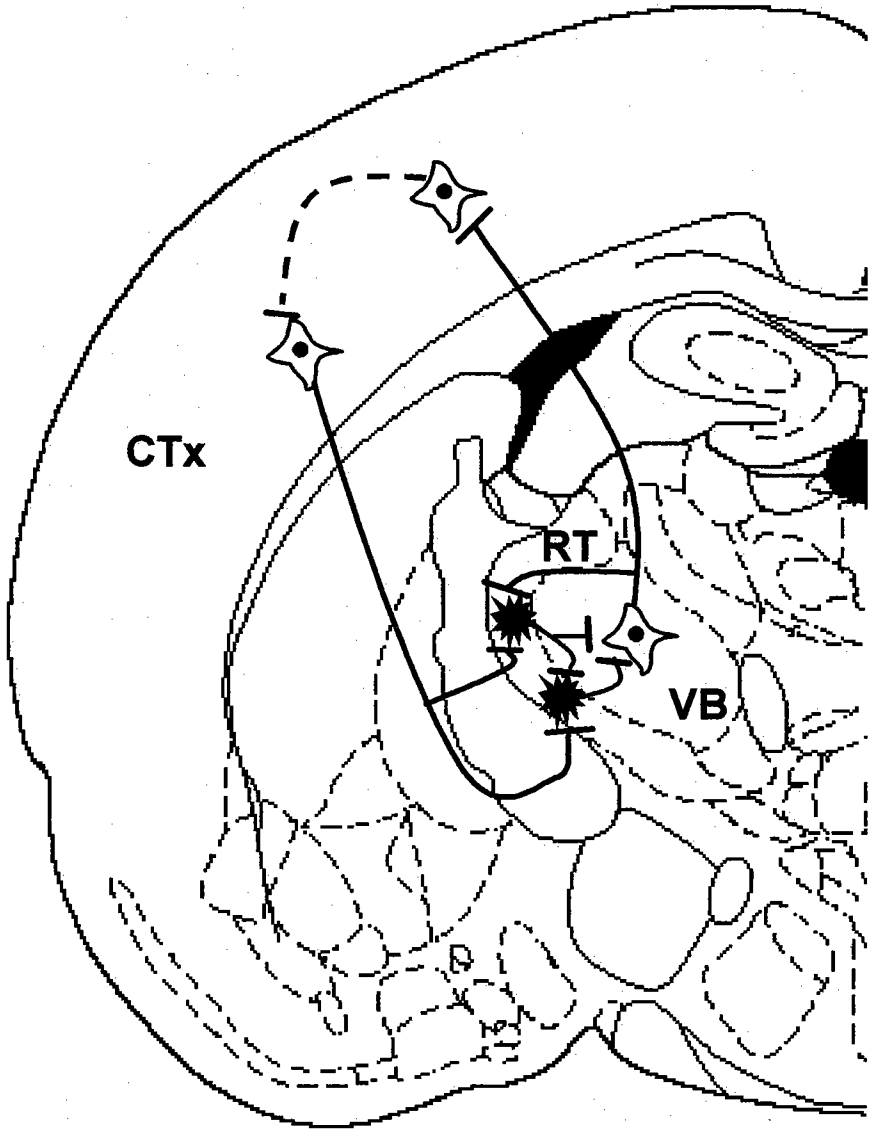

Figure 1. Corticothalamic connections in the rat brain. A coronal section through the rat brain shows some of the excitatory (blue) and inhibitory (red) connections within the corticothalamic circuit. Absence seizures seem to be related to a malfunction of this circuit. CTx, cortex; RT, nucleus reticularis; VB, ventrobasal thalamus (ventro-posteromedial/ventro-posterolateral thalamic nuclei).

Pathophysiology/Working Hypothesis

Determining the pathogenesis of this unique seizure type began with studies demonstrating in cats that electrical stimulation to the midline and intralaminar nuclei of the thalamus at a frequency of 3 Hz produced SWDs on EEG (17). This finding became more significant following work showing that depth electrodes in the thalamus of a child with absence seizures produced identical 3 Hz SWDs on EEG (18). Since this time, controversy has ensued regarding whether the structure that produces and controls the SWDs responsible for absence epilepsy is in the cortex, thalamus, or both. The generation of animal models for absence seizures has allowed this controversy to be partially resolved. Genetic rat models of absence epilepsy (WAG/Rij strain) have demonstrated a seizure "initiation site" in the somatosensory cortex with subsequent recruitment of the thalamus (19). Most people now accept the unifying hypothesis that the SWDs of absence seizures are probably produced via reciprocally connected neurons in the thalamus and cortex (20). Recent studies using animal models have shown that the nRt, thalamic relay neurons (RNs), and cortical pyramidal neurons form a circuit that sustains the thalamocortical synchronous burst firing of absence seizures (21).

Data from animal models and electrical recording from humans acquired over the past 25 years have shed some light on the pathogenesis of absence seizures. It appears the first crucial events leading to a generalized absence seizure are a glutamatergic-mediated excitatory post-synaptic potential (EPSP),

followed by a $GABA_A/GABA_B$ mediated IPSP (20). This ultimately leads to a low-threshold calcium current within the nRT neurons. The calcium current triggers another depolarization and the entire cycle is repeated (15). Since absence seizures do not occur constantly, it is believed there must be a process that controls the overall excitability of the thalamocortical circuit making it more or less resistant to the fluctuations that result in absence seizures. There is evidence of cholinergic, dopaminergic, and noradrenergic pathways projecting to thalamic and cortical endpoints of the corticothalamic circuit (22-24). Therefore, these systems may ultimately control the expression of absence seizures by their ability to modulate the corticothalamic system.

While much progress has been made in understanding the pathophysiology of generalized absence seizures, many fundamental questions still remain unanswered. Since most electrophysiology studies of seizures require the experimenter to place electrodes in specific structures, it is not completely known which brain structures contribute to the formation of SWDs. The mechanisms proposed for SWD formation do not explain what stops an absence seizure once it starts. In terms of development, it is not understood why children are particularly sensitive to this seizure disorder or why the seizures naturally begin to regress in some patients upon reaching adolescence or adulthood. Some evidence has been provided which implicates a maldevelopment of the GABAergic and glutamatergic systems or alterations of calcium channels, within the thalamocortical circuit. In the same regard, it is not

clear why a percentage of those with childhood absence epilepsy go on to develop more serious convulsive-type seizures. Also, the effect of repetitive absence seizures on psychosocial and cognitive development has not been well established. The development of appropriate animal models of absence epilepsy may lead to answers for some of these questions.

Treatment and Prognosis

Over the past three decades, the drugs of choice for treating absence epilepsy have been ethosuximide and sodium valproate. It appears as if ethosuximide exerts its inhibition of seizures by blocking low-threshold T-type Ca^{++} channels within the thalamus. Isolated nRT and thalamocortical neurons have demonstrated a depression of the amplification of the T-type calcium current upon treatment with ethosuximide (25). The mechanisms by which valproate suppresses absence seizures is less clear. It has been shown to increase GABA levels by inhibiting its metabolism and increasing its synthesis (26). Since this effect should increase rather than decrease seizure activity, the main anti-absence action of valproate seems to consist of its inhibition of voltage-gated Na^{+} channels (27).

While the majority of children with uncomplicated absence epilepsy have a favorable prognosis, the long term effects associated with the disorder have been debated. Total remission of absence seizures upon adolescence or adulthood is the normal outcome for many children, but it has been found that about 40% of

absence epilepsies can progress to more damaging, lifelong seizures such as generalized tonic-clonic seizures (28). In addition, generalized tonic-clonic seizures may be present in 75-90% of patients with a history of childhood absence seizures that persisted into adulthood (29-31).

The most common negative outcome of absence seizures is an increased risk of accidental injury (32). This is rather intuitive given the behavioral effect of the seizures but less clear is the reason why the increased incidence of accidents persists after the start of antiepileptic drug treatment. While studies have concluded that absence seizures result in no long term cellular damage, repetitive absence seizures have been shown to interfere with social and intellectual development during childhood (33-35). In a study comparing children with juvenile rheumatoid arthritis and childhood absence epilepsy, it was found that those with absence seizures had greater difficulties in the academic/personal and behavioral categories (34). These difficulties were considerably worse when seizures did not remit. It has also been reported that children with absence epilepsy have lower intelligent quotient (IQ) scores and decreased performance on general cognitive functioning and visuospatial tests than age matched controls (36). These studies highlight the fact that absence seizures may not have a completely benign outcome. Careful developmental studies of cognitive and psychosocial functioning in an animal model of absence seizures would provide a useful way of assessing the long-term effects of repetitive absence seizures.

Animal Models of Absence Epilepsy

Overview

Animal models of absence seizures exist and have been shown to possess EEG and behavioral findings similar to the human condition - attenuation with drugs used to treat absences, and SWDs that originate in the cortex, thalamus, or both (37). The desirable prerequisites of an animal model of absence seizures have been determined and include: (1) EEG and behavioral profiles similar to the human condition, (2) easy reproducibility, (3) predictability of effects and time course, (4) a similar pharmacologic response to drugs used for treatment in a clinical setting, (5) a developmental course similar to the human condition, and (6) exacerbation of the experimental seizure by GABAergic agonists (38-39). All the animal models discussed in this thesis have previously been shown to fulfill these criteria.

The first and best studied animal model of generalized absence seizures is the feline penicillin model. This resulted from observations that large intramuscular doses of penicillin could induce generalized SWDs in the cat, along with behavioral changes that seemed to mimic human absence seizures (40). More recently, other animal models, both pharmacologic and genetic, have been developed and found to meet the criteria for absence seizures. The pharmacologic models include low dose pentylenetetrazole and γ-hydroxybutyric acid (GHB) in the rat and monkey. Genetic models have included the genetic

absence epilepsy rat of Strasbourg (GAERS) and the WAG/Rij strain of rats. This thesis utilizes the GHB rat and monkey models as well as the WAG/Rij rat strain, as animal models of absence seizures.

GBL Rat Model

GHB was first synthesized in 1960 and its first use was as an anesthetic drug (41). In the 1970s GHB was found to be useful as a treatment for narcolepsy (42). In the 1990s it was manufactured and advertised as a dietary supplement. More recently, GHB has been found to have addictive properties and has become popular as a club drug and date rape drug (43). As a result of these illicit uses, the Food and Drug Administration banned the sale of non-prescription GHB in the 1990s and in 2000 it was classified and regulated as a Schedule I drug (44).

In addition to its uses listed above, GHB has been widely used as an experimental animal model of absence seizures for more than 30 years. GHB is a short-chain fatty acid that occurs naturally in the mammalian brain (45). The primary precursor of GHB in the brain is GABA and is formed by the conversion of GABA-derived succinic semialdehyde through the action of the succinic semialdehyde reductase (Figure 2) (46). GHB has properties that suggest it may play a role as a neurotransmitter although its precise function is not known. An endogenous GHB receptor has been found throughout the brain of mice, rats, monkeys, and humans with the greatest densities in the hippocampus, cortex,

and thalamus (47). Many of the effects of exogenously administered GHB seem to be a result of its interaction with $GABA_B$ receptors, either directly as a partial agonist or indirectly through a conversion of GHB to GABA (42,45). It has also been proposed that GHB activates presynaptic GHB receptors which in turn modulate GABA release through an interaction with the $GABA_B$ receptor (48). Therefore, while the exact mechanism of action of endogenous or exogenous GHB has not been established, the GHB and $GABA_B$ receptors seem to play an important role.

Normal mice, rats, cats, and monkeys given an injection of GHB will show all the behavioral and electrophysiological signs of generalized absence seizure (20). The EEG effect of GHB has been shown to be dose-dependant with 7-11 Hz SWD discharges at low dose and burst suppression patterns at higher doses (39). GHB-induced seizures have been found to be treatable with clinical anti-absence medications such as ethosuximide and valproate (49-50). In addition, the seizures are exacerbated by both $GABA_A$ and $GABA_B$ receptor agonists (51). GHB and $GABA_B$ receptor antagonists have been found to block the seizures, suggesting an interaction between these two receptors (52).

While the mechanism by which GHB causes absence seizures is unknown, three hypotheses have been proposed. First, some exogenous GHB might be converted to GABA which would then stimulate the $GABA_B$ receptor (45). Second, GHB has been found to alter the release of GABA and glutamate within the thalamus and cortex, which could shift the balance between inhibition

and excitation within the thalamocortical circuitry (48). Lastly, GHB has been found to affect the intracellular movements of the $GABA_B$ receptor which could result in an increase in the number of $GABA_B$ receptors on the cell surface of neurons (42).

It was discovered that gamma-butyrolactone (GBL), the precursor molecule to GHB, can induce the SWDs of absence seizures with better reproducibility, predictability, and rapidity of onset than GHB itself (53). GBL has no activity in the brain itself so it must first be converted to GHB to produce its effects (Figure 2). GBL is transformed to GHB in the peripheral blood by a lactonase enzyme (54). Whereas, it might take up to 20 min after intraperitoneal (i.p.) injection of GHB to induce absence seizures, GBL can produce bilaterally synchronous SWDs within 2-5 minutes of its peripheral administration along with behavioral arrest, facial myoclonus, and vibrissal twitching (37).

A few studies have looked at which brain structures are responsible for producing the SWDs induced by GHB or GBL. The thalamocortical system seems to be integral to GHB-induced seizures, since intrathalamic microinjection of GHB results in SWDs in both the thalamus and cortex (55). Electrophysiology studies have focused on measuring neuronal activity in the thalamus and cortex. Synchronized bursting activity from recording electrodes in the somatosensory, ventrobasal thalamic areas (i.e., ventral posteromedial thalamus and ventral posterolateral thalamus), nRT, and frontoparietal cortex has been demonstrated in rats treated with GHB (56). Specifically within the cortex, SWDs have been

Figure 2

GABA

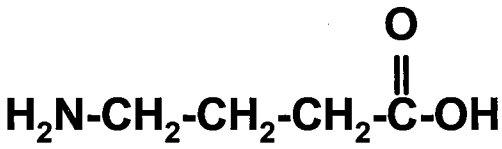

GHB

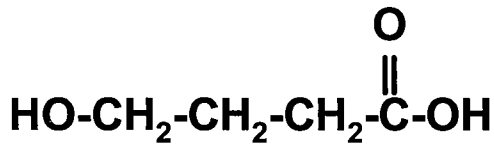

GBL

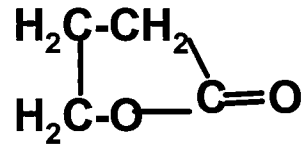

Figure 2. Chemical structures of GABA, GHB, and GBL. The structures of these three compounds are closely related. The precursor molecule, GBL, has its ring structure broken by a peripheral lactonase enzyme to form the active compound, GHB. Endogenous GHB and GABA are part of the same biosynthetic pathway in the mammalian brain.

measured within the superficial layers (I-IV) of the frontoparietal cortex.

WAG/Rij Model

Genetic rat models of absence epilepsy have been studied for many years and are thought to more accurately mimic the spontaneous seizures of human epilepsy than drug-induced animal models. The strain of rats named WAG/Rij (Wistar Albino Glaxo strain bred in Rijswijk, Netherlands) have been inbred for absence-like characteristics for more than 100 generations and are essentially homozygous for the trait (57-58). This strain exhibits spontaneous SWDs that have a frequency of 7-11 Hz, duration of 1-45 seconds, and amplitude of 200-1000 μV (59). As in the human condition, EEG changes are accompanied by immobile behavior and staring. Age related changes in the number of SWDs are reported. At an age of 75 days, only 17% of rats experience a single SWD in a four hour period, compared to 140 and 245 days where SWDs affected 83% and 100% of rats, respectively (60). This age-dependent increase in seizures has been seen in all genetic animal models of absence epilepsy. Sex differences have been found to be minimal (61).

In order to further validate the WAG/Rij strain as a model of absence epilepsy, its response to anti-epileptic medications has been assessed. Only the classical anti-absence drugs, such as ethosuximide and valproate, were found to decrease the number of SWDs (62). In addition, behavioral and reproductive characteristics of WAG/Rij rats have been studied extensively and found to be

very similar to those of the outbred, non-epileptic, Wistar rat strain, with which they have been compared (63-64). Therefore, other than spontaneous SWDs this strain appears to be behaviorally and reproductively normal.

Electrophysiological studies in genetic rodent models have helped identify key areas in the thalamus and cortex involved in absence seizures. Using the genetic rat model, GAERS, it was reported that the generation of SWDs are associated with concurrent multiunit activity in the ventral posteromedial and ventral posterolateral thalamus, layers IV/V of the somatosensory cortex, and the reticular thalamic nucleus (65). The onset of SWDs correlated with activity in somatosensory cortex followed by burst-like, rhythmic firing in thalamic nuclei. Lesioning the reticular thalamic nucleus in the GAERS abolishes SWDs underscoring the significance of this subcortical site in the pathogenesis of absence seizures (66). Indeed, the reticular thalamic nucleus has a high density of GABAergic neurons whose connections to other thalamic areas are critical in organizing the rhythmic bursting pattern characteristic of SWDs (67).

The genetic WAG/Rij rat model of absence seizure has been used to study the coordinated electrical field activity between thalamic and cortical sites using multielectrode recordings (68). Spontaneous SWDs were associated first with activity in the peri-oral region of the somatosensory cortex followed by cortical propagation and then thalamic activation. This finding suggests the somatosensory cortex may be the dominant factor initiating the oscillation between cortico-thalamic networks responsible for SWDs in absence seizures.

Non-Human Primate Model

Non-human primate models of generalized epilepsy have been used for many years to study convulsive seizures (69-73). A few studies have demonstrated that non-human primates mimic the behavior and characteristic EEG of childhood absence epilepsy, producing SWDs with a frequency of 3 Hz (74-75). Since rodent models of absence seizures produce SWDs of 7-11 Hz, the non-human primates are better suited to study the pathophysiology of the disorder. The behavior of monkeys given GHB is reported to be similar to that of humans during absence seizures with staring, immobility, and pupillary dilation. The behavioral and EEG changes experienced by monkeys that receive GHB can be reversed by oral or intravenous pretreatment with the anti-epileptics used to clinically treat absence seizures (49,76).

The common marmoset (*Callithrix jacchus*) monkey is a useful animal model for human research that displays fascinating behavioral and biological traits. Marmosets have an affiliative family structure similar to humans in which mother, father, and related siblings live together as a unit. Marmosets are also monogamous and usually pair-bond for life. In addition, they routinely give birth to dizygotic twins which improve experiment design. Marmoset development has a short time course in which the time from early childhood to early adulthood is approximately 20 months (77). This time course allows for easy developmental studies. In terms of imaging marmosets, their adult size (300-450 grams) is small meaning that they can easily fit into the small bore of a high field magnet.

This makes it possible to study developmental brain changes in the marmosets, over the course of their lives.

Imaging Human Absence Seizures with Multiple Techniques

Imaging studies of absence seizures can provide insight into their pathogenesis, but few research studies have been done in humans and fewer studies have been completed using animal models. Single photon emission computed tomography (SPECT) studies of children with absence epilepsy have shown that there is an overall increase in brain blood flow during seizure activity, but no local variations were detected (78). Some studies have been able to monitor blood flow during seizure activity using Doppler flow techniques. These methods provide acquisitions fast enough to determine changes associated with the seizure, but have poor spatial resolution so that structures involved cannot be identified. Doppler studies in humans have demonstrated that mean blood flow velocity increases a few seconds before clinical or EEG evidence of seizure activity is manifested and then rapidly decreases (79). A genetic rat model of absence epilepsy has also been studied with Doppler flow and it was found that during spontaneous absences the cerebral blood flow decreases when compared to the interictal period (80). Positron emission tomography (PET) studies have also been done which provide better spatial resolution but lack the temporal resolution to track rapid blood flow changes occurring during the seizure. The metabolic rate for glucose metabolism was studied with PET and it was found

that it increases by 2-3 times during the ictal period (81). PET studies have also provided contradictory results to the Doppler studies above by showing that there is an increase in global blood flow and an additional 4-8% increase in thalamic blood flow during absence seizure activity (82).

The utilization of BOLD fMRI to study absence seizures in animals has never been reported, however it has recently been used to investigate generalized absence seizures in humans. One study was a case report of a single patient experiencing absence seizures in the scanner (83). The thalamus showed bilateral increases in BOLD signal intensity, while there was a predominance of negative BOLD over most of the cortex. A second study employed spike triggered fMRI to study BOLD activation during SWDs in five humans (84). Based on group analysis, positive BOLD signal was found within the pre-central sulcus, while negative BOLD was found within the posterior cingulate cortex.

Principles of fMRI

The BOLD Technique

[A discussion of the principles of MRI physics can be found in Appendix I]. Functional magnetic resonance imaging (fMRI) is a technique which is sensitive to the oxygenation status of hemoglobin and therefore produces images that reflect changes in cerebral blood flow and volume (85-89). Increased neuronal

activity is accompanied by a regional increase in metabolism followed by a large change in cerebral blood flow which over compensates for the increase in oxygen consumption (Figure 3). The signal intensity changes related to blood oxygenation in regions close to blood vessels have been termed blood oxygenation-level-dependent (BOLD) contrast (87). The underlying mechanism of this technique is the paramagnetic contrast agent-like activity of deoxy-hemoglobin and the magnetic susceptibility effect it causes. Since deoxy-hemoglobin is paramagnetic it perturbs the local magnetic field into which it is placed and results in a shortening of the T_2^* parameter. Therefore, following neuronal activity, an *increase* in the level of blood oxygenation occurs which is associated with a *decrease* in the concentration of deoxy-hemoglobin and an *increase* in the MRI signal. When looking at a T_2^* contrast map this increased signal is reflected as positive BOLD.

It has been shown that activation maps produced using BOLD imaging correlate with the spatial location of synaptic activity (90). Therefore, changes in the status of oxygenation in the brain and blood flow correlate with brain activity in the region of interest. In addition, the fMRI BOLD signal has been shown to detect cerebral blood flow changes that occur during the ictal and interictal period in both humans and animal models of generalized and temporal lobe epilepsies (91-93). This imaging technique provides the necessary temporal and spatial resolution to detect BOLD signal caused by the seizure and correlate it with the brain area associated with the change.

Figure 3

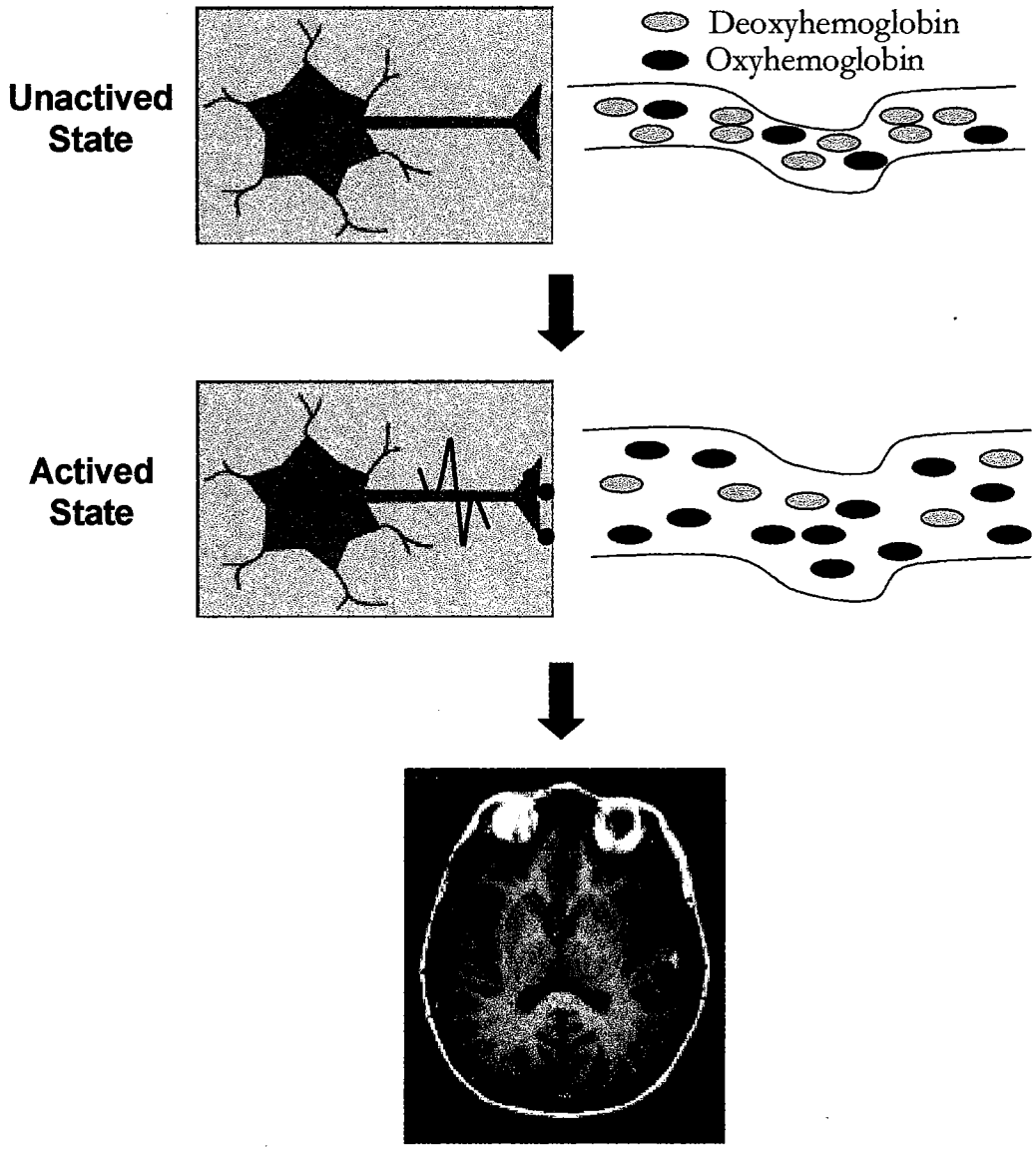
Unactived State
Deoxyhemoglobin
Oxyhemoglobin
Actived State

Figure 3. The basics of functional MRI. The unactivated state of neurons and cerebral vasculature is shown (top). This is compared with the activated state in which neurons have electrical discharges and, subsequently, the vasculature experiences an increased cerebral blood flow and volume (middle). Since there is an overcompensation of blood flow for the degree of metabolism, a decrease in the concentration of deoxyhemoglobin occurs. Since deoxyhemoglobin is a paramagnetic substance and perturbs the relaxation rate of protons, any change in its concentration causes a change in the local BOLD signal of the tissue (bottom). fMRI image is courtesy of the Oxford Centre for fMRI Research of the Brain.

Combining Electrophysiology with Functional MRI

Since electrical recordings of brain activity are the "gold standard" for identifying and characterizing seizure activity it is critical that EEG is included in fMRI studies of absence seizures. fMRI recorded along with EEG provides a method for localizing and identifying the neural structures responsible for electrical signals associated with seizures. However, concurrent acquisition of EEG and fMRI has proven challenging (94-97). When EEG leads are placed inside the magnet, the RF pulses required for MRI can induce large voltages that obscure the small EEG signal. In addition, introduction of EEG equipment into the scanner can disturb the homogeneity of the magnetic field and distort the MR images (98). One method used to overcome these difficulties in epilepsy studies has been to monitor the EEG in the absence of scanning, by using either spike-triggered fMRI techniques or interleaved EEG and fMRI methods (99-100). Both of these techniques have been utilized in the current thesis. In order to reduce artifacts on the EEG, the signal can be transmitted outside the magnetic field fiber-optically. In addition, in order to reduce EEG-related artifacts on the MR images several methods are employed. Non-magnetic electrodes, that do not create artifact, can be used for recording. Also, battery-operated recording devices can be used to reduce the amount of electrical current within the magnetic field (98,101-102).

Spike-Triggered BOLD fMRI

The ability to detect BOLD signal changes that correlate with spontaneous epileptiform activity is possible with the use of EEG-triggered fMRI (103-107). This technique essentially consists of continuously monitoring the EEG of a subject in the magnet, with the operator manually triggering image acquisition upon identifying seizure-related EEG changes (93,103,108-110). This procedure is possible due to the delay that exists between electrical neuronal activity and the associated hemodynamic changes (Figure 4). It has been shown that after brief neuronal activation, BOLD signal changes start to increase after approximately 2 seconds, peak after 4-7 seconds, and slowly return to baseline over 10 to 30 seconds (111). One study using EEG-triggered fMRI in patients during interictal epileptiform activity found that BOLD signal changes correlated with the spatial location of discharges seen with EEG (103). Another issue concerning EEG-triggered fMRI is the number of spikes necessary to produce significant fMRI activation. It has been shown that single spikes (occurring as briefly as 100 ms) can be associated with regional changes of cerebral hemodynamics and are detectable as a BOLD signal (105). Spike-triggered fMRI is a technique used to study the spontaneous seizures of WAG/Rij rats in the current thesis.

Figure 4

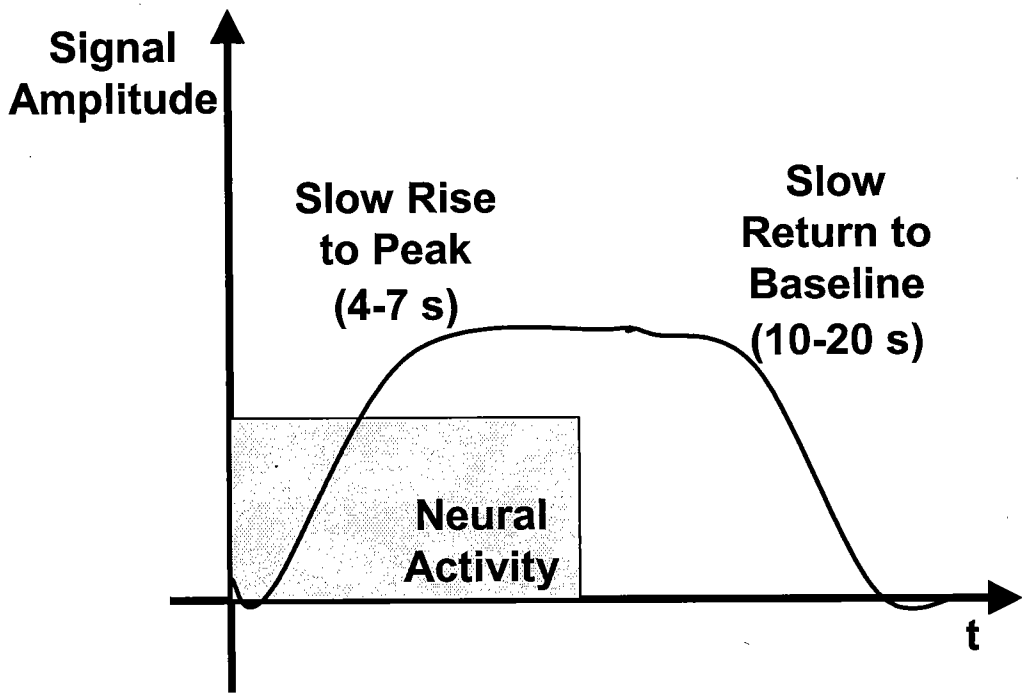
Signal
Amplitude
Slow Rise
to Peak
(4-7 s)
Slow
Return to
Baseline
(10-20 s)
Neural
Activity
t

Figure 4. The hemodynamic delay following neuronal activity. This delay accounts for the long time course of the BOLD signal (black line) compared with the fast activity of neurons (blue box). This hemodynamic delay is the reason that spike-triggered fMRI is possible and BOLD activation can be detected after an EEG change has occurred.

Functional Imaging of Awake Animals

While most fMRI work has been completed on humans and anesthetized animals, there have been a few fMRI studies in awake, restrained animals (112-124). fMRI of fully conscious animals offers many distinct advantages. First, the unwanted effects of anesthesia can be avoided. Second, general neural activity is not suppressed, which potentially yields increased fMRI signal changes and, thus, improved functional detection (120,122-124). Finally and most importantly, subcortical and higher order cognitive functions can be studied in the conscious model (118-119). Such studies would be very difficult if not impossible with anesthetized preparations.

Performing MRI experiments on awake rats is possible due to a MRI-compatible restrainer with built-in radiofrequency electronics (Figure 5). This dual coil design consists of a volume coil which is used to send the RF signal for enhanced homogeneity and a surface coil, placed over the head, which is used to receive the RF signal for increased signal-to-noise (125). These electronic components necessary for imaging are built into a plastic restraint device. A conscious animal can be immobilized by using a Plexiglas body tube and head restrainer. This restrainer has a mouth piece, nose bar, and position screws to keep the head immobile.

Figure 5

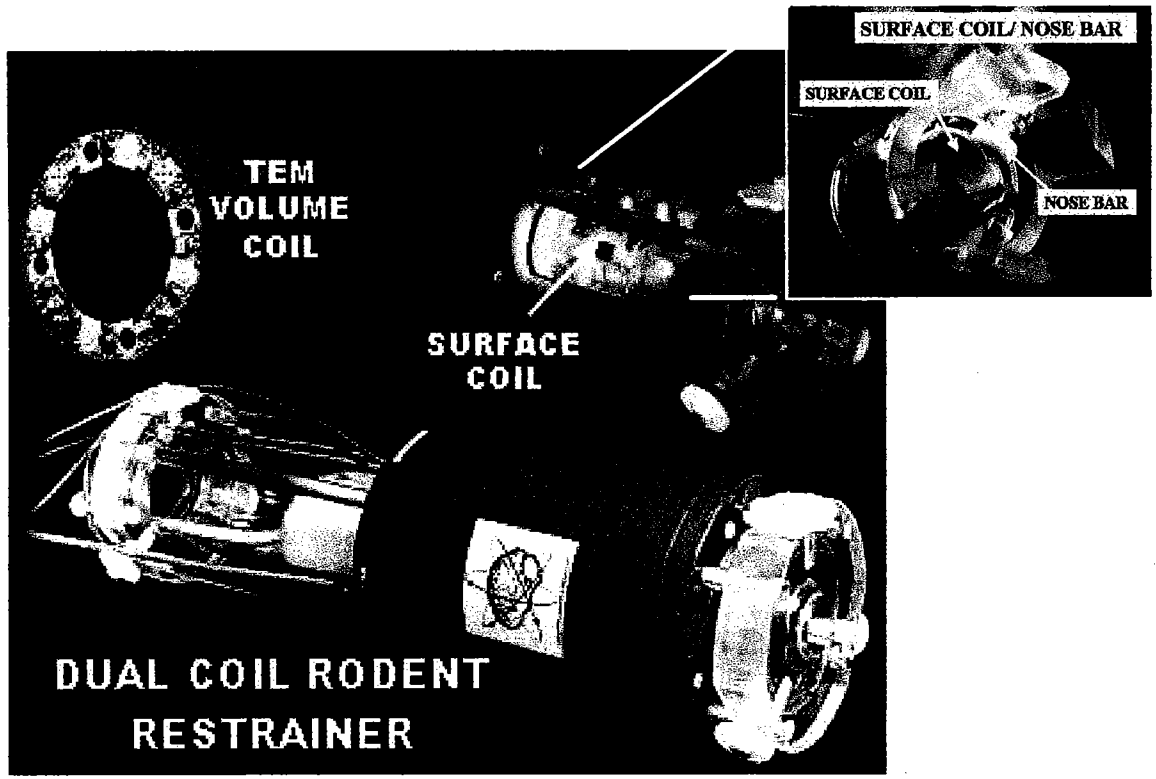
SURFACE COIL/ NOSE BAR
SURFACE COIL
NOSE BAR
TEM
VOLUME
COIL
SURFACE
COIL
DUAL COIL RODENT
RESTRAINER

Figure 5. Restrainer with built-in RF coils for MRI studies of awake animals. The apparatus consists of body. Head, and shoulder restrainers as well as ear, nose, and tooth bars to keep the animal immobilized. The RF coils consist of a large volume coil for transmitting signal and a surface coil, near the head, which receives the signal.

Objectives, Aims, Rationale, and Results

Current Objectives and Long-Term Goals

The long-term goal of this thesis is to study the psychosocial, cognitive and neurobiological consequences of childhood absence seizures. Since these goals cannot be met with a prospective study using humans they must be done in a relevant animal model. Yet monkeys do not have spontaneous absence seizures and can only be induced to seize with GBL. Would a GBL-induced seizure model be physiologically relevant? The genetic WAG/Rij rat has been adopted by researchers as being more relevant than the GBL rat model because the seizures are spontaneous and mimic the human clinical condition better. If these two rat models are determined to be the same in behavior, electrophysiology, and fMRI activation around the corticothalamic circuit then the use of the GBL drug to induce seizures in monkeys would be warranted. If it could be demonstrated that the monkey EEG during seizure accurately mimics that of humans then a relevant and useful animal model for studying the cognitive and psychosocial effects of absence epilepsy would be established.

Absence epilepsy is a disorder that primarily afflicts school-age children and adolescents. Much electrophysiology work has been done to try and determine the brain mechanisms underlying the generation and propagation of the seizures. While these studies have helped to determine that a malfunction of some part of the corticothalamic circuit seems to be present, the

electrophysiology techniques have limitations. It has been difficult to assess the global functioning of the entire brain during an absence seizure.

As absence seizures affect children during critical periods of development it is important to assess the effect of these seizures on cognitive and psychosocial functioning. Few studies have looked at the long-term effects of repetitive absence seizures during the developmental period. The few studies which exist seem to indicate that children with absence epilepsy have decreased academic performance and behavioral functioning.

A critical step in addressing the issues above is the development of an animal model of absence epilepsy which closely mimics the human condition. In addition, if this model can be used for functional imaging it may be possible to increase our understanding of the brain mechanisms which underlie the disorder. *The overall objective of this dissertation is to develop an animal model of absence epilepsy which closely mimics the EEG and behavior of humans and can subsequently be used to study corticothalamic activity with fMRI and assess the long term cognitive and psychosocial effects of the disorder.* Three specific aims are used to address this goal.

Specific Aim #1 (Chapter 2)

Development and fMRI of a Drug-Induced Rat Model of Absence Epilepsy

Rationale/Objectives for Aim #1

Drug-induced absence seizures can be elicited by administration of GBL to rats. Bench-top studies were necessary to assess the behavioral and EEG effects of various doses of GBL in order to establish the time course of seizure activity. Functional MRI paradigms for assessing corticothalamic activity during seizures were devised and SWDs were correlated with images in order to determine what brain areas experienced the greatest BOLD signal changes.

Summary of Results for Aim #1

GBL administration in rats, at a dose of 200 mg/kg, caused seizures that produced absence-like behaviors that were concurrent with 7-11 Hz SWDs. fMRI following GBL administration resulted in positive BOLD signal changes, bilaterally, in the cortex and throughout nuclei of the thalamus. Negative BOLD signal was also found symmetrically throughout the cortex.

Specific Aim #2 (Chapter 3)

fMRI of Spontaneous Absence Seizures in a Genetic Rat Model

Rationale/Objectives for Aim #2

While drug-induced seizures produce behaviors and EEG that mimic absence epilepsy, an animal having spontaneous seizures would be a better model for the human condition. The inbred rat strain, WAG/Rij, experience age-dependent spontaneous SWDs with absence-like behaviors. Bench-top studies were necessary to determine the most appropriate age of rats to use in order to maximize the number of seizures experienced within an imaging session. An

EEG-triggered fMRI technique was used to assess BOLD signal changes that occurred during spontaneous absence seizures. Activation maps were compared to that of the drug-induced seizure to determine similarities and differences.

Summary of Results for Aim #2

WAG/Rij rats experienced spontaneous seizures, with SWDs of 7-11 Hz, at an average rate of 5-6 per hour and an average duration of 8 seconds, which was appropriate for fMRI studies. EEG-triggered fMRI was reliably able to detect BOLD signal changes associated with spontaneous absence seizures. Positive BOLD signal occurred throughout the cortex and within several thalamic nuclei. Negative BOLD signal was not found to be correlated with these spontaneous seizures.

Specific Aim #3 (Chapter 4)

Development and fMRI of a Drug-Induced Monkey Model of Absence Epilepsy

Rationale/Objectives for Aim #3

Drug-induced absence seizures, by GBL administration, in non-human primates has previously been shown to produce SWDs of the same frequency and character of those on human EEG recordings. It was necessary to determine if the common marmoset, a small new world monkey, given GBL, would also produce a 3 Hz SWD. The behavioral, EEG, and pharmacological similarities of this seizure to human epilepsy condition was determined. The time

courses of SWD formation and behavioral changes were determined in order to complete functional MRI studies. BOLD activation maps of these non-human primates could then be compared to those of the two previous rat models.

Summary of Results for Aim #3

It was found that GBL induced absence-like behaviors in marmosets were correlated with SWDs of a frequency ranging from 2.5-3.5 Hz. These EEG changes, which mimic the human condition, were found to correlate with positive BOLD signal heterogeneously throughout the brain. Positive BOLD signal was found primarily with the cortex, thalamus, and hippocampus.

CHAPTER II

Development of a GBL Rat Model for fMRI

Summary

Functional MRI was used to identify areas of brain activation during absence seizures in an awake animal model. BOLD fMRI in the brain was measured using T_2*-weighted echo planar imaging at 4.7 Tesla. BOLD imaging was performed before, during, and after absence seizure induction using GBL (200 mg/kg, intraperitoneal). The cortico-thalamic circuitry, critical for SWD formation in absence seizure, showed robust BOLD signal changes after GBL administration, consistent with electroencephalographic recordings in the same animals. Predominantly positive BOLD changes occurred in the thalamus. Sensory and parietal cortices showed mixed positive and negative BOLD changes while temporal and motor cortices showed only negative BOLD changes. Using the BOLD fMRI technique, we have demonstrated signal changes in brain areas that have been shown, with electrophysiology experiments, to be important for generating and maintaining the SWDs that characterize absence seizures. These results corroborate previous findings from lesion and electrophysiological experiments and show the technical feasibility of non-invasively imaging absence seizures in fully conscious rodents.

Introduction

Gamma-hydroxybutyric acid (GHB) is a naturally occurring metabolite of the inhibitory neurotransmitter GABA. Normal rats given an i.p. injection of GHB show all the behavioral and electrophysiological signs of generalized absence seizure (20). Rats treated with GHB show synchronized bursting activity from recording electrodes in the somatosensory ventrobasal thalamic areas (i.e., ventral posteromedial thalamus and ventral posterolateral thalamus), reticular thalamic nucleus and frontoparietal cortex (56). Studies in the Genetic Absence Epilepsy Rats from Strasbourg (GAERS), report the generation of SWDs are associated with concurrent multiunit activity in the ventral posteriomedial and ventral posteriolateral thalamus, layers IV/V of the somatosensory cortex, and the reticular thalamic nucleus (21). The onset of SWDs correlate with activity in somatosensory cortex followed by burst-like, rhythmic firing in thalamic nuclei. Lesioning the reticular thalamic nucleus in the GAERS abolishes SWDs underscoring the significance of this subcortical site in the pathogenesis of absence seizures (126). Indeed, the reticular thalamic nucleus has a high density of GABAergic neurons whose connections to other thalamic areas are critical in organizing the rhythmic bursting pattern characteristic of SWDs (127).

In recent years, functional magnetic resonance imaging (fMRI) has come to the forefront as a powerful tool in neuroscience for non-invasive imaging of brain function. While many fMRI studies were confined to awake humans and

anesthetized animals, the technology was recently developed for imaging fully conscious animals (112-118,128). The use of fMRI in rodent models may facilitate the visualization of other functional neuroanatomical circuits involved in generalized absence seizures outside the cortico-thalamic circuit.

The present study was undertaken to examine the feasibility of using fMRI to study generalized absence seizure in rodent models. To this end, we chose to study the GHB model since it has a more predictable time-course than either of the genetic GAERS or WAG/Rij models. Moreover, it was discovered that GBL, the precursor molecule to GHB, can induce absence seizure with better reproducibility, predictability, and rapidity of onset than GHB itself (53). BOLD fMRI in the brain was measured using T_2*-weighted echo planar imaging at 4.7 Tesla. BOLD imaging was performed before, during, and after absence seizure induction using GBL. It was hypothesized that the ventral posteromedial and posterolateral thalamic nuclei, reticular thalamic nucleus and somatosensory cortex would show an increase in BOLD signal.

Materials and Methods

Animals

Male Sprague-Dawley rats weighing 200-300 grams were obtained from Charles River Laboratories (Charles River, MA). Animals were housed in pairs in Plexiglas cages (48 cm x 24 cm x 20 cm), maintained on 12:12 light:dark cycle

(lights on at 9:00 hr) and provided food and water *ad libitum*. All animals were acquired and cared for in accordance with the guidelines published in the *Guide for the Care and Use of Laboratory Animals* (National Institutes of Health Publications No. 85-23, Revised 1985).

Bench-top Studies

Prior to imaging, bench-top studies were run to characterize the dose/response effect of GBL on generalized absence seizures in both freely moving and restrained rats. Twelve rats were initially anesthetized with 2 mg ketamine (Ketaset, Fort Dodge Animal Health, Fort Dodge, IA) and 0.02 mg medetomidine (Domitor, Pfizer Animal Health, New York, NY). Epidural cortical electrodes were secured in the skull and connected to an EEG recorder using the Biopac system (BIOPAC Systems Inc., CA, USA). Animals were injected with 0.1 mg atipamezole (Antisedan, Pfizer Animal Health, New York, NY) to reverse the anesthesia and placed into an observation cage. EEG recordings were collected continuously from freely moving animals over the test period, during which four groups of three animals each were injected i.p. with GBL in doses of 50, 100, 200, or 400 mg/kg. Motor behavior was videotaped during the test period. The latency, pattern and duration of SWDs, and alterations in motor activity were measured for each dose to assess the reliability and reproducibility of GBL-induced seizure.

Following this dose/response study, three rats were observed for the seizure-inducing effects of the 200 mg/kg i.p. dose of GBL while secured in the restraining device used for functional imaging studies. These bench-top studies were important to test whether the stress of immobilization associated with imaging might alter the onset, time course, or EEG characteristics of GBL-induced seizure. The animal restrainer used for imaging consisted of a multiconcentric Plexiglas head and body holder with built-in radiofrequency dual coil electronics (Insight Neuroimaging Systems, LLC, Worcester MA). Animals were anesthetized with Domitor, fixed with epidural EEG electrodes, secured in the restrainer and awakened with Antiseden.

fMRI Studies

Prior to imaging studies, animals used for imaging were acclimated to the restrainer and the imaging protocol. Animals were lightly anesthetized with 2 % isoflurane and secured into the restrainer. When fully conscious, the restraining unit was placed into a black opaque tube that served as a "mock scanner" and a tape-recording of an MRI pulse sequence played for 90 minutes to simulate the bore of the magnet and an imaging protocol. This procedure was repeated every other day for three-four days. Previous work by our laboratory showed that this acclimation procedure in rats significantly reduces body temperature, motor movements, heart rate and plasma corticosterone levels by the third acclimation day (128).

Eight rats were anesthetized with Domitor and ketamine and implanted with an i.p. line for GBL injection, as described for the bench-top studies. A topical anesthetic of 2.5% lidocaine gel was applied to the skin of the scalp and MR compatible non-magnetic epidural EEG electrodes were fixed to the skull. In addition, lidocaine gel was applied to soft tissue around the ear canals and the bridge of the nose, as these are pressure points in the restrainer. A plastic semicircular headpiece with blunted ear supports that fits into the ear canals was positioned over the ears. The head was placed into a cylindrical head holder with the animal's canines secured over a bite bar and ears positioned inside the head holder with adjustable screws fitted into lateral sleeves. An adjustable surface coil built into the head holder was pressed firmly on the head and locked into place. The body of the animal was placed into a body restrainer. The body restrainer "floats" down the center of the chassis connecting at the front and rear end-plates and buffered by rubber gaskets. The head piece locks into a mounting post on the front of the chassis. This design isolates all of the body movement from the head restrainer and minimizes motion artifact. Once the animal was positioned in the body holder, a volume coil was slid over the head restrainer and locked into position. This procedure takes two to three minutes. Animals are usually fully conscious at the end of the set-up since Antisedan is administered at the point the animal is placed into the head holder, as in the bench-top studies described previously.

All images were acquired using a 4.7T/40-cm (Oxford magnet Technology, Oxford, UK) horizontal magnet interfaced to a Paravision console (Bruker Medical Instruments, MA, USA). High resolution anatomical data sets were acquired using a fast spin echo (RARE) sequence (TR=2.5s; TE=56ms; echo train length=8; field of view=3x3cm; data matrix=256x256; number of slices=4; slice thickness=1.0 mm) at the end of each imaging session. Functional images were acquired using a 2 segmented gradient echo planar imaging (EPI) sequence (TR=1000ms; TE=25ms; FOV=3x3cm; matrix=128x128; number of slices=4; slice thickness=1.0 mm).

EEG was recorded using nonmagnetic epidural electrodes, while the animal was in the magnet. The EEG signal was amplified inside the RF-shielded room using a battery-operated preamplifier and converted to a fiber-optic signal. This signal was passed outside the RF-shielded room and was converted back to an electrical signal before recording with MP100 hardware and analysis with MP100 Manager Software (BIOPAC Systems Inc., CA, USA). Similar setups have previously been used in human imaging experiments (98).

Functional imaging followed the experimental paradigm shown in Figure 6. A baseline set of images were acquired for 3 minutes, followed by an i.p. injection of 0.9% saline. EEG recordings were done for 2 minutes followed by image acquisition for 2 minutes. EEG was again recorded for 1 minute, followed by another image acquisition of 2 minutes. GBL was then administered and EEG

Figure 6

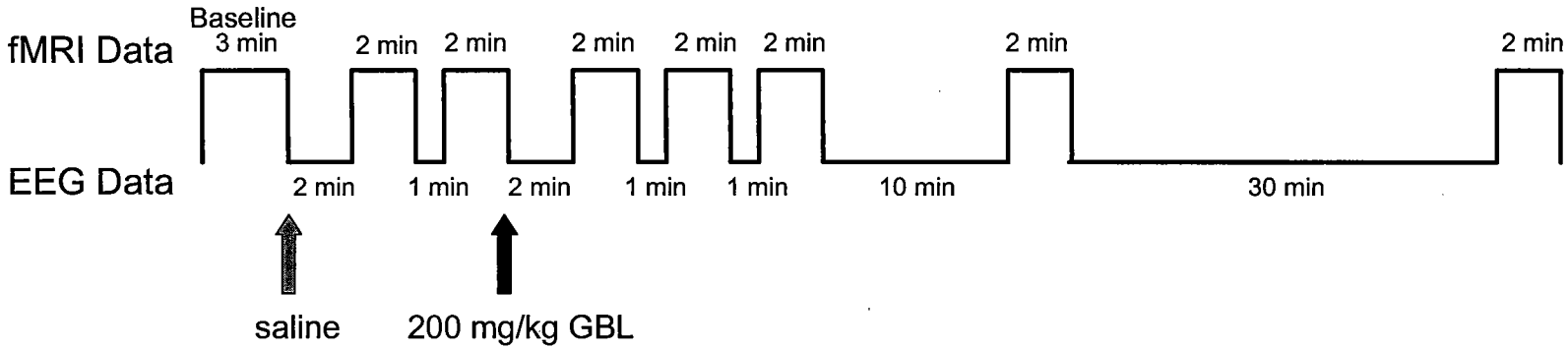
fMRI Data
EEG Data
Baseline
3 min
2 min
2 min
2 min
2 min
2 min
2 min
2 min
2 min
2 min
1 min
2 min
1 min
1 min
10 min
30 min
saline
200 mg/kg GBL

Figure 6. Experimental design used for functional imaging experiments. EEG data is collected during breaks in imaging because of the distortion caused by fMRI image acquisition.

was recorded for 2 minutes before starting image acquisition for 2 minutes. Scans were repeated four more times with wait times in between of 1 minute, 1 minute, 10 minutes, and 30 minutes, respectively. Cortical and thalamic regions of interest (ROI) were drawn manually on the images according to a rat brain atlas and analyzed for changes in BOLD signal intensity (10). STIMULATE software was used to perform statistical comparisons of control periods to absence seizure periods with the Student's paired t-test to generate an activation map of the ROIs for each dataset (129). The control imaging period was defined as the average value of the baseline data collected in the initial three minutes of the experiment. The absence seizure imaging period was defined as the average value of the time from the injection of GBL to the end of the experiment. The comparison for the t-tests, used to create activation maps, was the average of the baseline period and the average of the absence seizure period.

ROI analyses to calculate BOLD signal values and time course plots were based on the signal values averaged across the voxels in each respective region. These values were then averaged across all animals. Voxels whose BOLD percentage change, relative to the control period, was significant at a 95% confidence level were overlaid onto their respective anatomical data set. Activation maps are representative examples from one animal that have not been corrected for multiple comparisons.

Anesthetized vs. Awake Imaging Studies

Given the robust nature of the thalamocortical network in the initiation and maintenance of SWDs, we tested if it was possible to image changes in BOLD signal intensity in anesthetized animals treated with GBL. Three additional animals, under continuous 2% isoflurane anesthesia (Abbott Laboratories, IL, USA), were given 200 mg/kg GBL i.p. and imaged for changes in BOLD signal.

Results

Bench-top Studies

As expected, GBL produced dose dependent EEG and behavioral effects on rats. A dose of 50 mg/kg produced no observable change of the EEG or behavior. GBL at 100 mg/kg produced non-specific slowing of the EEG, followed by non-continuous SWDs (Figure 7). 200 mg/kg GBL resulted in the formation of continuous SWDs (Figure 8). The highest dose, 400 mg/kg, produced SWDs followed by a burst suppression pattern on EEG (Figure 9). GBL at 200 mg/kg was determined to be the lowest, most effective dose that produced clearly identifiable SWDs (Figure 10). All three animals treated with this dose showed onset of continuous SWDs within four minutes of injection, which persisted for almost two hours (Figure 11). The absence seizure was characterized by arrest of motor activity, vibrissal twitching, mild orofacial myoclonus, and impaired responsiveness concomitant with robust SWDs of approximately 7-8 Hz with

Figure 7

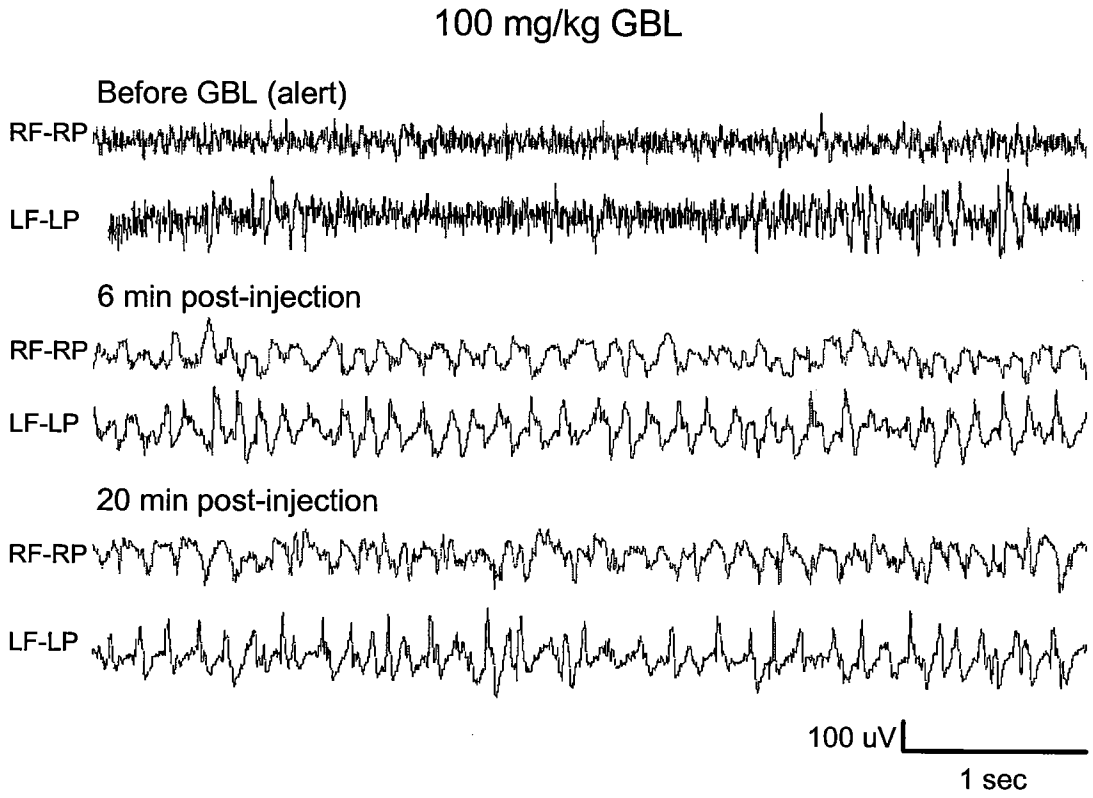
100 mg/kg GBL
Before GBL (alert)
RF-RP
LF-LP
6 min post-injection
RF-RP
LF-LP
20 min post-injection
RF-RP
LF-LP
100 uV
1 sec

Figure 7. EEG recording following injection of 100 mg/kg GBL. Epidural electrodes were placed in the frontal and parietal cortices in order to monitor seizure activity. Epochs corresponding to pre-injection, 6 minutes post-injection, and 20 minutes post-injection are shown. Placement of electrode leads is labeled. RF, right frontal cortex; RP, right parietal cortex; LF, left frontal cortex; LP, left parietal cortex.

Figure 8

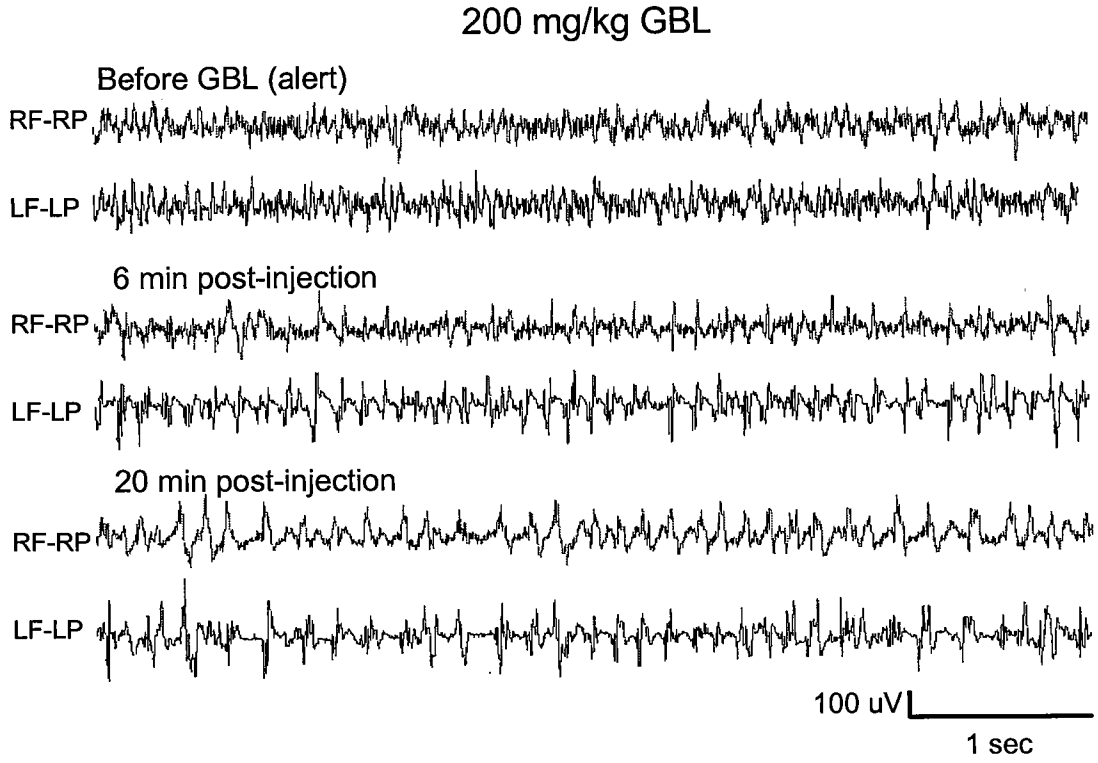
200 mg/kg GBL
Before GBL (alert)
RF-RP
LF-LP
6 min post-injection
RF-RP
LF-LP
20 min post-injection
RF-RP
LF-LP
100 uV
1 sec

Figure 8. EEG recording following injection of 200 mg/kg GBL. Epidural electrodes were placed in the frontal and parietal cortices in order to monitor seizure activity. Epochs corresponding to pre-injection, 6 minutes post-injection, and 20 minutes post-injection are shown. Placement of electrode leads is labeled. RF, right frontal cortex; RP, right parietal cortex; LF, left frontal cortex; LP, left parietal cortex.

Figure 9

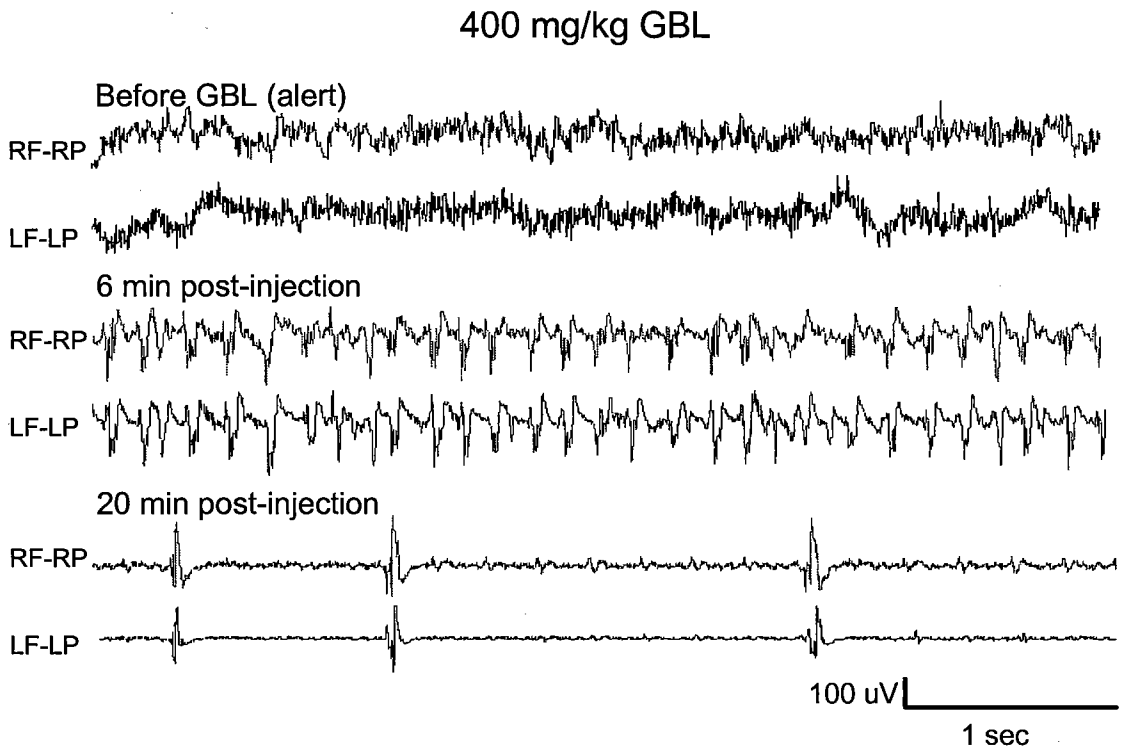
400 mg/kg GBL
Before GBL (alert)
RF-RP
LF-LP
6 min post-injection
RF-RP
LF-LP
20 min post-injection
RF-RP
LF-LP
100 uV
1 sec

Figure 9. EEG recording following injection of 400 mg/kg GBL. Epidural electrodes were placed in the frontal and parietal cortices in order to monitor seizure activity. Epochs corresponding to pre-injection, 6 minutes post-injection, and 20 minutes post-injection are shown. A burst-suppression pattern can be seen in the 20 minute epoch. Placement of electrode leads is labeled. RF, right frontal cortex; RP, right parietal cortex; LF, left frontal cortex; LP, left parietal cortex.

Figure 10

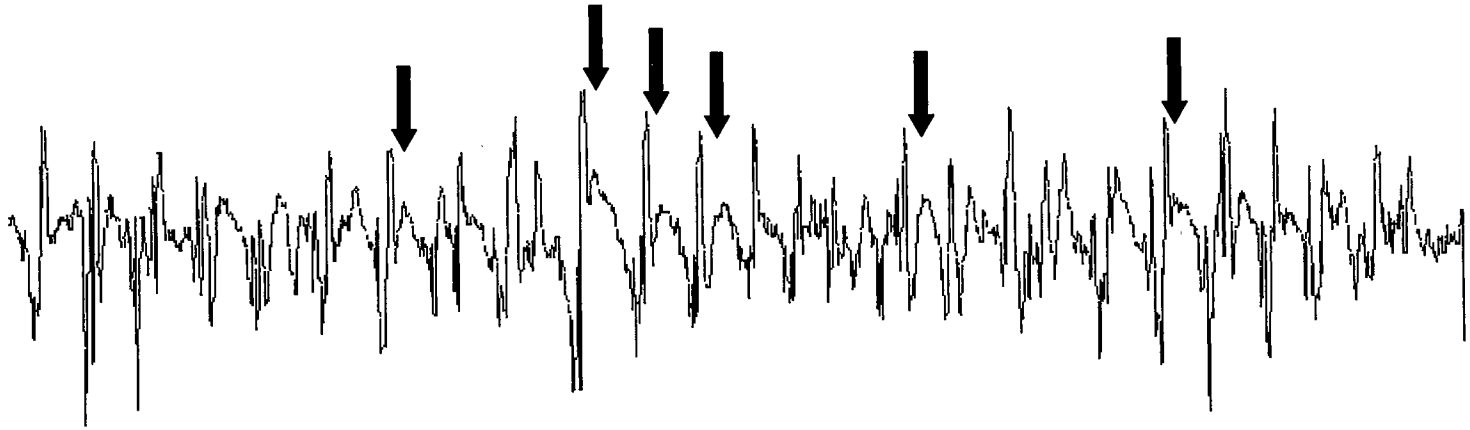

Figure 10. Expanded EEG showing SWD. A segment of the tracing following 200 mg/kg GBL is shown. Arrows indicate clear SWD formations.

Figure 11

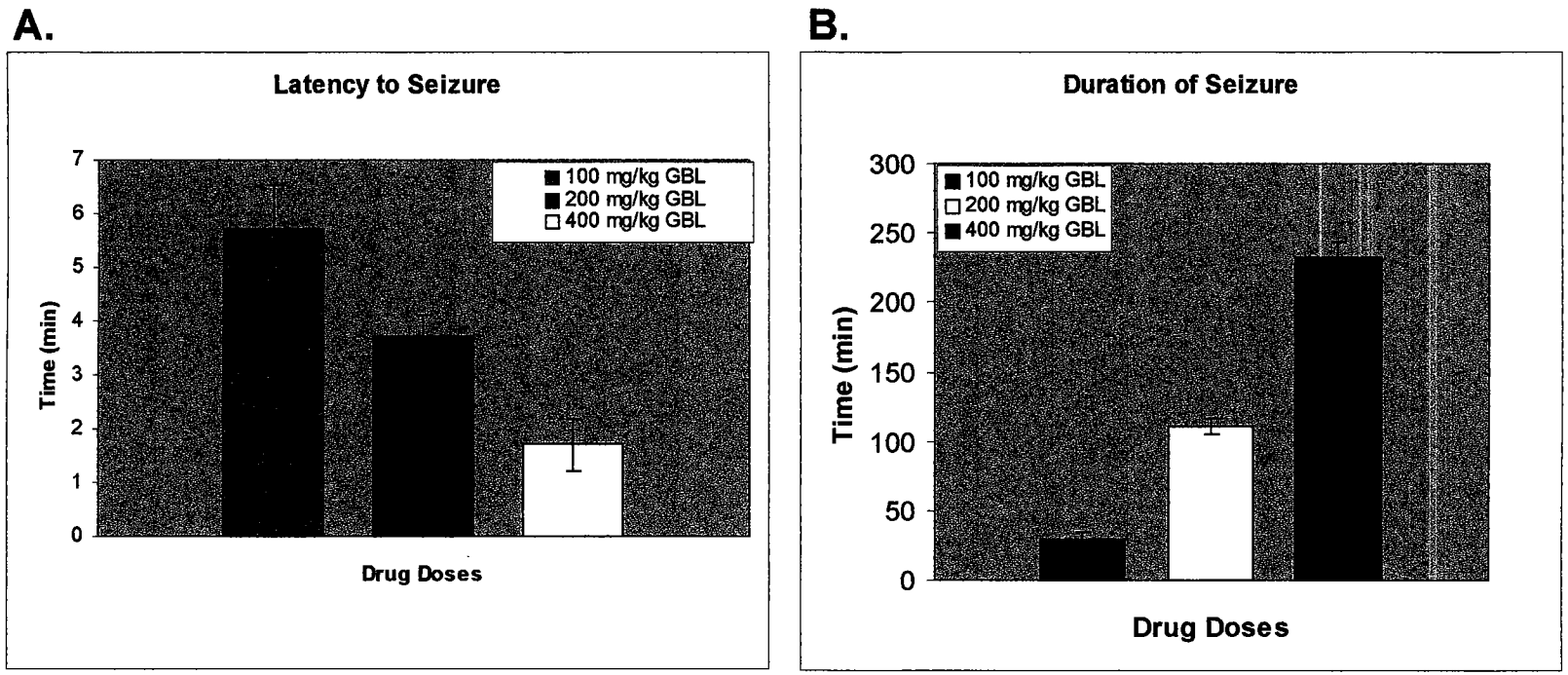
A.
Latency to Seizure
Time (min)
0
1
2
3
4
5
6
7
100 mg/kg GBL
200 mg/kg GBL
400 mg/kg GBL
Drug Doses
B.
Duration of Seizure
Time (min)
0
50
100
150
200
250
300
100 mg/kg GBL
200 mg/kg GBL
400 mg/kg GBL
Drug Doses

Figure 11. GBL-induced absence seizure characteristics. The average latency ± SEM, following GBL injection, to the start of SWD formation is shown for the doses measured (A). The average duration ± SEM of the GBL-induced SWDs is shown for each dose (B). The 50 mg/kg dose is not shown since it resulted in no EEG or behavioral changes.

amplitudes of 200-250 μV. At all doses, animals recovered to a normal EEG and no long-term alterations in behavior were noted. These behavioral and EEG data following i.p. GBL in this dose range, in freely moving rats, agrees with previously published studies (39). There were no differences in the onset, pattern and duration of GBL-induced SWDs between freely moving and restrained animals.

Anesthetized vs. Awake Imaging Studies

Figure 12 shows activation maps comparing changes in BOLD signal intensity in response to GBL with and without anesthesia. While SWDs were seen in both awake and anesthetized animals, isoflurane dramatically reduced BOLD signal changes precluding the use of this anesthetic in fMRI studies of GBL-induced seizures. This observation is consistent with the notion that anesthetics, in general, suppress synaptic activity (130-134). Therefore, all subsequent experiments were done on awake animals.

fMRI Studies

Over the course of each imaging session, EEG recordings were obtained between image acquisitions at the time intervals noted in Figure 6. Each of the eight animals studied showed GBL-induced bilateral SWDs, characteristic of absence seizures. A representative EEG tracing is shown in Figure 13. There were no EEG changes seen at any time point following the control injection of saline.

Figure 12

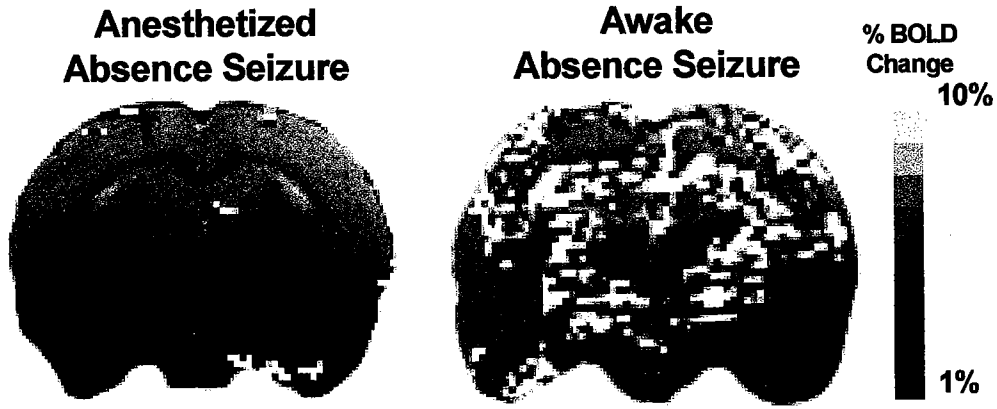
Anesthetized
Absence Seizure
Awake
Absence Seizure
% BOLD
Change
10%
1%

Figure 12. fMRI of drug-induced absence seizure in anesthetized versus conscious rats. The left side shows positive BOLD signal changes in an animal experiencing an absence seizure while continuously anesthetized with 2% isoflurane. The right side shows BOLD signal change in an animal experiencing an absence seizure, not anesthetized. The colored pixels indicate the statistically significant ($P<0.05$) pixels determined by t-test analysis and overlaid onto the corresponding anatomy (fast spin echo sequence). EPI image parameters were: TR=1000 ms; TE=25 ms; FOV=3 x 3 cm; matrix=128 x 128; slice thickness=1.0 mm and anatomical image parameters were: TR=2.5 s; TE=56 ms; echo train length=8; field of view= 3 x 3 cm; data matrix=256 x 256; slice thickness=1.0 mm. This a representative figure from a study with N=3.

Figure 13

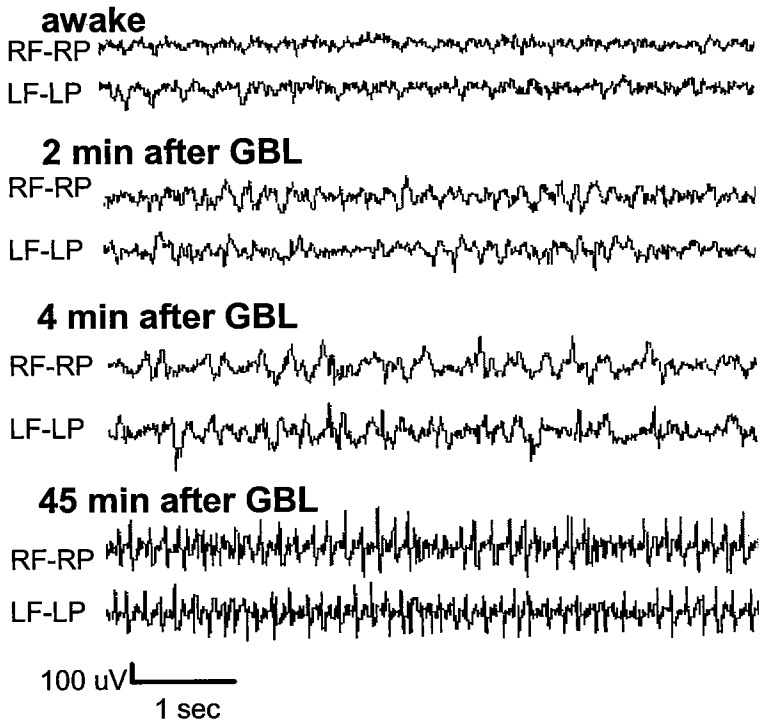
awake
RF-RP
LF-LP
2 min after GBL
RF-RP
LF-LP
4 min after GBL
RF-RP
LF-LP
45 min after GBL
RF-RP
LF-LP
100 uV
1 sec

Figure 13. EEG recording collected during the fMRI experiment. Nonmagnetic epidural electrodes were placed in the frontal and parietal cortices in order to monitor seizure activity during the imaging session. Placement of electrode leads is labeled. RF, right frontal cortex; RP, right parietal cortex; LF, left frontal cortex; LP, left parietal cortex.

Injection of GBL caused robust changes in BOLD signal intensity in the cortico-thalamic circuit. Representative activation maps of two consecutive brain slices together with delineations of representative thalamic and cortical ROIs are shown in Figure 14. The thalamic ROIs increased in the number of voxels with positive BOLD signal but there were few thalamic areas with negative BOLD signal in response to GBL. This is in sharp contrast to cortical ROIs which showed a preponderance of negative BOLD voxels during absence seizure. In addition, the sensory and parietal cortices have an increased number of voxels with positive BOLD signal.

Table 1 reports the group-average percent changes of positive and negative BOLD signal intensity for each of the ROIs (N=8 rats). Analysis of ROIs on left and right sides were initially analyzed separately and found to have statistically significant activations above baseline. Since all structures analyzed are bilateral and no significant differences were found between the left and right hemispheres, each rat included in the Table 1 analysis consists of a combination of both hemispheres. This was done because generalized SWDs are believed to be bilaterally synchronous and EEG showed SWDs in both hemispheres. In addition, for all significant positive BOLD changes, all eight animals experienced signal changes of at least 5%. All eight animals also experienced negative BOLD changes of at least 5% in the sensory and temporal cortices, while seven out of eight animals had signal changes of at least 5% in the motor and parietal cortices.

Figure 14

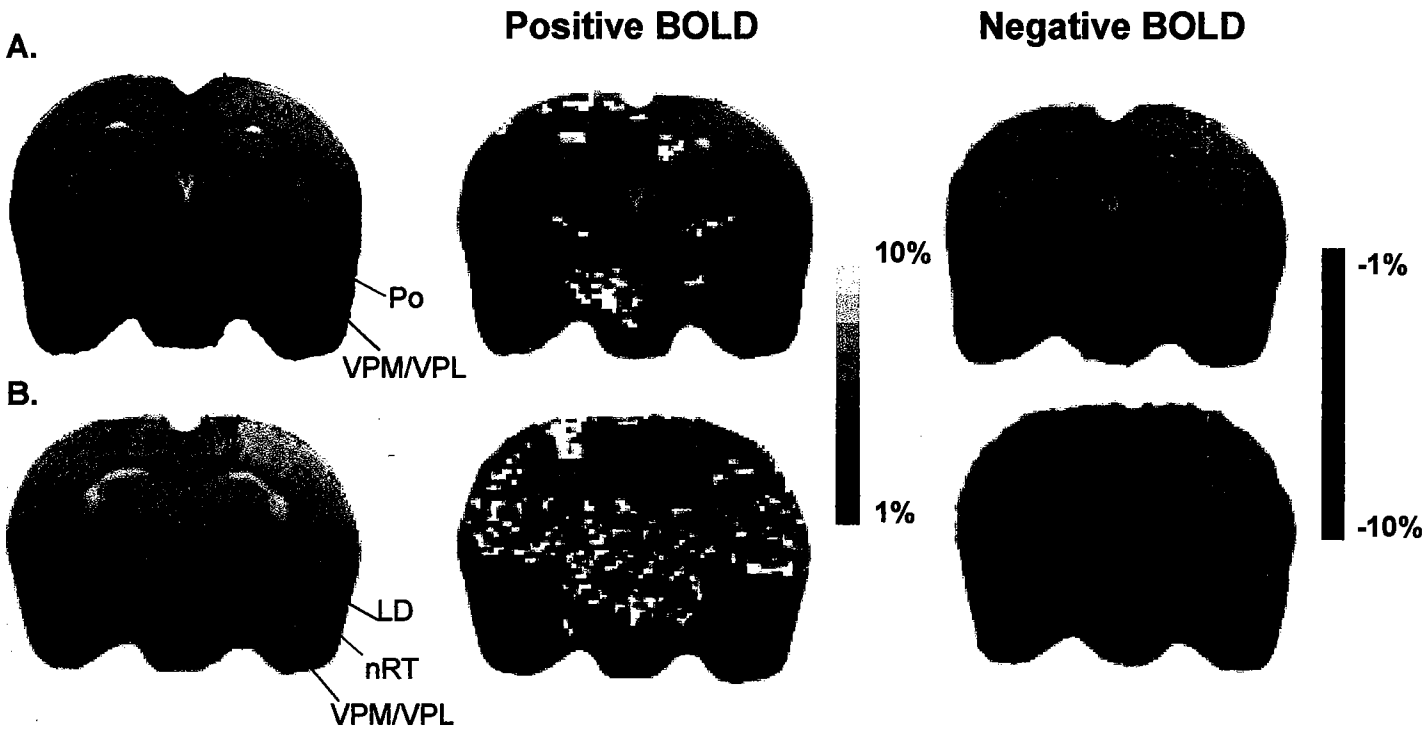
A.
Positive BOLD
Negative BOLD
Po
VPM/VPL
B.
LD
nRT
VPM/VPL
10%
1%
-1%
-10%

Figure 14. Activation maps of positive and negative BOLD signal responses during absence seizure. The colored pixels indicate the statistically significant ($P<0.05$) pixels determined by t-test analysis and overlaid onto the corresponding anatomy (fast spin echo sequence). (A) and (B) show BOLD activation maps for two consecutive slices through the brain. EPI image parameters were: TR=1000 ms; TE=25 ms; FOV=3 x 3 cm; matrix=128 x 128; slice thickness=1.0 mm and anatomical image parameters were: TR=2.5 s; TE=56 ms; echo train length=8; field of view= 3 x 3 cm; data matrix=256 x 256; slice thickness=1.0 mm. LD, laterodorsal thalamic nuclei; M, Motor Cortex; nRT, nucleus reticularis thalami; Po, posterior thalamic nuclear group; PtA, parietal cortex; S1, sensory cortex; Te, temporal cortex; VPM / VPL, ventral posteromedial / posterolateral thalamic nucleus.

Table 1. The percent changes of positive and negative BOLD signals (mean ± SEM, N=8 rats) over time. Regions that are significantly different from results obtained after the control saline injection are noted (* P< 0.01, **P<0.001).

ROI	Positive BOLD		Negative BOLD	
	Saline	GBL	Saline	GBL
Parietal Cortex	0.8 ± 0.3%	** 16.3 ± 2.2%	-1.8 ± 0.4%	* -11.9 ± 1.9%
Sensory Cortex	1.9 ± 0.6%	* 16.6 ± 2.3%	-2.2 ± 0.5%	* -11.1 ± 1.0%
Temporal Cortex	1.9 ± 0.7%	3.8 ± 0.5%	-2.3 ± 0.3%	** -14.6 ± 0.9%
Motor Cortex	1.8 ± 0.5%	3.9 ± 0.4%	-1.8 ± 0.3%	* -11.6 ± 1.7%
Ventral Posteromedial / Posterolateral Thalamic Nuclei	1.2 ± 0.4%	* 11.8 ± 1.8%	-1.0 ± 0.3%	-1.7 ± 0.1%
Nucleus Reticularis Thalami	2.3 ± 0.7%	* 9.7 ± 0.8%	-1.4 ± 0.3%	-1.8 ± 0.3%
Posterior Thalamic Nuclear Group	1.3 ± 0.4%	* 11.3 ± 1.5%	-1.4 ± 0.4%	-1.9 ± 0.4%
Laterodorsal Nucleus	1.3 ± 0.5%	** 14.7 ± 1.7%	-1.9 ± 0.4%	-1.8 ± 0.2%

As can be seen in Table 1, significant negative BOLD decreases were found in all cortical regions analyzed. These results are based on the signal values averaged across the voxels in a ROI. Parietal and somatosensory cortices had negative BOLD changes of -12% and -11.1%, while the motor and temporal cortices had negative BOLD changes of -11.7% and -14.7%, respectively. The nRT and laterodorsal thalamic nuclei (LD) showed average BOLD signal increases of 9.7% and 14.7% above baseline, respectively. Ventral posteromedial/posterolateral thalamic nuclei and the posterior thalamic nuclear group (VPM/VPL, Po) also showed increased positive BOLD changes of 11.8% and 11.4% above baseline, respectively. The somatosensory and parietal cortices had significant positive BOLD increases of 16.7% and 16.4%, respectively. These results following GBL injection can be compared to those following the control injection of saline, in which comparatively minor activations of less than 2.5% occurred.

BOLD signal time courses for each cortical ROI are plotted in Figure 15A. These percent change plots were constructed by averaging the values for the bilateral ROIs at each time point, for all eight rats. Following GBL injection, but before the onset of SWDs and absence seizure, the sensory cortex showed an increase in BOLD signal of about 10%. However, during absence seizure there was only a modest increase in BOLD signal intensity above pre-seizure levels. The parietal cortex showed a post-GBL, pre-seizure increase in BOLD signal of 10%, followed by a gradual increase in BOLD signal to about 20% during

seizure. All cortical ROIs demonstrated an increase in negative BOLD signal, which appeared to correlate with the absence seizure and decreased over the remainder of the study.

The percent change in BOLD signal intensity in the thalamus, following GBL injection, appears to have a biphasic "step-up" pattern (Figure 15B). This is an artifact of the experimental design and reflects stoppage of fMRI data acquisition for collection of EEG data (Figure 6). EEG data was collected for the first two minutes immediately after GBL injection. During this time there were slight changes in the EEG pattern, but no SWD formations for any of the eight animals studied (see Figure 13 for representative recording). With the resumption of imaging, BOLD signal intensity was found to be approximately 10% higher than the previous baseline taken before GBL injection. Four minutes after GBL injection imaging was stopped again and EEG data collected which showed the appearance of SWDs. With the resumption of imaging, approximately five minutes after GBL injection, BOLD signal changes were 10-20% higher than baseline. Over the experimental time course there was no significant negative BOLD signal in any of the thalamic ROIs.

Figure 15

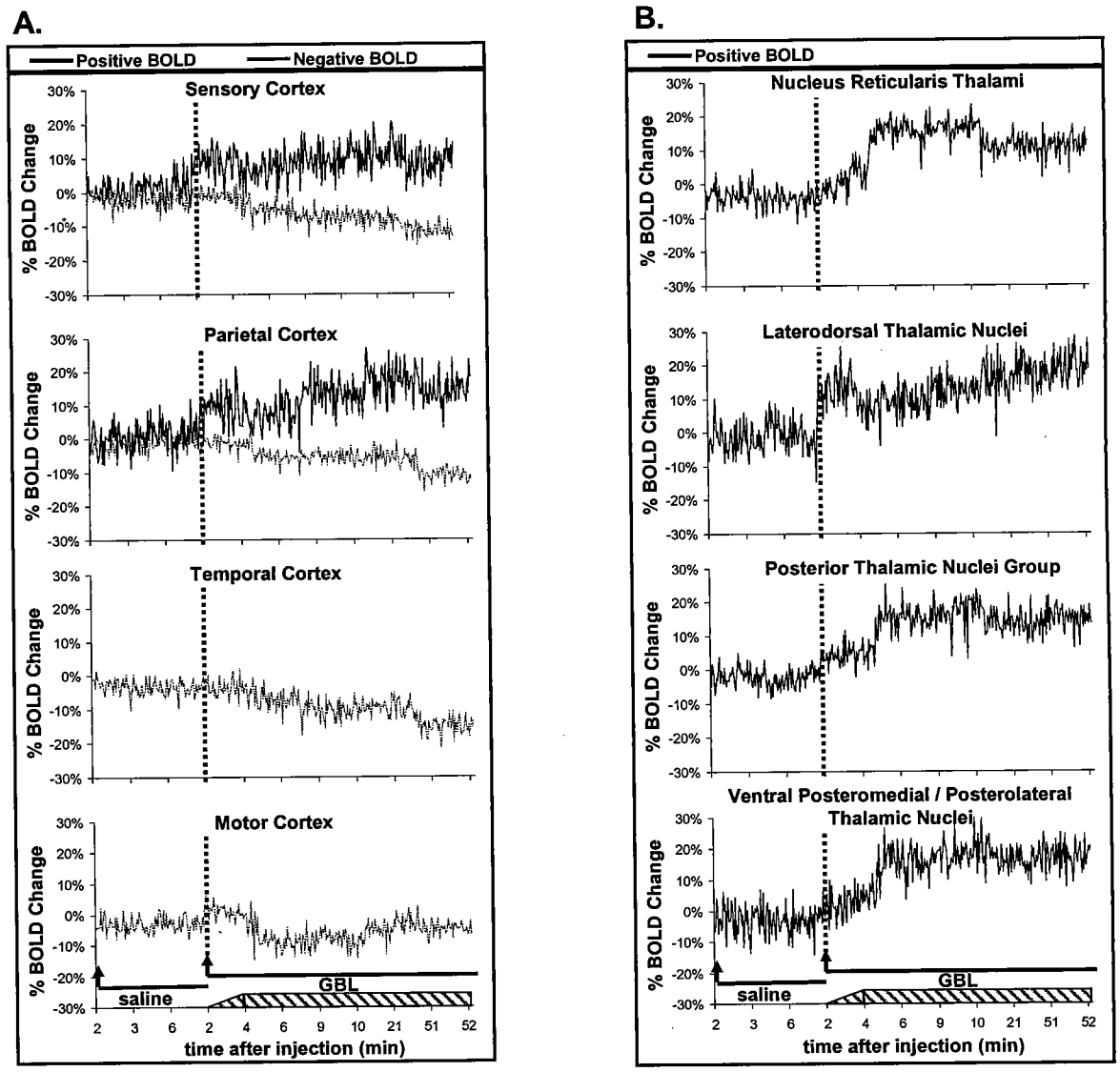
A.
Positive BOLD
Negative BOLD
Sensory Cortex
Parietal Cortex
Temporal Cortex
Motor Cortex
% BOLD Change
30%
20%
10%
0%
-10%
-20%
-30%
saline
GBL
2 3 6 2 4 6 9 10 21 51 52
time after injection (min)
B.
Positive BOLD
Nucleus Reticularis Thalami
Laterodorsal Thalamic Nuclei
Posterior Thalamic Nuclei Group
Ventral Posteromedial / Posterolateral Thalamic Nuclei
% BOLD Change
saline
GBL
2 3 6 2 4 6 9 10 21 51 52
time after injection (min)

Figure 15. Change in BOLD signal intensity over time for each ROI in the cortex (A) and thalamus (B). Temporal and motor cortices showed no significant positive BOLD changes. No significant negative BOLD changes occurred in any of the thalamic ROIs. These plots were created by averaging the value for each animal at each time point. Each image acquisition was 2 seconds. The start of imaging, 2 minutes following injection, is shown with an arrow and solid lines indicate images acquired during periods after either saline or GBL injections. Dashed lines correspond to the start of imaging, 2 minutes following the injection of GBL. The hatched box at the bottom of the graph indicates that SWDs began to form sometime between 2 and 4 minutes following GBL injection and lasted until the end of the imaging experiment.

Discussion

The data from this study, using fMRI to identify areas of brain activation during absence seizure, corroborate the findings from lesion and electrophysiological studies. The cortico-thalamic circuitry so critical for SWD formation shows robust changes in positive BOLD signal correlated with EEG changes showing the initiation of seizure activity following administration with GBL. The escalation of BOLD signal in the thalamus and cortex probably reflects increased blood flow associated with onset and maintenance of SWDs in absence seizures. These findings support the use of fMRI to study absence seizures in this rodent model and show the technical feasibility of imaging absence seizures in fully conscious rodents with minimal motion artifact.

The *a priori* hypothesis predicted activation of those ventrobasal thalamic sites, e.g., the ventral posteromedial and ventral posterolateral nuclei, with direct efferent connections to the sensory cortex. Neurotoxic lesions were used to identify several thalamic nuclei involved in the generation and maintenance of SWDs in the GBL rodent model (135-136). Bilateral lesions in the dorsal thalamic nuclei abolish SWDs from both the cortex and thalamus. In addition, ventral posterolateral thalamic lesions do not stop SWDs, but decrease their duration, while lesions in the reticular thalamic nucleus suppressed GBL-induced seizures. Data from the current study demonstrate that these thalamic areas

plus the sensory and parietal cortices show robust increases in positive BOLD signal with GBL treatment.

The results of the current study demonstrate a predominately positive BOLD signal change in the thalamus, likely reflecting an increase in neuronal activity associated with seizure. Interestingly, the sensory and parietal cortices presented a functional heterogeneity characterized by significant increases and decreases in BOLD signal. The sensory cortex, the primary afferent thalamic connection, shows the anticipated increase in BOLD with some adjacent areas, particularly along the superficial layers of the cortex, showing negative BOLD signal changes. Simultaneous positive and negative BOLD response in adjacent brain regions were reported also in humans during photic stimulus-triggered seizures (137). In contrast, the temporal and motor cortices show only a significant negative BOLD signal change most likely reflecting a decrease in neuronal activity. Prior to SWD formation, there were no changes seen in negative BOLD. However, at the resumption of imaging five minutes after GBL injection and with the onset of absence seizure there is a "step down" in negative BOLD signal that continues to decrease over the remainder of the study. It is interesting that the motor cortex shows deactivation since the seminal feature of the absence seizure is arrest of motor activity.

It is important when interpreting these results to choose an appropriate "control period" to use as a comparison. Since the control imaging period chosen in this study was the time before GBL injection and BOLD changes seem to

occur before the formation of identifiable SWDs, it is possible that these signal increases are due partly to an effect of the GBL, independent of seizure activity. It is also likely that seizure activity is occurring in subcortical structures or other areas not represented by the cortical EEG electrodes. If so, the results in figures 5 and 6 suggest that, in the GBL model, cortical activity is occurring before that in the thalamus. For this reason, the control imaging period used in this experiment was the time before GBL injection.

There are no published reports using BOLD fMRI to study absence seizure activity. However, several other imaging modalities were used to observe changes in cerebral blood flow and metabolism during absence seizures. Measures of metabolic activity using the ^{14}C-deoxyglucose autoradiographic technique in rats given GBL report a dose dependant decreases in glucose utilization (138). Studies using PET to measure cerebral glucose metabolism show global increases in activity during ictal periods, but limitations in temporal and spatial resolution preclude the identification of specific cortico-thalamic areas and their correlation with the generation of SWDs (81,139-140). Use of PET to follow changes in cerebral blood flow shows global increases in perfusion during absence seizures, with a higher focal increase in the thalamus, but again no clear delineation of cortico-thalamic structures or temporal correlation with EEG activity (82). Studies with single photon emission computed tomography (SPECT) in children show a homogenous, diffuse increase in cerebral blood flow during absence seizure activity, but no focal

changes (78). Better spatial resolution was reported in a recent SPECT study using adult patients and showing an increased perfusion in the cortex, cerebellum, thalamus, and basal ganglia (141).

Doppler flow techniques, providing good temporal resolution, were used to study blood flow changes in superficial cortical areas during absence seizure. Doppler studies in humans show mean blood flow velocity increases a few seconds before clinical or EEG evidence of seizure activity, with a peak value occurring 2-3 seconds after the start of clinical and EEG seizure activity (79). An abrupt decrease in blood flow velocity starts during seizure activity and reaches a minimum value within 4-6 seconds after the end of the seizure. Doppler studies with children and a genetic rat model of absence epilepsy report decreases in cerebral blood flow during the seizure, which subsequently returns to baseline values with the cessation of seizure activity (80). The decrease in blood flow during absence seizure was interpreted as a reduction in metabolism following reduced synaptic and neuronal activity. These data are not unlike our observation in the GBL model showing significant negative BOLD signal changes in the cortices, likely reflecting decreased cortical blood flow.

Despite the similarity of cortico-thalamic activity between human and rat models of absence seizure, there are fundamental differences. The data in this study is based on sustained spike and wave activity, whereas in humans, seizures of just several seconds occur. In addition, the GBL animal model produces SWDs with a frequency of 7-8 Hz, while human absence seizures are

characteristically 3 Hz. fMRI studies of a primate model of SWDs are necessary to make a closer approximation of the human condition since 3 Hz SWDs occur in this model.

In conclusion, using the BOLD fMRI technique, we demonstrated signal changes in brain areas previously shown to be important for generating and maintaining the SWDs that characterize absence seizures. These aberrant rhythms that characterize all epilepsies result from abnormal synchronous firing of neurons within neural networks. While these rhythms were studied extensively on a cellular and electrophysiological level, we show that fMRI, in awake animals, can non-invasively provide a global view of structures comprising the implicated networks, such as cortico-cortico and thalamo-cortico connections.

CHAPTER III

Development of a WAG/Rij Rat Model for fMRI

Summary

EEG-triggered fMRI was used to identify areas of brain activation during SWDs in an epileptic rat strain under awake conditions. Spontaneous absence seizures from ten WAG/Rij rats were imaged using T_2*-weighted echo planar imaging at 4.7 Tesla. Functional MRI of BOLD signal was triggered based on EEG recordings during imaging. Images obtained during spontaneous SWDs were compared with baseline images. Significant positive BOLD signal changes occurred in multiple cortical areas and several important nuclei of the thalamus. In addition, no negative BOLD signal was found in any brain area. No negative BOLD signal was found in any brain area. These findings show that EEG-triggered BOLD fMRI can be used to detect cortical and thalamic activation related to the spontaneous SWDs that characterize absence seizures in awake WAG/Rij rats. These results draw an anatomical correlation between areas in which there is increased BOLD signal and those where SWDs area recorded.

Introduction

Genetic rat models of absence epilepsy have been studied for many years and are thought to more accurately mimic the spontaneous seizures of human epilepsy than drug-induced animal models. The WAG/Rij strain exhibits spontaneous SWDs with a frequency of 7-11 Hz, duration of 1-45 seconds, and amplitude of 200-1000 uV (59). As in the human condition, EEG changes are accompanied by immobile behavior and staring. Electrophysiology recordings of the WAG/Rij model were used to uncover the neural structures responsible for the generation and propagation of SWDs. Many of these studies implicate the coupling of thalamic oscillations and cortical rhythms as the cause of the absence-like behaviors and EEG changes (65-67). Recently, this rat model was used to study the coordinated electrical field activity between thalamic and cortical sites using multielectrode recordings (68). Spontaneous SWDs were found to be associated first with activity in the peri-oral region of the somatosensory cortex followed by cortical propagation and then thalamic activation.

The ability to detect BOLD signal changes that correlate with spontaneous epileptiform activity is possible with the use of EEG-triggered fMRI (103-107). This technique essentially consists of continuously monitoring the EEG of a subject in the magnet, with the operator manually triggering image acquisition upon identifying seizure-related EEG changes (93, 103,108-110). In the present

study, EEG-triggered fMRI of SWDs was used in the WAG/Rij model to determine the activity of several thalamic nuclei and cortical areas proposed to be integral to the formation and propagation of SWDs.

Materials and Methods

Animals

Male WAG/Rij rats weighing 250-350 grams (150-200 days old) were obtained from Harlan Sprague-Dawley (The Netherlands). Animals were housed in pairs in Plexiglas cages (48 cm x 24 cm x 20 cm), maintained on 12:12 light:dark cycle (lights on at 7:00 hr) and provided food and water *ad libitum*. All animals were acquired and cared for in accordance with the guidelines published in the *Guide for the Care and Use of Laboratory Animals* (National Institutes of Health Publications No. 85-23, Revised 1985).

Bench-top Studies

Prior to imaging, studies were performed to characterize the number and duration of SWDs in awake, restrained rats. Five rats were initially anesthetized with 2 mg ketamine and 0.02 mg medetomidine and epidural cortical electrodes were secured in the skull and connected to an EEG recorder as described for the bench-top studies in Chapter 2. Electrodes were placed over the frontal and parietal cortices at the following stereotaxic positions from bregma (frontal –

1.6mm rostral, ± 2.5mm lateral, parietal – 1.6mm caudal, ± 2.5mm lateral). Animals were secured in the restraining device used for functional imaging studies and injected with 0.1 mg atipamezole to reverse the anesthesia. The animal restrainer used for imaging was the same as that described in Chapter 2. The average number and duration of SWDs were calculated based on 38 epochs of SWDs occurring in five rats.

Functional MRI Studies

Prior to imaging studies, animals used for imaging were acclimated to the restrainer and the imaging protocol as previously described in Chapter 2. Just prior to the imaging session, ten rats were anesthetized with ketamine and Domitor and placed into the MRI-compatible restraint device, as previously described in Chapter 2.

The EEG signal was amplified inside the RF-shielded room using a battery-operated preamplifier and converted to a fiber-optic signal which was recorded with MP100 hardware and MP100 Manager Software (BIOPAC Systems Inc., Goleta, CA). Similar setups have been used in previous human and animal imaging experiments (98, 123).

All images were acquired using a 4.7T/40-cm (Oxford magnet Technology, Oxford, UK) horizontal magnet interfaced to a Paravision console (Bruker, Billerica, MA). High resolution anatomical data sets were acquired using a fast spin echo (RARE) sequence (TR=2.5s; effective TE=56ms; echo train length=8;

field of view=3x3cm; data matrix=256x256; number of slices=4; slice thickness=1.0 mm). Functional images were acquired using a two-segment gradient echo planar imaging (EPI) sequence (TR=1000ms; TE=25ms; FOV=3x3cm; matrix=128x128; number of slices=4; slice thickness=1.0 mm). Four contiguous functional images were acquired in 2 seconds and each image acquisition included 15 sets of images for a total acquisition time of 30 seconds. The coordinates of slices collected, from rostral to caudal, are -1.5mm, -2.6mm, -3.8mm, and -4.8mm, from bregma, respectively. The most caudal slice (-4.8mm) was excluded from analysis because it did not include significant thalamic and frontal - parietal structures.

Seizure image acquisition was triggered when SWDs were two times the background amplitude and lasted for greater than one second (58). These criteria are important due to the fact that two distinct types of SWDs have been reported in WAG/Rij rats, with only the type I SWDs representing true absence seizures (65). Post-imaging analysis of the EEG changes was completed and imaging data discarded if these criteria were not met. Image acquisition was triggered manually, when SWDs were detected, with a delay of approximately 2.5 seconds. This delay is similar to other reports of EEG-triggered fMRI (103-107). Baseline images were acquired when the EEG showed a normal, awake pattern for greater than 30 seconds, similar to that used in other EEG-triggered fMRI studies (103-107). Baseline image acquisitions were interspersed throughout each 1-2 hour imaging session. Since artifact obscures the EEG during imaging,

it is possible that spikes could have occurred, undetected, during these baseline acquisitions. However, this is unlikely because there are only 5-6 SWD episodes per hour and more importantly, the seizure event has dramatic effects on BOLD signal activity as noted in the activational maps and time-course graphs. No such changes in BOLD activity occurred in any of the baseline acquisitions. Observations of movies comprising all images during acquisition showed little motion artifact. Muscle movement associated with swallowing would occasionally affect image quality slightly in a single slice.

Regions of interest (ROI) used for analysis included the sensory (S1), parietal (PtA), and temporal (Te) cortices and several thalamic nuclei including the reticular thalamic nuclei (nRT), mediodorsal nucleus (MD), ventral posteromedial / posterolateral nuclei (VPM/VPL), and posterior thalamic nuclei (Po). These ROIs were drawn manually on the images, according to the Paxinos and Watson rat brain atlas, and analyzed for changes in BOLD signal intensity (10). Comparisons to create activation maps were done by first appending three baseline periods, collected at various times throughout the imaging session, to create one continuous baseline. Using Stimulate's student's two tailed t-test, this appended baseline was then compared to each seizure period collected for a given animal (129). Voxels whose BOLD percentage change, relative to the control period, was significantly different (either increased or decreased) at a 95% confidence level were overlaid onto their respective anatomical data set. No correction was made for multiple comparisons.

ROI analyses to calculate BOLD signal values and time course plots were based on the signal values averaged across the voxels in each respective region. Since all ROIs are bilateral structures, the results from each hemisphere were combined. A total of 34 trains of SWDs in ten rats were used for these ROI analyses. The above values were averaged for the multiple seizures in each animal and then across all animals to determine average time courses and BOLD signal changes.

Results

Bench-top Studies

Bench-top studies were used to characterize the number and duration of SWDs in restrained rats. The number of seizures and their duration is age-dependent as has previously been shown. It was determined that the optimal age of WAG/Rij rat to use for imaging was approximately 150-200 days old. At this age the animals experience enough seizures to image in an imaging session and they are not too big for the restraint device used for imaging. For this age of animal the average number of SWDs was 5.7/hour (range 3.5-8.2) (Figure 16A). The average duration of SWDs was 45.1 seconds/hour (range 18.4-67.2), with the average duration of a single train of SWDs being 8.1 seconds (range 2.0-31.1) (Figure 16B). These measurements correlate well with previously published data concerning SWD characteristics in this rat strain (60).

Figure 16

A.

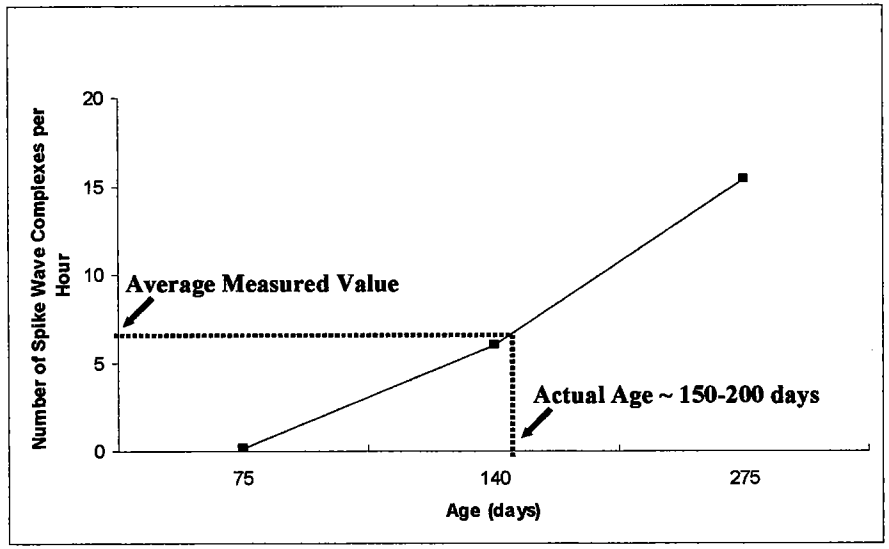
Number of Spike Wave Complexes per Hour
20
15
10
5
0
Average Measured Value
Actual Age ~ 150-200 days
75
140
275
Age (days)

B.

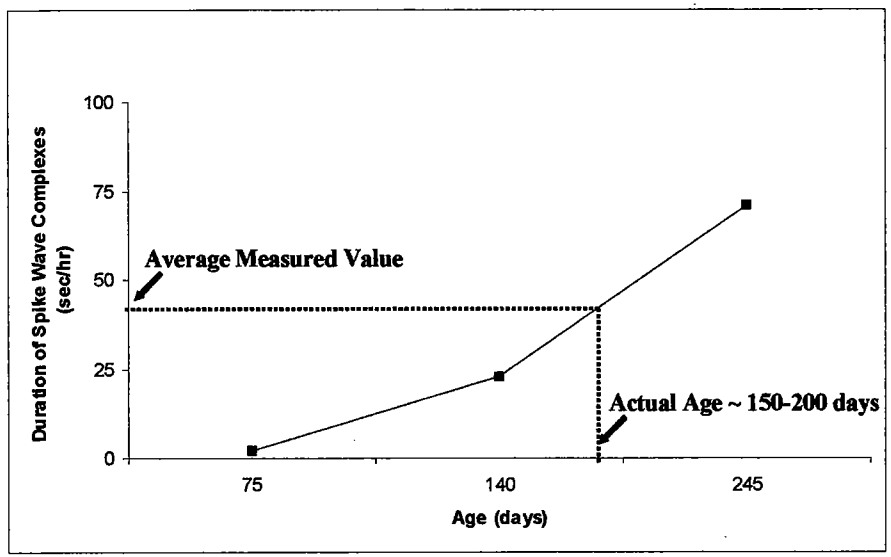
Duration of Spike Wave Complexes (sec/hr)
100
75
50
25
0
Average Measured Value
Actual Age ~ 150-200 days
75
140
245
Age (days)

Figure 16. Bench-top studies characterizing the SWDs in WAG/Rij rats. Previously published data (blue line) concerning the number of SWDs per hour is shown (A). In addition, the average value measured for rats used in this thesis is shown, along with the age of the animals used in the fMRI studies. Previously published data (blue line) is also shown concerning the duration of SWDs (B). The average value measured for rats used in this thesis is noted, along with the age of the animals used for fMRI studies.

Functional MRI Studies

EEG was recorded continuously while the animal was in the magnet and a representative trace can be seen in Figure 17. This trace shows an example of seizure activity, the delay before imaging, and the masking of EEG activity once image acquisition began. Representative activation maps of three consecutive brain slices, together with delineations of representative thalamic and cortical ROIs are shown in Figure 18. These are the activation maps of a single seizure. BOLD activation can be seen clustered throughout the S1, PtA, and Te cortices, along with several thalamic nuclei including the nRT, MD, VPM/VPL, and Po. No significant negative BOLD activation was seen for any seizures. In order to explore the negative BOLD response in the WAG/Rij model further, the pixel clustering and confidence interval used for creating the activation maps were decreased, to determine if the absence of negative BOLD was due to a lack of statistical power. The activation map in a few animals showed a few individual pixels of negative BOLD, which is not a significant finding.

Figure 19 shows the group-average percent changes of BOLD signal intensity for each of the ROIs (N=34 seizures), above the baseline values. All cortical and thalamic areas analyzed showed significant positive BOLD signal, above baseline values. During seizures, the BOLD signal changes were at least 4% in both cortical and thalamic ROIs.

BOLD signal time courses for each thalamic and cortical ROI are plotted in Figures 20A and 20B, respectively. These time course plots were constructed by

Figure 17

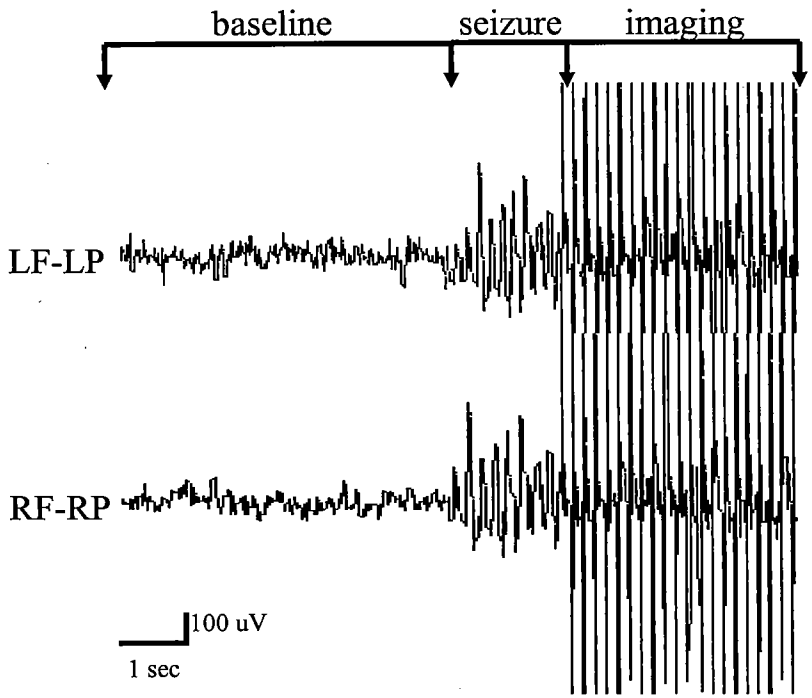

Figure 17. Representative EEG recording collected during fMRI. Nonmagnetic epidural electrodes were placed in the frontal and parietal cortices in order to monitor seizure activity during the imaging session. Normal, awake EEG was present during baseline imaging. Imaging was triggered following the formation of epileptiform activity similar to that shown during the seizure period. Artifact due to image acquisition can be seen with a delay of approximately two seconds following seizure activity. RF, right frontal cortex; RP, right parietal cortex; LF, left frontal cortex; LP, left parietal cortex.

Figure 18

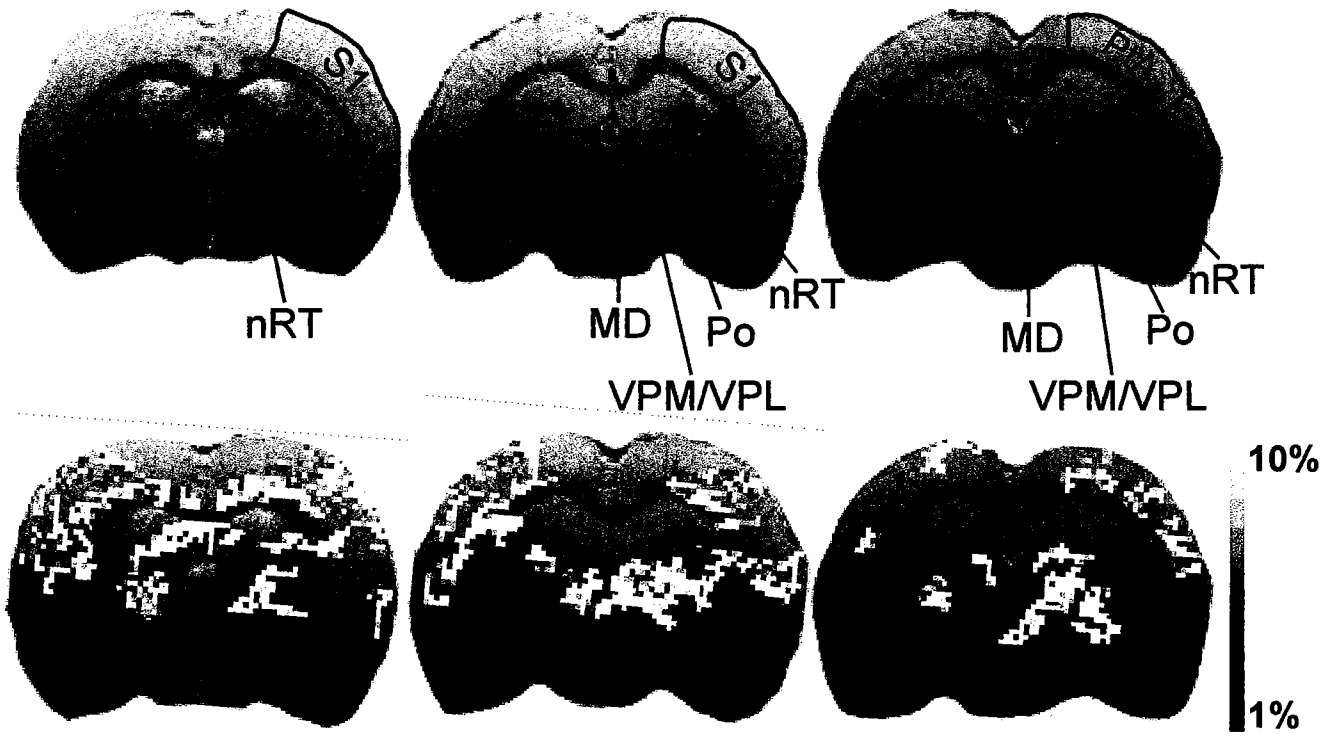

Figure 18. Activation maps of BOLD signal responses during spontaneous spike and wave discharges. The colored pixels indicate the statistically significant ($P<0.05$) pixels determined by t-test analysis (for a single seizure) and overlaid onto the corresponding anatomy. Three consecutive slices through the brain are shown for an individual rat. The top row shows the regions of interest used for analysis. MD, mediodorsal thalamic nuclei; nRT, nucleus reticularis thalami; Po, posterior thalamic nuclear group; PtA, parietal association cortex; S1, sensory cortex; Te, temporal cortex; VPM / VPL, ventral posteromedial / posterolateral thalamic nucleus.

Figure 19

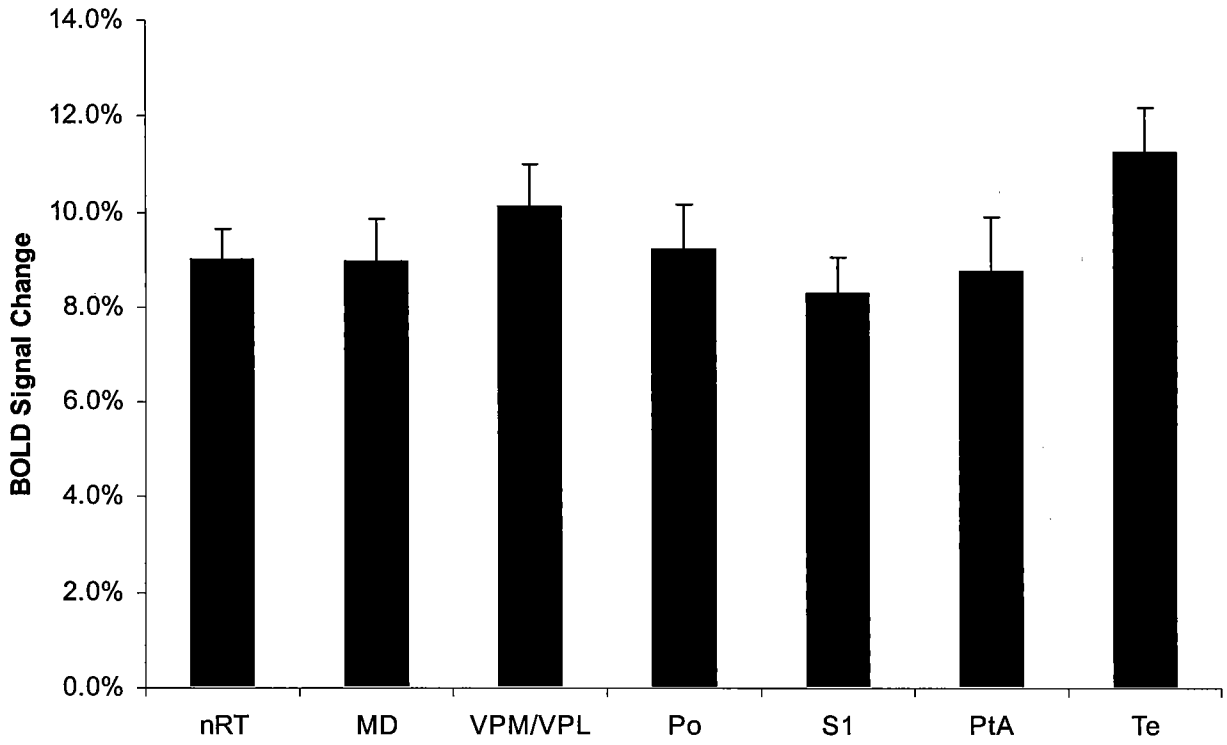
14.0%
12.0%
10.0%
8.0%
6.0%
4.0%
2.0%
0.0%
BOLD Signal Change
nRT
MD
VPM/VPL
Po
S1
PtA
Te

Figure 19. Change in BOLD signal intensity for each ROI. The BOLD signal intensity change during SWDs is shown for ROIs in the cortex and thalamus (mean ± SEM, N=34 seizures). All ROIs are bilateral structures, so the signal changes from each hemisphere were combined. BOLD signal was averaged for each seizure over the entire 30 second acquisition. MD, mediodorsal thalamic nuclei; nRT, nucleus reticularis thalami; Po, posterior thalamic nuclear group; PtA, parietal association cortex; S1, sensory cortex; Te, temporal cortex; VPM / VPL, ventral posteromedial / posterolateral thalamic nucleus.

Figure 20

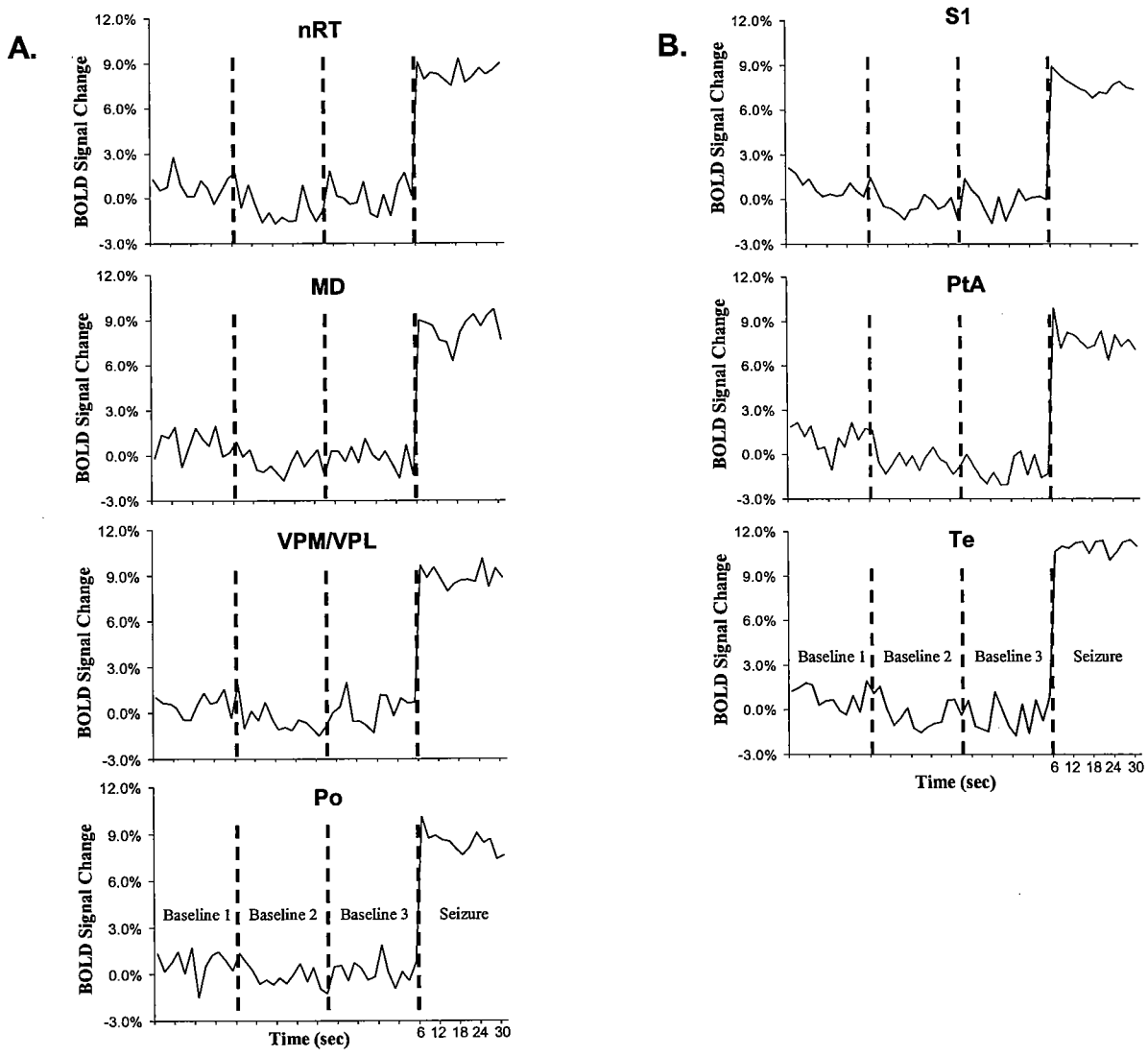
A.
nRT
MD
VPM/VPL
Po
B.
S1
PtA
Te
BOLD Signal Change
12.0%
9.0%
6.0%
3.0%
0.0%
-3.0%
Baseline 1
Baseline 2
Baseline 3
Seizure
6 12 18 24 30
Time (sec)

Figure 20. Change in BOLD signal intensity over time for each ROI in the thalamus. All thalamic (A) and cortical (B) ROIs showed significant BOLD signal changes from baseline. All ROIs are bilateral structures so, the signal intensities from each hemisphere were combined. These plots were created by averaging the value for all seizures at each time point. Each image acquisition was 2 seconds. BOLD signal changes are shown for each baseline period, which were collected at different points throughout the imaging session. MD, mediodorsal thalamic nuclei; nRT, nucleus reticularis thalami; Po, posterior thalamic nuclear group; VPM / VPL, ventral posteromedial / posterolateral thalamic nucleus.

averaging the BOLD signal values for the ROIs at each time point, for both baseline and seizure periods. Three baseline periods, acquired during normal, awake EEG activity and lasting for greater than 30 seconds are shown in the plots. The baseline periods lasted 30 seconds and were interspersed over the imaging session for each rat. Average baseline data varied approximately 2%, which is consistent with other fMRI studies of awake animals (120). BOLD activation corresponding to seizure activity is increased from the start of the image acquisition and remains elevated for most ROIs until the end of the acquisition period.

Discussion

The present data show that spontaneous SWDs in the WAG/Rij rat strain correlate with cortical and thalamic BOLD fMRI signal activation. Cortical areas and thalamic nuclei that show BOLD activation in the current study have been implicated in the pathogenesis of SWDs in previous neurophysiological studies. Electrophysiology recordings of SWDs in WAG/Rij rats have implicated the same cortical areas and thalamic nuclei which have shown BOLD activation in the current study (65-67). Specific thalamic relay nuclei, such as the VPM/VPL, and non-specific relay nuclei, such as the MD and Po, were found to contribute to the generation and diffuse nature of SWDs (65). In addition, the nRT is believed to be crucial for the synchronization of thalamic rhythmic oscillations (142-143).

The robust BOLD activation seen in all these nuclei underscore their importance to the pathophysiology of this seizure disorder. Also, since SWDs are generalized over the cortex, it is not surprising that BOLD activation was found in the S1, PtA, and Te cortical areas. Conversely, no significant BOLD activation was found in the hippocampus, an area devoid of SWDs during generalized absence (144-145). Therefore, it appears that the BOLD signal of fMRI is specific for areas and structures that contribute to or participate in the production of SWDs.

A few studies have measured brain metabolism during SWDs in rats. Cerebral energy metabolism in a strain of genetic absence epilepsy rats was measured and widespread increases were found in all brain structures, regardless of their ability to form SWDs (146). A previous fMRI study of SWDs in WAG/Rij rats, under continuous anesthesia, showed focal BOLD activation in anterior brain regions (147). Therefore, fMRI patterns of BOLD activation appear to correlate better with the brain areas responsible for the generation and propagation of SWDs.

The data in chapter two demonstrated similar positive BOLD activation patterns to the current spontaneous seizure model (123). The GBL drug-induced seizure caused positive BOLD activation in similar cortical areas and thalamic nuclei as those of the spontaneous seizure model. One difference between the two models, however, was the negative BOLD signal decreases present throughout the cortex in the GBL model. The WAG/Rij model had diffuse positive

BOLD activations in the cortex, but no significant negative BOLD changes were found. It is possible that the negative BOLD changes of the previous study were specific for the GBL drug used to induce the seizures.

There are three primary reasons for the occurrence of negative BOLD: 1) the rate of oxygen consumption ($CMRO_2$) from areas of high synaptic and neuronal activity exceeds compensatory blood flow, 2) "vascular steal" i.e., preferential flow to the most metabolically active areas leaving the abandoned areas facing less blood flow in the presence of a constant $CMRO_2$ and, 3) a reduction in brain activity and blood flow from basal levels (48). Since negative BOLD can occur as a result of one area of the brain being activated while another is deactivated, this discrepancy might simply be due to different neural pathways and mechanisms contributing to seizure activation in the drug model versus the genetic model. This is unlikely because alterations in GABA neurotransmission are responsible, in part, for both the GBL and genetic models of absence seizures (48, 61). A more plausible explanation is the severity of the seizures. In the WAG/Rij model absences occur a few times per hour and last less than ten seconds. With GBL, the seizure activity is unremitting and more representative of status epilepticus. The intense synaptic and neuronal activity with enhanced $CMRO_2$ may exceed compensatory blood flow in areas outside the corticothalamic loop that is responsible for the initiation and maintenance of the SWDs.

Patterns of positive BOLD activation in both animal models implicate the same cortical and thalamic structures in the generation and propagation of SWDs. Therefore, both the GBL drug-induced and WAG/Rij spontaneous models result in fMRI activation of the same brain structures during the SWDs that characterize absence epilepsy.

CHAPTER IV

Development of a GBL Monkey Model for fMRI

Summary

A typical absence seizure is manifested behaviorally as a "staring spell" and can be accompanied by atonic postures and automatisms. Children may have 10 to 200 of these seizures in a day and in the more severe case of absence status epilepticus the seizures are unremitting and can last for hours. To elucidate the brain mechanisms underlying this disorder, a non-human primate model of absence epilepsy was developed, which could be used for functional imaging in conscious monkeys. Marmoset monkeys (*Callithrix jacchus*) were treated with GBL to induce absence seizures during BOLD fMRI. Electroencephalographic recordings during imaging showed 3 Hz SWD typical of human absence seizures. This synchronized EEG pattern started within 15-20 minutes of drug administration and persisted for over 60 minutes. In addition, pre-treatment with the antiepileptic drug, ethosuximide, blocked the behavioral and EEG changes caused by GBL. Changes in BOLD signal intensity in the thalamus and sensorimotor cortex correlated with the onset of 3 Hz SWD. The change in BOLD signal intensity was bilateral but heterogeneous, affecting some brain areas more than others. There were no significant negative BOLD changes. These results support the use of fMRI in conscious marmoset

monkeys as a method for studying the neurobiology of absence seizures in a non-human primate.

Introduction

Non-human primate models of generalized epilepsy were used for many years to study convulsive seizures (69-73). A few studies demonstrated that non-human primates mimic the behavior and characteristic EEG of childhood absence epilepsy, producing SWDs with a frequency of 3 Hz (74-75). Primates and rodents given GHB show behavioral and EEG changes consistent with generalized absence seizures (20, 74). In addition, GHB-induced seizures respond to the anticonvulsant ethosuximide, the drug of choice for treatment of absence epilepsy (49, 76).

Functional MRI studies of GBL-induced SWDs in rats showed that BOLD signal is increased in the corticothalamic circuit as discussed in Chapter 2 (123). Likewise, the BOLD fMRI studies of spontaneous SWDs in the epileptic WAG/Rij rat strain, presented in Chapter 3, have shown similar activation in the cortex and thalamus (124). While these results suggest drug-induced and spontaneous rat models of absence epilepsy produce similar activation, they do not accurately mimic the neurophysiology responsible for the human EEG that characterizes epilepsy. In the current study, we have used BOLD fMRI to determine the neural

structures activated during 3 Hz SWDs in a small non-human primate model of absence epilepsy.

Materials and Methods

Animals

Imaging studies were conducted on adult male common marmoset monkeys (*Callithrix jacchus*) weighing 300-450 grams. Animals were family reared and socially housed. All animals were cared for in accordance with the guidelines published in the *Guide for the Care and Use of Laboratory Animals* (National Institutes of Health Publications No. 85-23, Revised 1985).

Bench-top Studies

Prior to imaging, studies were performed to characterize the dose-response effect of GBL in both freely moving and restrained marmosets. Marmosets (n = 6) were lightly anesthetized with 1 mg ketamine (Ketaset, Fort Dodge Animal Health, Fort Dodge, IA) and 0.05 mg medetomidine (Domitor, Pfizer Animal Health, New York, NY). Anesthesia was maintained through the use of 1.5% isoflurane gas. Subdermal needle electrodes (Grass Telefactor, West Warwick, RI) were secured under the scalp and connected to an EEG recorder using the Biopac system (BIOPAC Systems Inc., Goleta, CA). Electrodes were placed over the frontal and parietal cortices. Animals were

injected with 0.1 mg atipamezole (Antisedan, Pfizer Animal Health, New York, NY) to reverse anesthesia and placed into a body tube for light restraint in order to minimize motion artifact on the EEG. EEG recordings were collected continuously over a 120-min test period, during which three groups of two animals each were injected subcutaneously (s.c.) with GBL in doses of 50, 100, or 200 mg/kg. A higher dose than 200 mg/kg was not used due to our previous experience with GBL in rats and its tendency to produce prolonged periods of burst-suppression pattern on EEG. The latency, duration, and pattern of SWDs were measured for each dose, to determine the most appropriate concentration to use for imaging experiments. Behavioral alterations following GBL administration were videotaped. In order to quantify the frequency of the SWDs, a fast fourier transformation (FFT) of a segment of seizure EEG was run for each marmoset used in the baseline study.

Antiepileptic Drug Study

Further characterization of the GBL-induced marmoset model of absence seizures was carried out by testing the efficacy of an antiepileptic drug routinely used to treat human absence seizures. Three adult male marmosets were pre-treated with 30 mg/Kg ethosuximide (Sigma-Aldrich, St. Louis, MO) made in sterile water. The daily dose was divided by 3 in order to give the drug three times a day. The drug was disguised in a marshmallow treat and administered three times a day (6:30am, 12:30pm, 6:30pm) for three days. This dosing

schedule is similar to that used in children with absence epilepsy (148). After three days of pre-treatment, marmosets were given 200 mg/Kg GBL as described for bench-top studies with behavior and EEG videotaped for analysis.

Imaging Studies

Prior to imaging studies, marmosets were acclimated to the restrainer and imaging protocol as previously described (119). Animals were lightly anesthetized and secured in the restrainer. When fully conscious, the restraining unit was placed into a black opaque tube that served as a "mock scanner" and a tape-recording of MRI pulse sequences played for 90 minutes to simulate the bore of the magnet and an imaging protocol. This procedure was repeated every other day for two-three days.

Just prior to the imaging session, marmosets (n=5) were anesthetized with ketamine, Domitor, and isoflurane regimen. A topical anesthetic of 2.5% lidocaine gel was applied to the skin of the scalp and MR compatible non-magnetic subdermal needle EEG electrodes were fixed to the scalp, as in the bench-top studies previously described. In addition, lidocaine gel was applied to soft tissue around the ear canals, as these are pressure points in the restrainer. A plastic semicircular headpiece with blunted ear supports that fits into the ear canals was positioned over the ears. The head was placed into a cylindrical head holder with the animal's canines secured over a bite bar and ears positioned inside the head holder with adjustable screws fitted into lateral

sleeves. An adjustable surface coil built into the head holder was pressed firmly on the head and locked into place. The body of the animal was placed into a heavy cotton sock to keep it warm and then placed into a body restrainer. The body restrainer "floats" down the center of the chassis connecting at the front and rear end-plates and buffered by rubber gaskets. The head piece locks into a mounting post on the front of the chassis. This design isolates all of the body movement from the head restrainer and minimizes motion artifact. Once the animal was positioned in the body holder, a volume coil was slid over the head restrainer and locked into position. This procedure took five to six minutes. Animals are usually fully conscious at the end of the set-up since Antisedan is administered at the point the animal is placed into the head holder, as in the bench-top studies described above. The animal restrainer used for imaging consisted of a multiconcentric Plexiglas head and body holder with built-in radiofrequency dual coil electronics (Insight Neuroimaging Systems, LLC, Worcester MA) (125).

All images were acquired using a 4.7T/40-cm (Oxford magnet Technology, Oxford, UK) horizontal magnet interfaced to a Paravision console (Bruker, Billerica, MA). High resolution anatomical data sets were acquired using a fast spin echo (RARE) sequence (TR=2.5s; effective TE=56ms; echo train length=8; field of view=3x3cm; data matrix=256x256; number of slices=4; slice thickness=1.0 mm). Functional images were acquired using a spin echo (RARE) sequence (TR=2.4s; TE=8ms; FOV=3x3cm; matrix=64x64; slice thickness=1.5

mm; number of slices=18; averages=2). Eighteen contiguous functional images were acquired in 20 seconds and each image acquisition included 15 sets of images for a total acquisition time of 5 minutes.

The EEG signal was amplified inside the RF-shielded room using a battery-operated preamplifier and converted to a fiber-optic signal which was recorded with MP100 hardware and MP100 Manager Software (BIOPAC Systems Inc., Goleta, CA). Similar setups have been used in previous human and animal imaging experiments (98, 123-124).

Functional imaging followed the paradigm shown in Figure 21. A baseline set of images was acquired for 5 min, followed by an s.c. injection of 0.9% saline. EEG recordings were done for 2 min, followed by image acquisition for 5 min. 200 mg/kg GBL was then administered, s.c., and EEG was recorded for 2 min before starting image acquisition for 5 min. Scans were repeated 5 more times with wait times in between of 2 min, 2 min, 2 min, 2 min, and 20 min, respectively.

Regions of interest (ROI) used for analysis included the thalamus (Thal), hippocampus (Hipp), and frontal (Fr), temporal (Te), pre-central (PrC), post-central (PoC), anterior cingulate (aCg), and posterior cingulate (pCg) cortices. These ROIs were drawn manually on the images, according to the common marmoset and macaque brain atlases, and analyzed for changes in BOLD signal intensity (149-150). STIMULATE software was used to perform statistical comparisons of control periods to absence seizure periods with the Student's two

tailed t-test to generate an activation map of the ROIs for each dataset (129). The control imaging period was defined as the average value of the baseline data collected in the initial 5 min of the experiment. The absence seizure imaging periods were defined as the 5 min imaging blocks acquired following the GBL injection. Each block of absence seizure images were individually compared to the baseline period. Voxels whose BOLD percentage change, relative to the control period, was significantly different (either increased or decreased) at a 95% confidence level were overlaid onto their respective anatomical data set. Only clusters of four or more voxels were displayed in activation maps. No correction was made for multiple comparisons.

ROI analyses to calculate BOLD signal values were based on the signal values averaged across the voxels in each respective region. Since activation maps are examples from an individual animal, the number of pixels activated within ROIs was calculated and averaged for all animals. This area of activation calculation was done using the STIMULATE program to determine the percent of activated voxels within an ROI, out of all the voxels that constitute the ROI. Since all ROIs are bilateral structures and comparisons between the left and right hemispheres showed no significant differences, the results from each hemisphere were combined. The above values were averaged for the multiple seizures in each animal and then across all animals to determine average BOLD signal changes and area of activation.

Figure 21

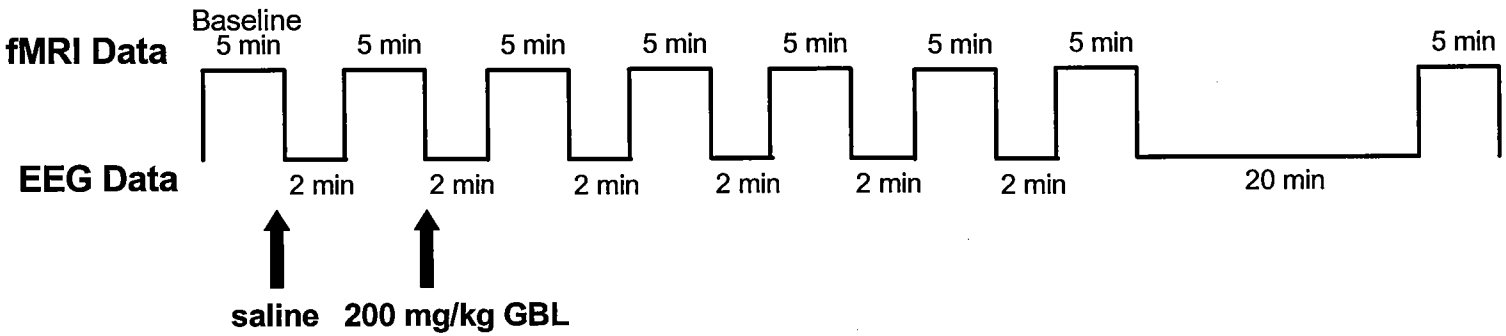
fMRI Data
EEG Data
Baseline
5 min
5 min
5 min
5 min
5 min
5 min
5 min
5 min
2 min
2 min
2 min
2 min
2 min
2 min
20 min
saline
200 mg/kg GBL

Figure 21. Experimental paradigm used for functional imaging experiments. EEG data are collected during breaks in imaging because of the distortion caused by functional magnetic resonance imaging acquisition.

Results

Bench-top Studies

Bench-top studies indicated that GBL at 200 mg/kg was the most effective dose for eliciting absence seizures in marmosets. SWDs, with amplitudes of 200-250 *μV,* began approximately 15 min following the GBL injection. Before the 3 Hz SWDs began to form, a non-specific slowing of the EEG occurred at higher frequencies. A representative EEG tracing is shown in Figure 22. The SWDs take the form of waves with embedded spikes that are not easily discernable. This type of SWD is similar to ones previously reported in a non-human primate model administered GHB and the feline penicillin model of absence seizures (49, 74, 76, 151). Independent analyses of these EEG tracings confirm their identity as a 3 Hz SWD characteristic of non-human primate absence (Elliott Marcus, personal communication). No EEG changes were seen following the control injection of saline. These EEG changes correlated with absence-like behaviors that included arrest of motor activity, orofacial myoclonus, and impaired responsiveness. A comparison of 3 Hz SWDs in cats and rhesus monkeys are compared to a segment collected from marmoset monkeys (Figure 23). A FFT of the EEG during the seizures showed that the average frequency of the SWDs ranged from 2.5-3.5 Hz, consistent with human recordings (Figure 24).

Figure 22

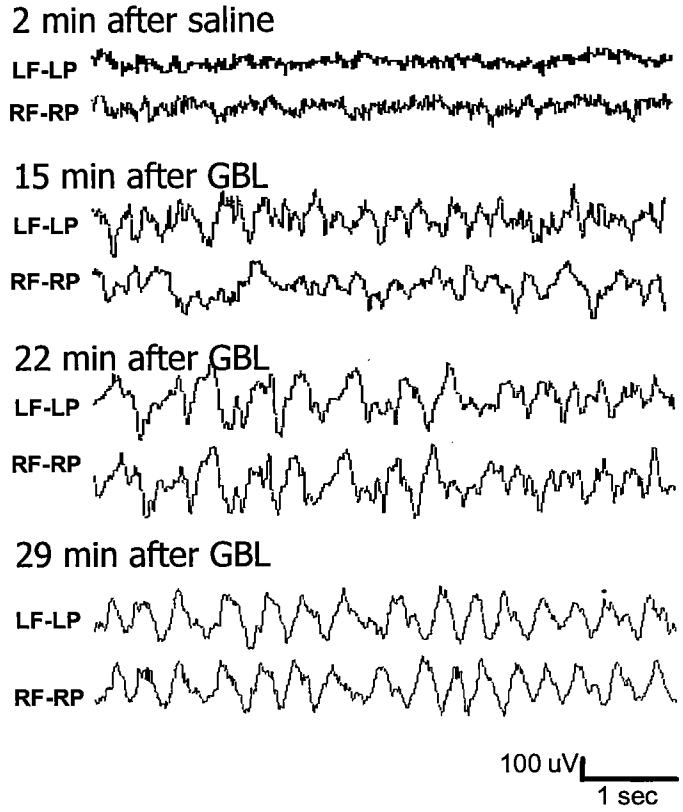
2 min after saline
LF-LP
RF-RP
15 min after GBL
LF-LP
RF-RP
22 min after GBL
LF-LP
RF-RP
29 min after GBL
LF-LP
RF-RP
100 uV
1 sec

Figure 22. Representative EEG recording collected during fMRI. Nonmagnetic subdermal needle electrodes were placed in the scalp over the frontal and parietal cortices in order to monitor seizure activity during the imaging session. Placement of electrode leads is labeled. RF, right frontal cortex; RP, right parietal cortex; LF, left frontal cortex; LP, left parietal cortex.

Figure 23

Cat SWDs
(Marcus and Watson, 1966)

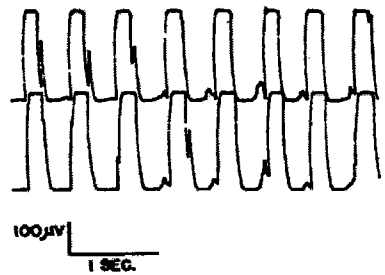

Rhesus Monkey SWDs
(Snead, 1978)

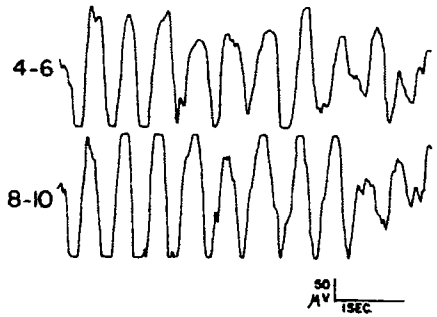

Marmoset Monkey SWDs

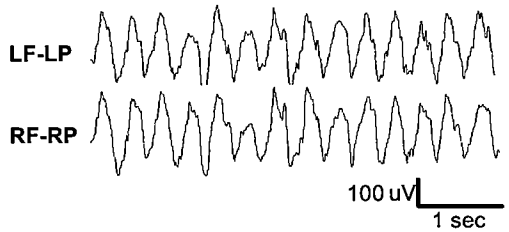

Figure 23. Comparison of experimental 3 Hz SWDs in cats (top), rhesus monkeys (middle), and marmoset monkeys (bottom). Both previous tracings were described as waves with embedded spikes, similar to that shown for the current marmoset model. Placement of electrode leads is labeled. RF, right frontal cortex; RP, right parietal cortex; LF, left frontal cortex; LP, left parietal cortex.

Figure 24

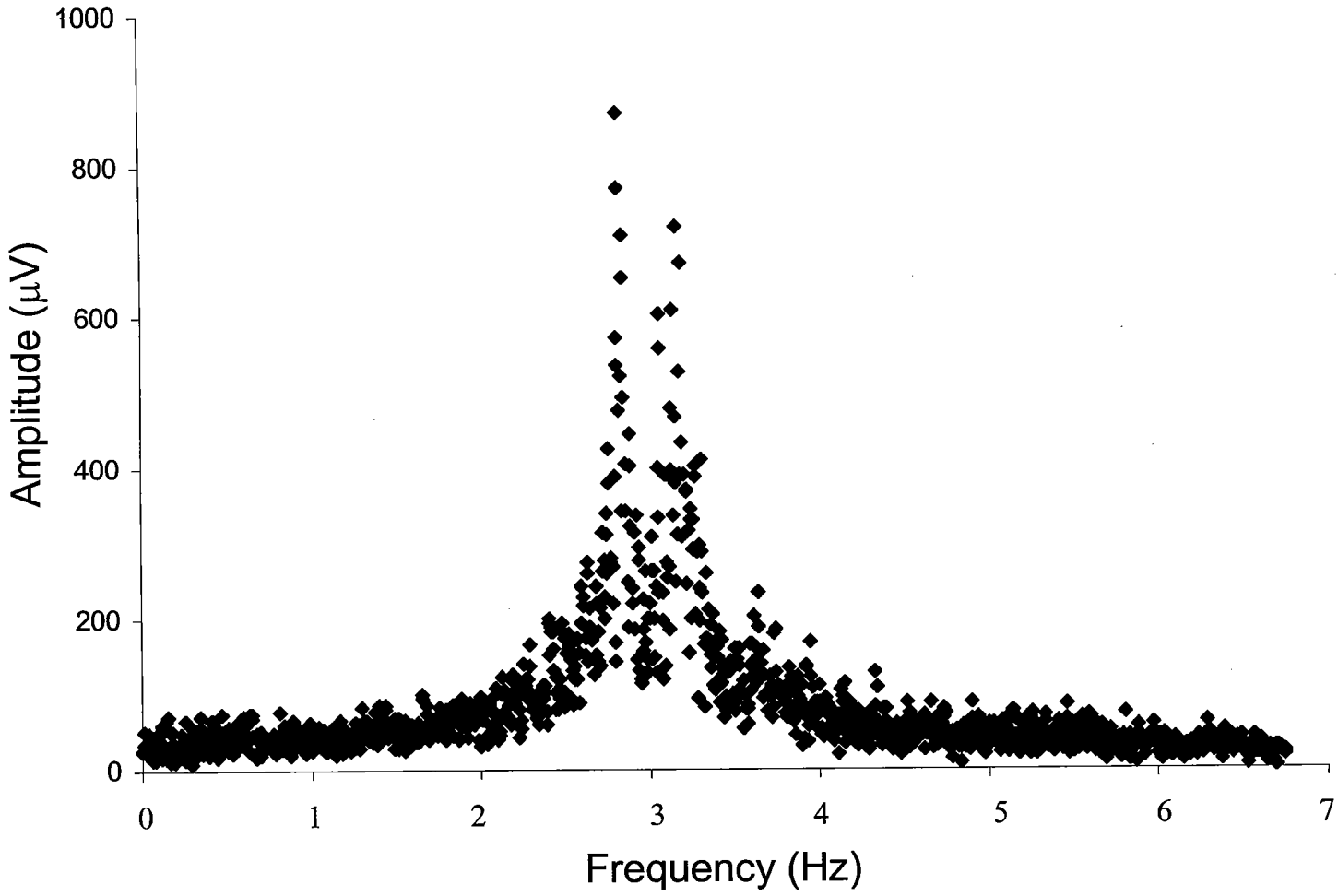

Figure 24. Spectral analysis of marmoset SWDs on EEG. To quantify the frequency of SWDs in marmosets a fast fourier transform of the EEG was run. The average frequency versus amplitude for all monkeys is shown.

Antiepileptic Drug Study

All marmosets pre-treated with ethosuximide for three days and subsequently given 200 mg/kg GBL showed none of the behavioral alterations associated with an absence seizure. Animals were fully conscious and awake, with no change from baseline up to 60 minutes following GBL administration. In addition, no seizure-associated EEG changes were noted following administration of GBL, with constant low amplitude, high frequency waveforms identical to that of the baseline occurring.

Imaging Studies

With the onset of 3 Hz SWDs, positive BOLD activation was seen throughout the marmoset cortex and subcortical structures, including the thalamus and hippocampus. Representative activation maps of four consecutive brain slices, in a single animal and at various time points are shown in Figure 25. Areas used for cortical and subcortical ROIs are indicated in Figure 25A. Figures 25B, 25C, and 25D correspond to images acquired, after GBL administration, during the following five minute blocks – 16-21 min, 23-28 min, and 30-35 min, respectively. The number of activated pixels increased in most areas, over the times shown. No significant negative BOLD pixels were seen for any seizures, in any animals.

Figure 26 shows the group-average percent changes of positive BOLD signal intensity for ROIs and each time block, above the baseline values. ROIs

Figure 25

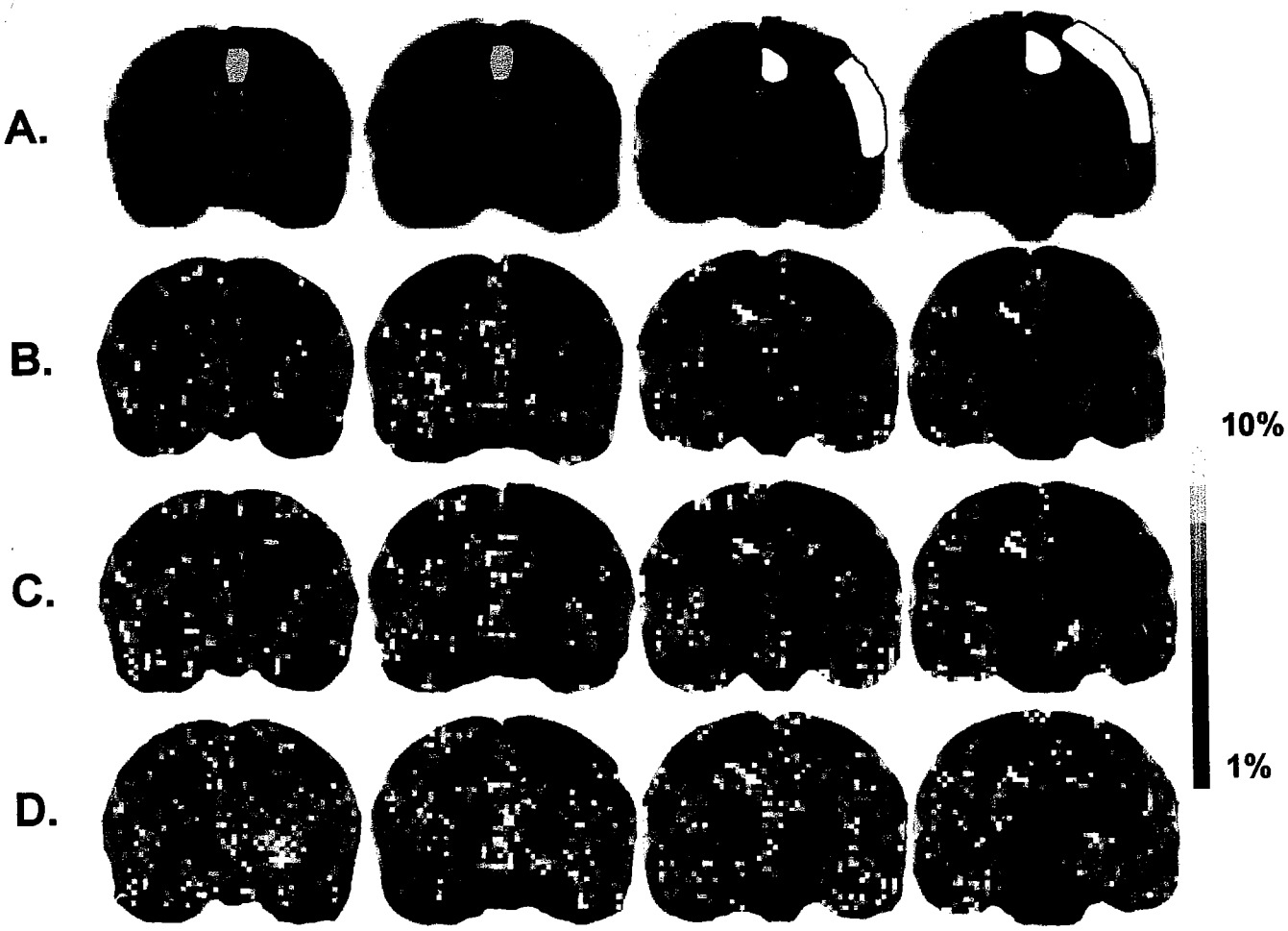

Figure 25. Activation maps of blood-oxygenation-level-dependent (BOLD) signal responses during absence seizure. The colored pixels indicate the statistically significant ($p<0.05$) pixels determined by t-test analysis and overlaid onto the corresponding anatomy. Four consecutive slices through the brain are shown for an individual marmoset. A) Anatomical images with ROIs used for analysis outlined according to the following color code - thalamus (blue), hippocampus (orange), frontal cortex (red), temporal cortex (purple), pre-central cortex (green), post-central cortex (yellow), anterior cingulate cortex (light blue), posterior cingulate cortex (white). B, C, D) Activation corresponding to images collected 16-21 min, 23-28 min, and 30-35 min following GBL injection, respectively.

on the left and right sides were initially analyzed separately and found to have statistically significant activations above baseline. Because all structures analyzed are bilateral and no significant differences were found between the right and left hemispheres, each marmoset included in the Figure 26 analysis consists of a combination of both hemispheres. As can be seen in Figure 26, significant positive BOLD signal changes were seen in all ROIs, at all time points, with the exception of the Hipp and aCg, where positive BOLD signal was non-significant at both the 16-21 min and 30-35 min time blocks. The control saline injection produced a minimal signal change of <2.0% in all ROIs except for Hipp and aCg, where the saline injection caused an average positive BOLD signal change of 2.0% to 3.5%. The most significant positive BOLD signal changes were found within the Thal, Te, PrC, and PoC.

The area of activation plot in Figure 27 shows the percentage of voxels activated out of the total voxel number (volume of the ROI). These results were averaged across all animals, for each time point. An increasing area of activation over time was seen in all ROIs except for the pCg, where there was little variation over time. Following the control injection of saline, the area of activation was <1.5% in all ROIs.

Figure 26

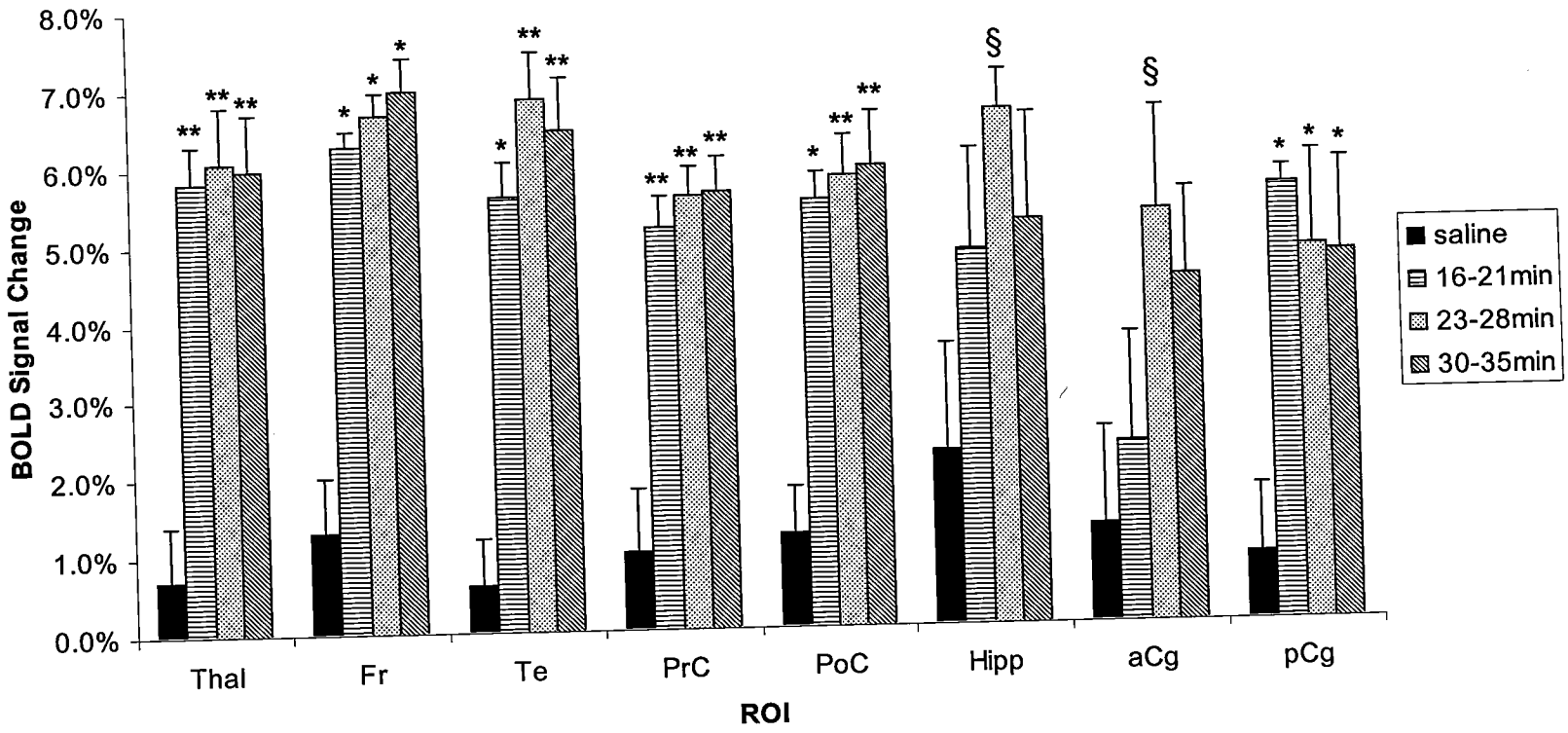
8.0%
7.0%
6.0%
5.0%
4.0%
3.0%
2.0%
1.0%
0.0%
BOLD Signal Change
Thal
Fr
Te
PrC
PoC
Hipp
aCg
pCg
ROI
saline
16-21min
23-28min
30-35min

Figure 26. Change in BOLD signal intensity for each ROI. The BOLD signal intensity change during 3 Hz SWDs is shown for cortical and subcortical ROIs (mean ± SEM, N=5 marmosets). Signal changes following the control injection for saline are shown, along with signal changes occurring 16-21 min, 23-28 min, and 30-35 min following the GBL injection. Time blocks with significantly different signal changes from the control injection are noted (§$P<0.05$, *$P<0.01$, **$P<0.001$). All ROIs are bilateral structures, so the signal changes from each hemisphere were combined. Thal, thalamus; Fr, frontal cortex; Te, temporal cortex; PrC, pre-central cortex; PoC, post-central cortex; Hipp, hippocampus; aCg, anterior cingulate cortex; pCg, posterior cingulate cortex.

Figure 27

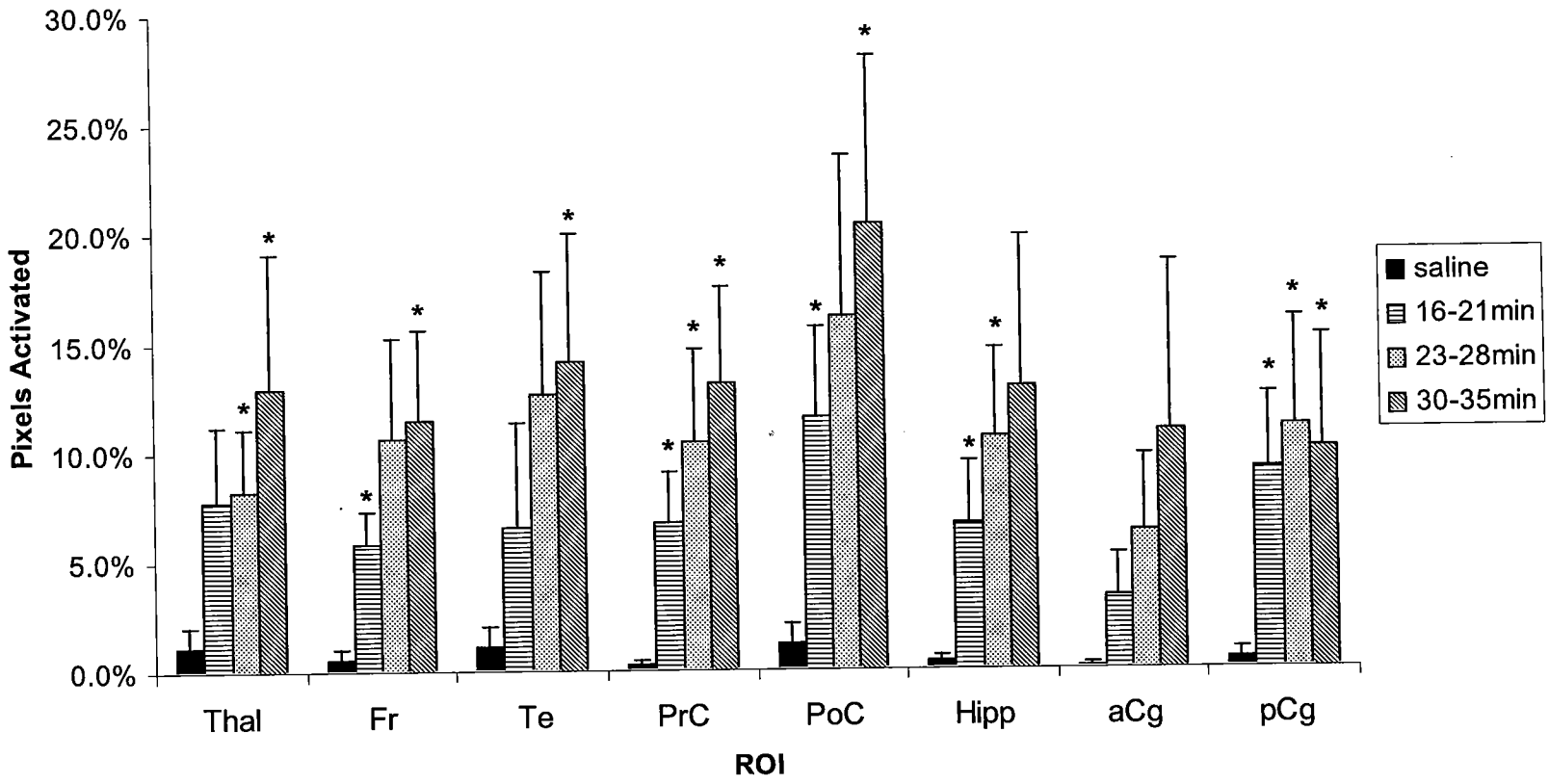
30.0%
25.0%
20.0%
15.0%
10.0%
5.0%
0.0%
Pixels Activated
Thal
Fr
Te
PrC
PoC
Hipp
aCg
pCg
ROI
saline
16-21min
23-28min
30-35min

Figure 27. Change in area of activation for each ROI. The area of activation during 3 Hz SWDs is shown for cortical and subcortical ROIs (mean ± SEM, N=5 marmosets). Area of activation following the control injection for saline is shown, along with the area of activation corresponding to 16-21 min, 23-28 min, and 30-35 min following the GBL injection. Time blocks with significantly different signal changes from the control injection are noted (*P<0.05). All ROIs are bilateral structures, so the signal changes from each hemisphere were combined. Thal, thalamus; Fr, frontal cortex; Te, temporal cortex; PrC, pre-central cortex; PoC, post-central cortex; Hipp, hippocampus; aCg, anterior cingulate cortex; pCg, posterior cingulate cortex.

Discussion

The data from the current study show GBL-induced generalized seizure in the common marmoset, is similar in EEG and behavioral alterations to human absence epilepsy. The GBL-induced SWDs appear similar those previously published for other animal models of absence seizures in non-human primates and felines. Fast FT shows that the frequency of SWDs in marmosets given GBL is 3 Hz, as is seen in humans. In addition, pre-treatment of marmosets with ehtosuximide, an antiepileptic drug used routinely to treat human absence, prevents the occurrence of the GBL-induced seizure. The specificity of ethosuximide in the treatment of absence seizures, supports the notion that the GBL-induced seizure is not unlike that experienced in humans.

The 3 Hz SWDs induced by GBL correlates with positive BOLD activation in the corticothalamic circuit. Many electrophysiology studies in rats implicate this circuit as being critical to the pathophysiology of absence epilepsy (19, 126-127, 135, 142-143). While the temporal resolution of BOLD fMRI is not comparable to that of electrophysiological recordings, functional imaging has the advantage of providing a global view of changes in brain activity. The current experiment demonstrates that this non-human primate model of generalized epilepsy correlates with positive BOLD signal changes that are bilateral, but heterogeneous as some brain areas are affected more than others. In addition, the area of activation increased with the duration of the seizure, indicating that

more brain area is being recruited for activation as the seizure progresses. Since typical absence seizures last seconds, the current model is more applicable to absence status epilepticus. While positive BOLD activation in the corticothalamic circuit correlates with electrophysiological recordings of structures contributing to SWD formation, the hippocampus, a structure where SWDs have not previously been recorded, showed positive BOLD signal in the current study (144-145). A possible explanation for this activation is that GHB, the active GBL metabolite, has a receptor that is most concentrated in the hippocampus of mammalian brains including the human and squirrel monkey (47). It is possible that a high level of GHB binding in the hippocampus could produce increased synaptic activity that correlates with positive BOLD measurements. Indeed many of the areas showing increased BOLD signal during absence seizures may be metabolically active but not electrically synchronized.

While no other fMRI studies of absence seizures in non-human primates have been reported, two recent studies have reported BOLD signal changes during 3 Hz SWDs in humans. The first was a case report of a single patient experiencing absence seizures in the scanner (83). The thalamus showed bilateral increases in BOLD signal intensity, while there was a predominance of negative BOLD over most of the cortex. A second study employed spike triggered fMRI to study BOLD activation during SWDs in five humans (84). Based on group analysis, positive BOLD signal was found within the pre-central sulcus, while negative BOLD was found within the posterior cingulate cortex.

Positive BOLD signal in the marmoset GBL model was also found in the pre-central cortex, but no negative BOLD signal was found in any brain area. In order to explore the negative BOLD response in the monkey model further, we decreased the pixel clustering and also the confidence interval used for creating the activation map, to see if the absence of negative BOLD was due to a lack of statistical power. The activation map in a few animals showed a few individual pixels of negative BOLD, which we do not believe to be significant findings.

Chapters 2 and 3 provided imaging data of absence seizures in fully conscious rats treated with GBL (123) and in the genetic strain of Wag/Rij rats showing spontaneous seizure activity (124). Both chemical and genetic models of absence seizures showed the same pattern of positive BOLD activation in the cortex and thalamus in the presence of 9 -11 Hz SWD. Marmosets given GBL showed the same anticipated bilateral corticothalamic activation; however, the EEG showed the prominent 3 Hz SWDs that are characteristic of human absence seizures. In addition, the clinically used antiabsence drug, ethosuximide, was able to prevent the GBL seizures from occurring in the marmosets. Thus the use of GBL in marmoset monkeys may hold promise as an animal model of human absence epilepsy. Since MRI is a non-invasive technology it is possible to carry out prospective studies following developmental changes in brain anatomy, function and chemistry in marmosets with a history of GBL-induced, prepubescent absence seizures.

CHAPTER V

Comprehensive Discussion

Rationale for Studies

An absence seizure is a brief, paroxysmal loss of consciousness that is associated with bilaterally synchronous 3 Hz SWDs recorded on an EEG. Even though the first description of this interesting epileptic condition appeared in 1705, many fundamental questions concerning its pathogenesis, pathophysiology, and psychological/neurological sequela are still unanswered (20). These questions remain largely unanswered for many reasons. The optimal way to understand any disease state is to study it within the human. Unfortunately, well controlled experiments in humans are difficult due to small patient populations, treatment medications which alter the seizure, and the ethical problems associated with invasive experimental procedures. Animal models of absence seizures provide a means of avoiding the above difficulties but the model should mimic, as closely as possible, the human condition.

The goal of this thesis was to develop an animal model of absence epilepsy that closely parallels the human condition and could be used to explore, non-invasively, the underlying mechanisms of absence seizures as well as the long-term psychosocial and cognitive effects of early repetitive seizures. Functional MRI was used to non-invasively monitor brain activity. This technique

allows one to measure neuronal activity in all brain structures simultaneously and correlate the results with seizure-related EEG changes.

Review of Findings

Overall Results

This dissertation began with the development of a pharmacological rat model of absence seizures for fMRI experimentation. A major disadvantage of this model, however, is that it produces acute, drug-induced seizures rather than spontaneous, chronic seizures. For this reason, a genetic rat model of absence epilepsy was then developed for fMRI. The inbred strain of rats, WAG/Rij, mimic the human condition better because they experience spontaneous, short, paroxysmal absence seizures. One way in which absences differ between humans and both of these rat models is that the SWD frequency in humans is classically 3 Hz while in rats it varies from 7 to 11 Hz.

Upon comparison of the BOLD activation patterns during absence seizures in the two rat models it was determined that both experienced activity within the same brain regions. This similarity between drug-induced and spontaneous seizures was significant because it warranted the use of the GBL drug in monkeys. Marmoset monkeys were found to model the human absence seizure condition better than other animals because GBL induced the formation of 3 Hz SWDs. In addition, the development of this non-human primate model is

important because it is phylogenetically closer to humans and amenable to psychosocial and cognitive evaluations that are more relevant than those obtained from rodents.

Review of Results from Chapter 2 (GBL Rat Model)

It was concluded from bench-top studies that 200 mg/kg of GBL was the optimal dose to use for fMRI experiments. This dosage caused absence-like behaviors and 7-8 Hz SWDs within four minutes, which lasted for 90-120 minutes. Preliminary fMRI experiments showed that anesthesia during imaging suppresses much of the BOLD signal that is present during a seizure in an unanesthetized animal. Functional MRI experiments revealed activation within the thalamus and cortex, bilaterally. The thalamus had a predominantly positive BOLD response within several nuclei previously shown to be electrically active during the seizure including the nRT and VPM/VPL. The sensory and parietal cortices, on the other hand, experienced simultaneous negative and positive BOLD responses. The motor and temporal cortices, in contrast, showed only a negative BOLD response. These fMRI results suggest that, while the EEG of absence seizures is generalized, neuronal activity, measured with the BOLD signal is preferentially focused within the thalamus and its corresponding cortex.

Review of Results from Chapter 3 (WAG/Rij Rat Model)

Based on the spontaneous incidence of EEG recordings in the WAG/Rij rat it was determined that animals 150-200 days old were best suited for fMRI studies. At this age the rats produced seizures of sufficient number and duration to make imaging with EEG-triggered fMRI a possibility. It was found that this technique could be used to image the brief, spontaneous absence seizures experienced by WAG/Rij rats. Positive BOLD signal was found throughout nuclei of the thalamus including the nRT, VPM/VPL, MD, and Po. In addition, positive BOLD signal was found throughout the cortex including the sensory, parietal, and temporal areas, but not within subcortical structures such as the hippocampus. No negative BOLD signal was found in any brain areas analyzed. The spontaneous seizures seem to result in brain activations similar to those induced by the GBL drug. This significant finding lends support to the development of a monkey GBL model of absence seizures that should be similar to seizures occurring spontaneously.

Review of Results from Chapter 4 (GBL Monkey Model)

As in the rat GBL studies, bench-top studies in the marmoset revealed that 200 mg/kg GBL was the appropriate dose for use in fMRI. In contrast to the rat model, however, GBL administration produced 3 Hz SWDs on EEG, similar to the human, which started 15 minutes after giving the drug and lasted for approximately 60 minutes. It was found that fMRI could be used to detect BOLD

signal changes in awake marmoset monkeys during 3 Hz SWDs. Positive BOLD activation was found to be present throughout corticothalamic structures. The hippocampus was also detected as an area with increased positive BOLD and it was hypothesized that this was due to the high level of GHB receptors in that region. No negative BOLD signal was detected during seizures in the marmosets. GBL-induced absence in marmosets appears to be a relevant model of human absence because the brain activation pattern is similar to spontaneous occurring seizures, has the same 3 Hz SWDs, and can be blocked with ethosuximide.

Working Hypothesis of Absence Seizures

Chapter one described the current working hypothesis used to explain the pathophysiology of absence seizures. The data presented in this thesis complement and add to what is known concerning the pathophysiology of these seizures. The BOLD fMRI results in the rat and monkey GBL models and the WAG/Rij rat model support the unifying hypothesis that SWDs are produced via reciprocally connected neurons in the thalamus and cortex. In all animal models used for fMRI, BOLD signal was found within specific thalamic nuclei and throughout the sensory and parietal cortices. These structures are similar to those that were implicated in previous electrophysiology experiments (20-21). One drawback of fMRI is the limited temporal resolution it provides when

compared with electrophysiology. Perhaps in the future, simultaneous fMRI and intracellular electrical recordings will be possible and therefore could be used to determine the initiation site and propagation patterns of the SWDs of absence seizures.

In terms of the development and validation of animal models of absence epilepsy, the data in this thesis contribute much to what is already known. The GBL and WAG/Rij rat models, which are used frequently by researchers, were further validated as models of human absence epilepsy by the expression of BOLD signal within the corticothalamic circuit. In addition, it was shown that the longer, drug-induced and shorter spontaneous seizures of these two rat models were similar in terms of their BOLD activation patterns and presumably their neuronal activity during SWD formation. This indicates that either model is equally useful for studying absence seizures although the WAG/Rij rats may be more suited to studying typical absence epilepsy and the GBL model more suited for absence status epilepticus, due to the length of the respective seizures.

The development of a non-human primate model with 3 Hz SWDs could contribute greatly to the neurobiologic understanding of absence seizures. The behavioral, EEG, and pharmacologic profile of the marmoset GBL model developed in this thesis indicates that it mimics the human epilepsy condition better than the rat models previously described. This monkey model may prove to be a significant tool for understanding the pathophysiology of 3 Hz SWDs and also the long-term effects of prolonged, repetitive absence seizures on the brain.

The unique characteristics of marmosets may allow long-term prospective studies of the neuropathologic, cognitive, and psychosocial changes associated with absence seizures that would be very difficult, if not impossible, to carry out in humans.

Impact of the Findings

The corticothalamic system of the brain plays a major role in the underlying pathophysiology of generalized absence epilepsy in humans, monkeys, rats, and mice. The specific areas of thalamus and cortex that are crucial for the initiation, propagation, and termination of the SWDs which characterize absence seizures are still unclear, in part because it has been difficult to couple the temporal resolution of a seizure with the spatial resolution needed to identify specific groups of neurons. In this dissertation I have developed and validated rat and monkey models of absence seizures that can be used for high field fMRI research. These data have been discussed in detail, but what is their potential benefit for ultimately treating absence epilepsy?

A great deal of interest has been recently shown in the development of implantable devices that can be used to stop seizures before they begin. These devices work by predicting seizure activity and halting it through the localized delivery of electrical stimulation or drug infusion. The data from the current thesis indicate that this type of treatment for absence epilepsy might be feasible

due to the fact that brain areas are focally, rather than generally activated during a seizure. It is critical to the success of this therapy that an initiation site for the seizures be determined. As fMRI technology progresses towards millisecond temporal resolution and microscopic spatial resolution it is quite possible that this technique could be used to "watch" the initiation and progression of an absence seizure in these animal models. Indeed researchers have recently demonstrated fMRI techniques that can be used to map sub-millimeter structures and to detect tens of millisecond neural activity (90, 152-153). This possibility warrants continued study.

Future Directions

Data presented in this dissertation provide several major avenues for the future study of absence epilepsy and the more severe case of absence status epilepticus. During typical absence status epilepticus the seizures are unremitting and last for hours and have been reported to occur in 10-30% of idiopathic generalized epilepsies with absences (154-155). The prognosis for "pure" childhood absence epilepsy is very favorable but tonic-clonic seizures appear in about 40% of all children with absence seizures as they grow into adolescence and early adulthood (3, 29, 156-159). This progression from absence alone to an absence/tonic-clonic profile in adolescence is particularly true in children with untreated absence status epilepticus. Indeed, generalized

tonic-clonic seizures may be present in 75-90% of patients with a history of childhood absence that persisted into adulthood (31, 157, 159). This continuum from early absence seizures to the more severe tonic-clonic seizures raises questions about the developmental pathophysiology of idiopathic generalized epilepsies. Do persistent, untreated absences in childhood lower the threshold of activation in epiletogenic neural circuits increasing the risk of generalized tonic-conic seizures in adolescence? Do persistent, untreated absence seizures in childhood alter long-term psychosocial and cognitive development?

Any neurological and psychological illness is a progressive, developmental problem. Outcomes in psychosocial behavior and cognition involve the interaction between brain and environment over the life of the individual. Controlled, prospective studies on the long-term pathophysiology of naturally occurring childhood absence seizures are not feasible. Initiating absence seizures in healthy children is unethical. Consequently, animal models, such as the marmoset monkey developed for this thesis are needed. Therefore, long-term cognitive and psychosocial effects of persistent absence seizures during the developmental period of non-human primates should be investigated with the use of the marmoset absence seizure model proposed in this thesis. Also, the ability of absence seizures to alter neural pathways and influence the development of convulsive, generalized seizures in marmosets should be evaluated.

In addition, in order to better understand the pathophysiology of absence seizures a well controlled fMRI study of these seizures in humans should be completed. Together, these future studies should contribute greatly to our understanding of the long-term effects of absence seizures in the nervous system and may shed additional light on the mechanism of the disease in the human.

Neuropathologic Effects of Absence Seizures

Absence in children may go undetected for long periods of time before treatment, but no reports of structural changes resulting from absence epilepsy have ever been published (3, 159). In this dissertation, however, I have shown that robust BOLD signal changes accompany these seizures and other studies have shown that absences alter cerebral blood flow and metabolism (78, 81-82). It is quite possible that neuro-structural changes associated with absence seizures may not be detected grossly, but rather they might be comprised of subtle changes in cell/receptor structure and functioning or synaptic alterations that predispose to more serious convulsive generalized seizures. It should be possible, through the use of quantitative high resolution MRI and MR spectroscopy (MRS), to monitor any subtle cellular damage resulting from repetitive absence seizures in marmosets. Quantitative MRI can be used to measure volumes of brain substructures as chronic absence seizures progress while MRS can be used to monitor GABA levels within the corticothalamic loop

and major brain metabolites that reflect neuronal cellular integrity. These include the neuronal axonal marker N-acetylaspartate (NAA), which putatively reflects neuronal viability and function. Also included are creatine, an important energy metabolite and constituent of all cells, chorine-containing compounds representing formation and degradation of products of cell membranes, myo-inosital as a marker of astrocytes, and glutamate the excitatory amino acid (160).

Indeed, there is evidence from human studies on generalized idiopathic epilepsy of a decrease in $GABA_A$ receptor binding that might reflect a state of microdysgenesis or cortical hyperexcitability (161-163). In order to study developmental changes in the brain in response to persistent absence seizures it should be possible to use non-invasive fMRI, quantitative MRI and MRS. It was previously reported that quantitative volumetric MRI could detect abnormalities in cortical and subcortical grey matter of subjects with a history of childhood absence epilepsy (164). Also, patients with idiopathic generalized epilepsy show a reduction in NAA levels and elevation in glutamate/glutamine levels in the frontal cortex (165). In another group of patients with idiopathic generalized epilepsy a reduction of NAA levels were found within the thalamus (166). These studies show that it is feasible to use quantitative MRI and MRS to identify neuroanatomical and chemical changes in the brain, associated with generalized seizures. Long-term neuropathologic studies may help to better understand the neurobiology of generalized idiopathic epilepsy.

BOLD fMRI of Absence Seizures in Humans

The technique of fMRI is readily translatable to humans, due to its non-invasive nature. Therefore, a logical extension of this dissertation would be to use fMRI to study absence seizures in humans. It would be important to have a well-controlled study that had age, sex, and syndrome matched patients. As the effects of anticonvulsants on the brain are not clearly understood, it would be important to employ a drug-free period or choose subjects early in the course of treatment. EEG-triggered fMRI could be used acquire images related to the spontaneous seizures and techniques, such as hyperventilation and sleep deprivation, could be used to increase the number of seizures experienced in an imaging session as have been used in other studies (167-168). The BOLD activation map of humans during absence seizures would add to our understanding of the mechanisms underlying this disorder and help to further validate the marmoset model presented in this dissertation.

Final Comments

In this dissertation I have presented a monkey model of absence epilepsy that may be useful in determining the underlying mechanism of absences and the long-term effects of these seizures on the developing brain. In addition, I have shown that functional MRI can be used to detect brain activation associated with absence seizures in rat and monkey models. The non-invasive nature of this

technique lends itself to use in humans. It is my hope that, by developing and validating animal models of absence epilepsy that can be used for fMRI, these data may provide insight into the pathophysiology and treatment of this and other epilepsy conditions.

CHAPTER VI

References

1. Annegers JF. The epidemiology of epilepsy. In: Wyllie E, ed. The treatment of epilepsy: principles and practice. 3rd ed. Philadelphia: Lippincott Williams & Wilkins, 2001: 131-8.
2. Benbadis SR. Epileptic seizures and syndromes. *Neurol Clin* 2001;19:251-70.
3. Panayiotopoulos CP. Absence Epilepsies. In: Engel JJ, Pedley TA, eds. Epilepsy: a comprehensive textbook. Philadelphia: Lippincott-Raven Publishers, 1997. 2327-2346.
4. Berkovic SF, Howell RA, Hay DA, Hopper JL. Epilepsies in twins: genetics of the major epilepsy syndromes. *Ann Neurol* 1998;43:435-45.
5. Crunelli V, Leresche N. Childhood absence epilepsy: genes, channels, neurons, and networks. *Nat Rev Neurosci* 2002;3:371-82.
6. Steriade M, Gloor P, Llinas RR, Lopes de Silva FH, Mesulam MM. Basic mechanisms of cerebral rhythmic activities. *Electroencephalogr Clin Neurophysiol* 1990;76:481-508.
7. Steriade M, Llinas RR. The functional states of the thalamus and the associated neuronal interplay. *Physiol Rev* 1988;68:649-742.
8. Steriade M, McCormick DA, Sejnowski TJ. Thalamocortical oscillations in the sleeping and aroused brains. *Science* 1993;262:679-85.

9. Jones EG. The thalamus. New York: Plenum, 1985.

10. Paxinos G and Watson C. The Rat Brain in Stereotaxic Coordinates. San Diego: Academic Press, 1998.

11. McCormick DA, von Krosigk M. Corticothalamic activation modulates thalamic firing through activation of glutamate metabotropic receptors. *Proc Natl Acad Sci USA* 1992;89:2774-8.

12. Bal T, McCormick DA. Mechanisms of oscillatory activity in guinea pig nucleus reticularis thalami in vitro: a mammalian pacemaker. *J Physiol* 1993;468:669-91.

13. Steriade M, Domich L, Oakson G. Reticularis thalami neurons revisited: activity changes during shifts in states of vigilance. *J Neurosci* 1986;6:68-81.

14. Contreras D, Dossi RC, Steriade M. Electrophysiological properties of cat reticular thalamic neurons in vivo. *J Physiol* 1993;470:273-94.

15. von Krosigk M, Bal T, McCormick DA. Cellular mechanisms of a synchronized oscillation in the thalamus. *Science* 1993;261:361-4.

16. Coulter DA, Huguenard JR, Prince DA. Differential effects of petit mal anticonvulsants and convulsants on thalamic neurons: calcium current reduction. *Br J Pharmacol* 1990;100:800-5.

17. Jasper HH and Droogleever-Fortuynn J. Experimental studies on the functional anatomy of petit epilepsy. *Res Publ Assoc Nerv Ment Dis* 1947;26:272-298.

18. Williams D. A study of thalamic and cortical rhythms in petit mal. *Brain* 1953;76:50-69.

19. Meeren H, Pijn J, Luijtelaar E, Coenen A, Lopes da Silva F. Cortical focus drives widespread corticothalamic networks during spontaneous absence seizures in rats. *J Neurosci* 2002;22:1480-95.

20. Snead OC. Basic mechanisms of generalized absence seizures. *Ann Neurol* 1995;37:146-157.

21. Seidenbecher T, Staak R, Pape HC. Relations between cortical and thalamic cellular activities during absence seizures in rats. *Eur J Neurosci* 1998;10:1103-1112.

22. Micheletti G, Warter JM, Marescaux C, Depaulis A, Tranchant C, Rumbach C, Vergnes M. Effects of drugs affecting noradrenergic neurotransmission in rats with spontaneous petit mal-like seizures. *Eur J Pharmacol* 1987;135:397-402.

23. Warter JM, Vergnes M, Depaulis A, Tranchant C, Rumbach L, Micheletti G, Marescaux C. Effects of drugs affecting dopaminergic neurotransmission in rats with spontaneous petit mal-like seizures. *Neuropharmacology* 1988;27:269-74.

24. Danober L, Depaulis A, Marescaux C, Vergnes M. Effects of cholinergic drugs on genetic absence seizures in rats. *Eur J Pharmacol* 1993;234:263-8.

25. Coulter DA, Huguenard JR, Prince DA. Characterization of ethosuximide reduction of low-threshold calcium current in thalamic neurons. *Ann Neurol* 1989;25:582-93.

26. Winterer G. Valproate and GABAergic system effects. *Neuropsychopharmacology* 2003;28:2050-1.

27. Manning JA, Richards DA, Bowery NG. Pharmacology of absence epilepsy. *Trends Pharmacol Sci* 2003;24:542-9.

28. Mattson RH. Overview: idiopathic generalized epilepsies. *Epilepsia* 2003;44(Suppl 2):2-6.

29. Dieterich E, Baier WK, Doose H, Tuxhorn I, Fichsel H. Longterm follow-up of childhood epilepsy with absences. I. Epilepsy with absences at onset. *Neuropediatrics* 1985;16:149-54.

30. Loiseau P, Duche B, Pedespan JM. Absence epilepsies. *Epilepsia* 1995;36:1182-6.

31. Panayiotopoulus CP. Treatment of typical absence seizures and related epileptic syndromes. *Paedriatr Drugs* 2001;3:379-403.

32. Wirrell EC, Camfield CS, Dooley JM, Gordon KE. Long-term prognosis of typical childhood absence epilepsy: remission or progression to juvenile myoclonic epilepsy. *Neurology* 1996;47:912-18.

33. Olsson I, Campenhausen G. Social adjustment in young adults with absence epilepsies. *Epilepsia* 1993;34:846-51.

34. Wirrell EC, Camfield CS, Camfield PR, Dooley JM, Gordon KE, Smith B. Long-term psychosocial outcome in typical absence epilepsy. *Arch Pediatr Adolesc Med* 1997;151:152-8.

35. Sato S, Dreifuss FE, Penry K, Kirby DD, Palesch Y. Long-term follow-up of absence seizures. *Neurology* 1983;33:1590-1595.

36. Pavone P, Bianchini R, Trifiletti RR, Incorpora G, Pavone A, Parano E. Neuropsychological assessment in children with absence epilepsy. *Neurology* 2001;56:1047-51.

37. Snead OC, Depaulis A, Vergnes M, Marescaux C. Absence epilepsy: advances in experimental animal models. *Adv Neurol* 1999;79:253-78.

38. Fariello RG, Golden GT. The THIP-induced model of bilateral synchronous spike and wave in rodents. *Neuropharmacology* 1987;26:161-5.

39. Snead OC. γ-hydroxybutyrate model of generalized absence seizures: further characterization and comparison with other absence models. *Epilepsia* 1988;29:361-68.

40. Prince D, Farrell D. "Centrecephalic" spike wave discharges following parenteral penicillin injection in the cat. *Neurology* 1969;19:309-10.

41. Vickers MD. Gamma hydroxybutyric acid. *Int Anesthesiol Clin* 1969;7:75-9.

42. Wong CG, Gibson KM, Snead OC. From the street to the brain: neurobiology of the recreational drug γ-hydroxybutyric acid. *Trends Pharmacol Sci* 2004;25:29-34.

43. Freese TE, Miotto K, Reback CJ. The effects and consequences of selected club drugs. *J Subst Abuse Treat* 2002;23:151-6.

44. Smith KM, Larive LL, Romanelli F. Club drugs: methylenedioxymethamphetamine, flunitrazepam, ketamine hydrochloride, and gamma-hydroxy-butyrate. *Am J Health Syst Pharm* 2002;59:1067-76.

45. Maitre M. The gamma-hydroxybutyrate signaling system in brain: organization and functional implications. *Prog Neurobiol* 1997;51:337-61.

46. Hogema BM, Gupta M, Senephansiri H, et al. Pharmacological rescue of lethal seizures in mice deficient in succinate semialdehyde dehydrogenase. *Nat Genet* 2001;29:212-6.

47. Castelli MP, Mocci I, Langlois X, Gommerendagger W, Luyten WH, Leysen JE, Gessa GL. Quantitative autoradiographic distribution of gamma-hydroxybutyric acid binding sites in human and monkey brain. *Brain Res Mol Brain Res* 2000;78:91-9.

48. Hu RQ, Banerjee PK, Snead OC. Regulation of gamma-aminobutyric acid (GABA) release in cerebral cortex in the gamma-hydroxybutyric acid (GHB) model of absence seizures in rat. *Neuropharmacology* 2000;39:427-39.

49. Snead OC. Gamma hydroxybutyrate in the monkey. II. Effect of chronic oral anticonvulsant drugs. *Neurology* 1978;28:643-8.

50. Snead OC. Evidence for GABAB-mediated mechanisms in experimental generalized absence seizures. *Eur J Pharmacol* 1992;213:343-9.

51. Colombo G, Agabio R, Lobina C, Reali R, Gessa GL. Involvement of GABA(A) and GABA(B) receptors in the mediation of discriminative stimulus effects of gamma-hydroxybutyric acid. *Physiol Behav* 1998;64:293-302.

52. Snead OC. Antiabsence seizure activity of specific GABAB and gamma-hydroxybutyric acid receptor antagonists. *Pharmacol Biochem Behav* 1996;53:73-9.

53. Bearden LJ, Snead OC, Healy CT, Pegram GV. Antagonism of gamma-hydroxybutyrate induced frequency shifts in the cortical EEG of rats by dipropylacetate. *Electroencephalogr Clin Neurophysiol* 1980;49:181-3.

54. Mason PE, Kerns WP. Gamma hydroxybutyric acid (GHB) intoxication. *Acad Emerg Med* 2002;9:730-9.

55. Gervasi N, Monnier Z, Vincent P, Paupardin-Tritsch D, Hughes SW, Crunelli V, Leresche N. Pathway-specific action of gamma-hydroxybutyric acid in sensory thalamus and its relevance to absence seizures. *J Neurosci* 2003;23:11469-78.

56. Banerjee PK, Snead OC. Presynaptic gamma-hydroxybutyric acid (GHB) and gamma-aminobutyric acid (GABAB) receptor-mediated release of GABA and glutamate (GLU) in rat ventrobasal nucleus (VB): a possible mechanism for the generation of absence-like seizures induced by GHB. *J Pharmacol Exp Ther* 1995;273:1534-43.

57. Festing MF. *Inbred strains in biomedical research*. London: MacMillan Press, 1979:267-96.

58. van Luijtelaar ELMJ, Coenen AM. Two types of electrocortical paroxysms in an inbred strain of rats. *Neurosci Lett* 1986;70:393-7.

59. Coenen AM, Drinkenburg WH, Inoue M, van Luijtelaar ELMJ. Genetic models of absence epilepsy, with emphasis on the WAG/Rij strain of rats. *Epilepsy Res* 1992;12:75-86.

60. Coenen AM, van Luijtelaar ELMJ. The WAG/Rij rat model for absence epilepsy: age and sex factors. *Epilepsy Res* 1987;1:297-301.

61. Coenen AM, van Luijtelaar ELMJ. Genetic animal models for absence epilepsy: a review of the WAG/Rij strain of rats. *Behav Genet* 2003;33:635-55.

62. Peeters BW, van Rijn CM, Vossen JM, Coenen AM. Effects of GABA-ergic agents on spontaneous non-convulsive epilepsy, EEG and behavior, in the WAG/Rij inbred strain of rats. *Life Sci* 1989;45:1171-6.

63. van Luijtelaar EMJL, Coenen AM. Circadian rhythmicity in absence epilepsy in rats. *Epilepsy Res* 1988;2:331-6.

64. de Bruin NM, van Luijtelaar ELMJ, Cools AR, Ellenbroek BA. Dopamine characteristics in rat genotypes with distinct susceptibility to epileptic activity: apomorphine-induced stereotyped gnawing and novelty/ amphetamine-induced locomotor stimulation. *Behav Pharmacol* 2001;12:517-25.

65. Inoue M, Duysens J, Vossen JM, Coenen AM. Thalamic multiple-unit activity underlying spike-wave discharges in anesthetized rats. *Brain Res* 1993;612:35-40.

66. Midzianovskaia IS, Kuznetsova GD, Coenen AM, Spiridonov AM, van Luijtelaar ELMJ. Electrophysiological and pharmacological characteristics of two types of spike-wave discharges in WAG/Rij rats. *Brain Res* 2001;911:62-70.

67. D'Arcangelo G, D'Antuono M, Biagini G, Warren R, Tancredi V, Avoli M. Thalamocortical oscillations in a genetic model of absence seizures. *Eur J Neurosci* 2002;16:2383-93.

68. Meeren HK, Pijn HP, van Luijtelaar ELMJ, Coenen AM, Lopes da Silva FH. Cortical focus drives widespread corticothalamic networks during spontaneous absence seizures in rats. *J Neurosci* 2002;22:1480-95.

69. Dwyer BE, Fujikawa DG, Wasterlain CG. Metabolic anatomy of generalized bicuculline seizures in the newborn marmoset monkey. *Exp Neurol* 1986;94:213-227.

70. Fujikawa DG, Dwyer BE, Wasterlain CG. Preferential blood flow to brainstem during generalized seizures in the newborn marmoset monkey. *Brain Res* 1986;397:61-72.

71. Fujikawa DG, Vannucci RC, Dwyer BE, Wasterlain CG. Generalized seizures deplete brain energy reserves in normoxemic newborn monkeys. *Brain Res* 1988;454:51-9.

72. Fujikawa DG, Dwyer BE, Lake RR, Wasterlain CG. Local cerebral glucose utilization during status epilepticus in newborn primates. *Am J Physiol* 1989;256:1160-7.

73. Gunderson VM, Dubach M, Szot P, Born DE, Wenzel HJ, Maravilla KR, Zierath DK, Robbins CA, Schwartzkroin PA. Development of a model of status epilepticus in pigtailed macaque infant monkeys. *Dev Neurosci* 1999;21:352-64.

74. Snead OC. Gamma hydroxybutyrate in the monkey. I. Electroencephalographic, behavioral, and pharmacokinetic studies. *Neurology* 1978;28:636-42.

75. David J, Marathe SB, Patil SD, Grewal RS. Arrest reaction with concomitant spike and wave afterdischarge following thalamic stimulation in conscious juvenile monkeys with $Al(OH)_3$ focal premotor regions. *Ind J Physiol Pharmac* 1981;25:209-18.

76. Snead OC. Gamma hydroxybutyrate in the monkey. II. Effect of intravenous anticonvulsant drugs. *Neurology* 1978;28:1173-8.

77. Stevenson M. The common marmoset (*Callathrix jacchus jacchus*) as a model for ethological research. *Lab Anim Sci* 1977;27:895-900.

78. Yeni SN, Kabasakal L, Yalcinkaya C, Nisli C, Dervent A. Ictal and interictal SPECT findings in childhood absence epilepsy. *Seizure* 2000;9:265-9.

79. DeSimone R, Silvestrini M, Marciani MG, Curatolo P. Changes in cerebral blood flow velocities during childhood absence seizures. *Pediatr Neurol* 1998;18:132-5.

80. Nehlig A, Wergnes M, Waydelich R, Hirsch E, Charbonne R, Marescaux C, Seylaz J. Absence seizures induce a decrease in cerebral blood flow: human and animal data. *J Cereb Blood Flow Metab* 1996;16:147-55.

81. Engel J, Lubens O, Kuhl DE, Phelps ME. Local cerebral metabolic rate for glucose during petit mal absences. *Ann Neurol* 1985;17:121-8.

82. Prevett MC, Duncan JS, Jones T, Fish DR, Brooks DJ. Demonstration of thalamic activation during typical absence seizures using H2(15)O and PET. *Neurology* 1995;45:1396-402.

83. Salek-Haddadi A, Lemieux L, Merschhemke M, Friston KJ, Duncan JS, Fish DR. Functional magnetic resonance imaging of human absence seizures. *Ann Neurol* 2003;53:663-7.

84. Archer JS, Abbott DF, Waites AB, Jackson GD. fMRI "deactivation" of the posterior cingulated during generalized spike and wave. *Neuroimage* 2003;20:1915-22.

85. Ogawa S, Lee TM, Nayak AS, Glynn P. Oxygenation-sensitive contrast in magnetic resonance image of rodent brain at high magnetic fields. *Magn Reson Med* 1990;14:68-78.

86. Ogawa S, Tank DW, Menon R, Ellermann JM, Kin SG, Merkle H, Ugurbil K. Intrinsic signal changes accompanying sensory stimulation: functional brain

mapping with magnetic resonance imaging. *Proc Natl Acad Sci USA* 1992;89:5951-5.

87. Ogawa S, Menon RS, Tank DW, Kim SG, Merkle H, Ellermann JM, Ugurbil K. Functional brain mapping by blood oxygenation level-dependent contrast magnetic resonance imaging. A comparison of signal characteristics with a biophysical model. *Biophys J* 1993;64:803-12.
88. Kwong KK, Belliveau JW, Chesler DA, et al. Dynamic magnetic resonance imaging of human brain activity during primary sensory stimulation. *Proc Natl Acad Sci USA* 1992;89:5675-9.
89. Bandettini PA, Wong EC, Hinks RS, Tikofsky RS, Hyde JS. Time course EPI of human brain function during task activation. *Magn Reson Med* 1992;25:390-7.
90. Logothetis NK, Pauls J, Augath M, Trinath T, Oeltermann A. Neurophysiological investigation of the basis of the fMRI signal. *Nature* 2001;412:150-7.
91. Jackson GD, Connelly A, Cross JH, Gordon I, Gadian DG. Functional magnetic resonance imaging of focal seizures. *Neurology* 1994;44:850-6.
92. Detre JA, Sirven JI, Alsop DC, O'Conner MJ, French JA. Localization of subclinical ictal activity by functional magnetic resonance imaging: correlation with invasive monitoring. *Ann Neurol* 1995;38:618-24.
93. Warach S, Ives JR, Schlaug G, et al. EEG-triggered echo-planar functional MRI in epilepsy. *Neurology* 1996;47:89-93.

94. Allen PJ, Polizzi G, Krakow K, Fish DR, Lemieux L. Identification of EEG events in the MR scanner: the problem of pulse artifact and a method for its subtraction. *Neuroimage* 1998;8:229-39.

95. Goldmann RI, Stern JM, Engel J, Cohen MS. Acquiring simultaneous EEG and functional MRI. *Clin Neurophysiol* 2000;111:1974-80.

96. Lemieux L, Salek-Haddadi A, Josephs O, et al. Event-related fMRI with simultaneous and continuous EEG: description of the method and initial case report. *Neuroimage* 2001:14:780-7.

97. Benar C, Aghakhani Y, Wang Y, Izenberg A, Al-Asmi A, Dubeau F, Gotman J. Quality of EEG in simultaneous EEG-fMRi for epilepsy. *Clin Neurophysiol* 2003;114:569-80.

98. Ives JR, Warach S, Schmitt F, Edelmann RR, Schomer DL. Monitoring the patient's EEG during echo planar MRI. *Electroencephalgr Clin Neurophysiol* 1993;87:417-20.

99. Krakow K, Allen PJ, Lemieux L, Symms MR, Fish DR. Methodology: EEG correlated fMRI. *Adv Neurol* 2000;83:187-201.

100. Schomer DL, Bonmassar G, Lazeyras F, et al. EEG-linked functional magnetic resonance imaging in epilepsy and cognitive neurophysiology. *J Clin Neurophysiol* 2000;17:43-58.

101. Hill RA, Chiappa KH, Huang-Hellinger F, Jenkins BG. EEG during MR imaging: differentiation of movement artifact from paroxysmal cortical activity. *Neurology* 1995;45:1942-3.

102. Lemieux L, Allen PJ, Franconi F, Symms MR, Fish DR. Recording of EEG during fMRI experiments: patient safety. *Magn Reson Med* 1997;38:943-52.

103. Krakow K, Woermann FG, Symms MR, et al. EEG-triggered functional MRI of interictal epileptiform activity in patients with partial seizures. *Brain* 1999;122:1679-88.

104. Krakow K, Lemieux L, Messina D, Scott CA, Symms MR, Duncan JS, Fish DR. Spatio-temporal imaging of focal interictal epileptiform activity using EEG-triggered functional MRI. *Epileptic Disord* 2001;3:67-74.

105. Krakow K, Messina D, Lemieux L, Duncan JS, Fish DR. Functional MRI activation of individual interictal epileptiform spikes. *Neuroimage* 2001;13:502-5.

106. Archer JS, Briellmann RS, Sygeniotis A, Abbott DF, Jackson GD. Spike-triggered fMRI in reading epilepsy: involvement of left frontal cortex working memory area. *Neurology* 2003;60:415-21.

107. Archer JS, Briellmann RS, Abbott DF, Sygeniotis A, Wellard RM, Jackson GD. Benign epilepsy with centro-temporal spikes: spike triggered fMRI shows somatosensory cortex activity. *Epilepsia* 2003;44:200-4.

108. Seeck M, Lazeyras F, Michel CM, et al. Non-invasive epileptic focus localization using EEG-triggered functional MRI and electromagnetic tomography. *Electroencephalogr Clin Neurophysiol* 1998;106:508-12.

109. Patel MR, Blum A, Pearlman JD, et al. Echo-planar functional MRI imaging of epilepsy with concurrent EEG monitoring. *Am J Neuroradiol* 1999;20:1916-9.

110. Symms MR, Allen PJ, Woermann FG, et al. Reproducible localization of interictal epileptiform discharges using EEG-triggered fMRI. *Phys Med Biol* 1999;44:N161-8.

111. Rosen BR, Buckner RL, Dale AM. Event-related functional MRI: past, present, and future. *Proc Natl Acad Sci USA* 1998;95:773-80.

112. Dubowitz DJ, Chen DY, Atkinson DJ, et al. Functional magnetic resonance imaging in macaque cortex. *Neuroreport* 1998;9:2213-8.

113. Dubowitz DJ, Chen DY, Atkinson DJ, et al. Direct comparison of visual cortex in human and non-human primates using functional magnetic resonance imaging. *J Neurosci Methods* 2001;107:71-80.

114. Lahti KM, Ferris CF, Li F, Sotak CH, King JA. Imaging brain activity in conscious animals using functional MRI. *J Neurosci Methods* 1998;82:75-82.

115. Logothetis NK, Guggenberger H, Peled S, Pauls J. Functional imaging of the monkey brain. *Nat Neurosci* 1999;2:555-62.

116. Zhang Z, Andersen AH, Avison MJ, Gerhardt GA, Gash DM. Functional MRI of apomorphine activation of the basal ganglia in awake rhesus monkeys. *Brain Res* 2000;852:290-6.

117. Zhang Z, Andersen AH, Grondin R, Barber T, Avison R, Gerhardt G, Gash D. Pharmacological MRI mapping of age-associated changes in basal ganglia circuitry of awake rhesus monkeys. *Neuroimage* 2001;14:1159-67.

118. Ferris CF, Snowden CT, King JA, et al. Functional imaging of brain activity in conscious monkeys responding to sexually arousing cues. *Neuroreport* 2001;12:2231-6.

119. Ferris CF, Snowden CT, King JA, et al. Activation of neural pathways associated with sexual arousal in non-human primates. *J Magn Reson Imaging* 2004;19:168-75.

120. Brevard ME, Duong TQ, King JA, Ferris CF. Changes in MRI signal intensity during hypercapnic challenge under conscious and anesthetized conditions. *Magn Reson Imaging* 2003;21:995-1001.

121. Khubchandani M, Mallick HN, Jagannathan NR, Mohan Kumar V. Stereotaxic assembly and procedures for simultaneous electrophysiological and MRI study of conscious rat. *Magn Reson Med* 2003;49:962-7.

122. Sicard K, Shen Q, Brevard ME, Sullivan R, Ferris CF, King JA, Duong TQ. Regional cerebral blood flow and BOLD responses in conscious and anesthetized rats under basal and hypercapnic conditions: implications for functional MRI studies. *J Cereb Blood Flow Metab* 2003;23:472-81.

123. Tenney JR, Duong TQ, King JA, Ludwig R, Ferris CF. Corticothalamic modulation during absence seizures in rats: a functional MRI assessment. *Epilepsia* 2003;44:1133-40.

124. Tenney JR, Duong TQ, King JA, Ferris CF. fMRI of brain activation in a genetic rat model of absence seizures. *Epilepsia* 2004;45:1-6.

125. Ludwig R, Bodgdanov G, King J, Allard A, Ferris CF. A dual RF resonator system for high field functional magnetic resonance imaging of small animals. *J Neurosci Methods* 2004;132:125-35.

126. Avanzini G, Vergnes M, Spreafico R, Marescaux C. Calcium-dependent regulation of genetically determined spike and waves by the RTN of rats. *Epilepsia* 1993;34:1-7.

127. Avanzini G, Panzica F, de Curtis M. The role of the thalamus in vigilance and epileptogenic mechanisms. *Clin Neurophysiol* 2000;111:S19-26.

128. King JA, Brevard ME, Messenger TL, Duong TQ, Ferris CF. Evaluation of acclimation of conscious rats for magnetic resonance imaging studies. *Behav Brain Res* 2003;submitted.

129. Strupp JP. Stimulate: a GUI based fMRI analysis software package. *Neuroimage* 1996;3:S607.

130. el-Beheiry H, Puil E. Anesthetic depression of excitatory synaptic transmission in neocortex. *Exp Brain Res* 1989;77:87-93.

131. Richards CD. On the mechanism of barbiturate anesthesia. *J Physiol* 1972;227:749-67.

132. Richards CD. On the mechanism of halothane anesthesia. *J Physiol* 1973;233:439-56.

133. Richards CD, Strupinski K. An analysis of the action of pentobarbitone on the excitatory post-synaptic potentials and membrane properties of neurons in the guinea-pig olfactory cortex. *Br J Pharmacol* 1986;89:321-5.

134. Richards CD, White AE. The actions of volatile anesthetics on synaptic transmission in the dentate gyrus. *J Physiol* 1975;252:241-57.

135. Banerjee PK, Snead OC. Thalamic mediodorsal and intralaminar nuclear lesions disrupt the generation of experimentally induced generalized absence-like seizures in rats. *Epilepsy Res* 1994;17:193-205.

136. Pohl M, Mares P, Langmeier M. Localization of the origin of self-sustained afterdischarges (SSADs) in the rat: the spike and wave type of SSAD. *Epilepsia* 1986;27:516-22.

137. Hill RA, Chiappa KH, Huang-Hellinger F, Jenkins BG. Hemodynamic and metabolic aspects of photosensitive epilepsy revealed by functional magnetic resonance imaging and magnetic resonance spectroscopy. *Epilepsia* 1999;40:912-20.

138. Wolfson LI, Sakurada O, Sokoloff L. Effects of γ-butyrolactone on local cerebral glucose utilization in the rat. *J Neurochem* 1977;29:777-83.

139. Theodore WH, Brooks R, Margolin R, et al. Positron emission tomography in generalized seizures. *Neurology* 35:684-90.

140. Ochs RF, Gloor P, Tyler JL, et al. Effect of generalized spike-and-wave discharge on glucose metabolism measured by positron emission tomography. *Ann Neurol* 1987;21:458-64.

141. Iannetti P, Spalice A, De Luca F, Boemi S, Festa A, Maini CL. Ictal signle photon emission computed tomography in absence seizures: apparent implication of different neuronal mechanisms. *J Child Neurol* 2001;16:339-44.

142. Vergnes M, Marescaux C. Cortical and thalamic lesions in rats with genetic absence epilepsy. *J Neural Transm* 1992;35:71-83.

143. Seidenbecher T, Staak R, Pape HC. Relations between cortical and thalamic cellular activities during absence seizures in rats. *Eur J Neurosci* 1998;10:1103-12.

144. Vergnes M, Marescaux C, Depaulis A, Micheletti G, Warter JM. Spontaneous spike and wave discharges in thalamus and cortex in a rat model of genetic petit mal-like seizures. *Exp Neurol* 1987;96:127-36.

145. Vergnes M, Marescaux C, Depaulis A. Mapping of spontaneous spike and wave discharges in Wistar rats with genetic generalized non-convulsive epilepsy. *Brain Res* 1990;523:87-91.

146. Nehlig A, Vergnes M, Marescaux C, Boyet S. Mapping of cerebral energy metabolism in rats with genetic generalized nonconvulsive epilepsy. *J Neural Transm* 1992;35:141-53.

147. Blumenfeld H. From molecules to networks:cortical/subcortical interactions in the pathophysiology of idiopathic generalized epilepsy. *Epilepsia* 2003;44:7-15.

148. Holland KD. Efficacy, pharmacology, and adverse effects of antiepileptic

drugs. *Neurol Clin* 2001;19:313-45.

149. Stephan H, Baron G, Schwerdtfeger WK. The brain of the common marmoset (*Callathrix jacchus*). New York, NY: Springer-Verlag Press, 1980.

150. Martin RF, Bowden DM. Primate brain maps: Structure of the macaque brain. New York, NY: Elsevier Press, 2000.

151. Marcus EM, Watson CM. Bilateral synchronous spike wave electrographic patterns in the cat. *Arch Neurol* 1966;14:601-10.

152. Kim SG, Ogawa S. Insights into new techniques for high resolution functional MRI. *Curr Opin Neurobiol* 2002;12:607-15.

153. Ogawa S, Lee TM, Stepnoski R, Chen W, Zhu XH, Ugurbil K. An approach to probe some neural systems interaction by functional MRI at neural time scale down to milliseconds. *Proc Natl Acad Sci USA* 2000;97:11026-31.

154. Livingston J. Status Epilepticus: In Wallace S, ed. *Epilepsy in Children*. London: Chapman and Hall Medical, 1996.

155. Agathonikou A, Panayiotopoulos CP, Giannakodimos S, Koutroumanidis. Typical absence status in adults: diagnostic and syndromic considerations. *Epilepsia* 1998;39:1265-76.

156. Livingston S, Torres I, Pauli LL, Rider RV. Results of a prolonged follow-up study of 117 patients. *JAMA* 1965;194:113-8.

157. Charlton MH, Yahr MD. Long-term follow-up of patients with petit mal. *Arch Neurol* 1967;16:595-8.

158. Drury I, Dreifuss FE. Pyknoleptic petit mal. *Acta Neurol Scand* 1985;72:353-62.

159. Loiseau P, Douche B. In: *Typical absences and related epileptic syndromes*. Duncan Js, Panayiotopoulos CP, eds. London: Churchill Livingston Press, 1995.

160. Birken DL, Oldendorf WH. N-acetyl-L-aspartic acid: a literature review of a compound prominent in 1H-NMR spectroscopy studies of the brain. *Neurosci Biobehav Rev* 1989;13:23-31.

161. Meencke HJ, Janz D. Neuropathologic findings in primary generalized epilepsy: a study of eight cases. *Epilepsia* 1984;25:8-21.

162. Koepp MJ, Richardson MP, Brooks DJ, Cunningham VJ, Duncan JS. Central benzodiazepine / gamma-aminobutyric acid A receptors in idiopathic generalized epilepsy: an [11C]flumazenil positron emission tomography study. *Epilepsia* 1997;38:1089-97.

163. Roper SN, Yachnis AT. Cortical dysgenesis and epilepsy. *Neuroscientist* 2002;8:356-71.

164. Woermann FG, Sisodiya SM, Free SL, Duncan JS. Quantitative MRI in patients with idiopathic generalized epilepsy. *Brain* 1998;121:1661-7.

165. Simister RJ, McLean MA, Barker GJ, Duncan JS. Proton MRS reveals frontal lobe metabolite abnormalities in idiopathic generalized epilepsy. *Neurology* 2003;61:897-902.

166. Bernasconi A, Bernasconi N, Natsume J, Antel SB, Andermann AF, Arnold DL. Magnetic resonance spectroscopy and imaging of the thalamus in idiopathic generalized epilepsy. *Brain* 2003;126:2447-54.

167. Kapucu LO, Serdaroglu A, Okuyaz C, Kose G, Gucuyener K. Brain single photon emission computed tomographic evaluation of patients with childhood absence epilepsy. *J Child Neurol* 2003;18:542-8.

168. Lum LM, Connolly MB, Farrell K, Wong PK. Hyperventilation-induced high-amplitude rhythmic slowing with altered awareness: a video-EEG comparison with absence seizures. *Epilepsia* 2002;43:1372-8.

169. Buxton RB. *An introduction to functional magnetic resonance imaging: principles and techniques*. Cambridge: Cambridge University Press, 2001.

APPENDIX I

Basics of Magnetic Resonance Imaging

A moving electric charge produces a magnetic field. A proton does not have much of an electric charge, but it spins rapidly and therefore produces a small, but noticeable, magnetic field. The hydrogen nucleus with its single charged proton spins creating a surrounding electromagnetic field with the characteristics of a magnetic dipole (think of a tiny bar magnet). When placed in an external magnet field, quantum mechanics tells us this hydrogen nucleus can have two "spin" states or energy levels. Most of the nuclei prefer the lower energy state rather than the higher. When electromagnetic radiation in the radiofrequency range (MHz) is applied, nuclei can absorb energy and be elevated to the higher energy state. The energy given off as these nuclei "relax" back into their lower state is the source of the MR signal.

The greatest sources of mobile protons in the human body are water and fat and the direction of their spins is normally randomly distributed (Figure 28A) (169). When placed in the large magnetic field of an MRI, the spins become aligned with or against the field. Importantly, a slight excess of protons align with the field and therefore a net magnetization (M_o) in this direction results (Figure 28B). The advantage of high field imaging can be understood in this regard since at a higher field strength a larger excess of protons are aligned, resulting in a larger M_o.

The spinning hydrogen nuclei "wobble" or show an angular precessional frequency when placed in the main magnetic field as depicted by the red circles in Figure 28. This precessional frequency is directly related to field strength of the magnet. Animal magnets with field strengths of 4.7, 7.0 and 9.4 Tesla create precessional frequencies for hydrogen nuclei of 200, 300 and 400 MHz, respectively. Once the protons are aligned within the magnetic field an electromagnetic radio frequency (RF) pulse is applied and the resulting energy is absorbed by the protons (Figure 28C). If these RF pulses have the same frequency as the precessing hydrogen nuclei the resonant energy is absorbed. This absorption causes M_o to flip towards the x-y plane and dephase in the transverse direction (Figure 28D). The time constant which describes the return of transverse magnetization to its equilibrium position is referred to as the T2/T2* relaxation time. As soon as the RF pulse is turned off M_o goes back into phase and returns to its equilibrium position over a relaxation time know as T1 (longitudinal relaxation). Both time courses are exponential functions. T_1 is measured in seconds while T_2 is measured in milliseconds. As the protons relax back to their equilibrium position, the RF energy which was previously absorbed is re-transmitted, producing the signal necessary for magnetic resonance imaging.

It is important to note, as long as there is net magnetization in the transverse plane there is potential for generating a series of MR signals. Is there

Figure 28

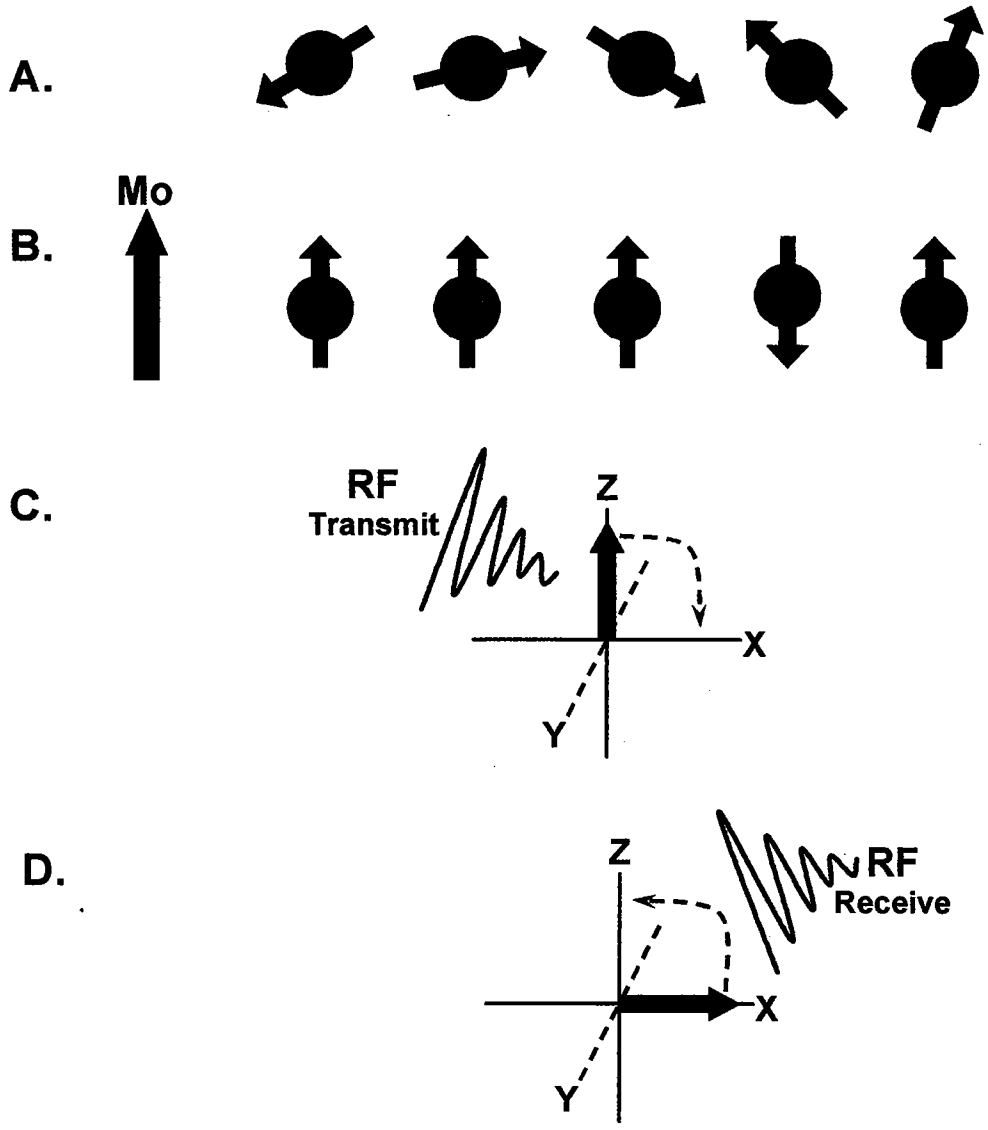

Figure 28. The basics of magnetic resonance imaging. Normally, proton spins (green) are pointed in random directions (A). When placed in a magnetic field, such as that of an MRI, the spins line up either with or against the direction of the field producing a net magnetization, Mo (B). During imaging, RF signal is transmitted and absorbed by the protons. This results in the net magnetization vector (green arrow) being flipped into the x-y plane (C). Once the RF pulse is turned off, the magnetization vector relaxes back to its equilibrium position according to the relaxation rates, T1 and T2/T2* (D). As relaxation occurs, the protons emit an RF signal which is received by the surface coil and processed into an image.

a way to bring the hydrogen nuclei back into phase or have them "echo" repeatedly until the system comes back to equilibrium? Spin echo and gradient echo pulse sequences have been developed to do just this. In a spin echo pulse sequence the initial 90° pulse flips the hydrogen nuclei into the transverse plane. Afterward, a refocusing 180° pulse is applied reversing the direction of the precessional spins. The faster spinning hydrogen nuclei now have been turned around and are facing the slower spinning nuclei. The MR signal waxes and wanes as the faster nuclei catch up and pass the slower nuclei. The 180° refocusing pulse can be applied several times while there is transverse magnetization. Usually after 1.5 to 2.5 seconds the sequence is repeated (time to repeat or T_R) and another 90° pulse is applied to flip the hydrogen nuclei into the transverse plane and the echo series begins again. One of the major advantages of fast spin echo pulse technique, particularly in imaging fully conscious animals, is its tolerance to artifacts from physiologic motion (e.g. cerebrospinal fluid movement) or magnetic susceptibility (e.g. distorted signal at air/liquid interfaces). However, magnetic susceptibility caused by deoxygenated hemoglobin is a key component in the BOLD signal. Hence, fast spin echo technique is less sensitive to changes in BOLD signal than gradient echo technique.

In a gradient echo pulse sequence the initial RF pulse only partially flips the hydrogen nuclei into the transverse plane. Since these nuclei are only partially flipped they rapidly loose their transverse magnetization as they return to

equilibrium in the main magnetic field. Hence a series of short T_Rs usually between 50-75 msec are necessary in order to collect multiple MR signals. Indeed, the purpose of gradient echo technique is to increase the speed of the scan. The rephasing event required for echo generation is accomplished by reversing the local magnetic field with special gradient coils. Gradient echo is particularly sensitive to magnetic susceptibility and commonly used in functional imaging. But this major advantage is also its major disadvantage because of the susceptibility artifacts most noticeably at air/tissue interfaces associated with sinuses. Gradient echo is also very sensitive to shimming (improving the field homogeneity) making it difficult to collect undistorted slices across the entire brain.